BORNEO
INTERNATIONAL JOURNAL OF BIOTECHNOLOGY

Volume 1, December 2020
e-ISSN 2716-697X

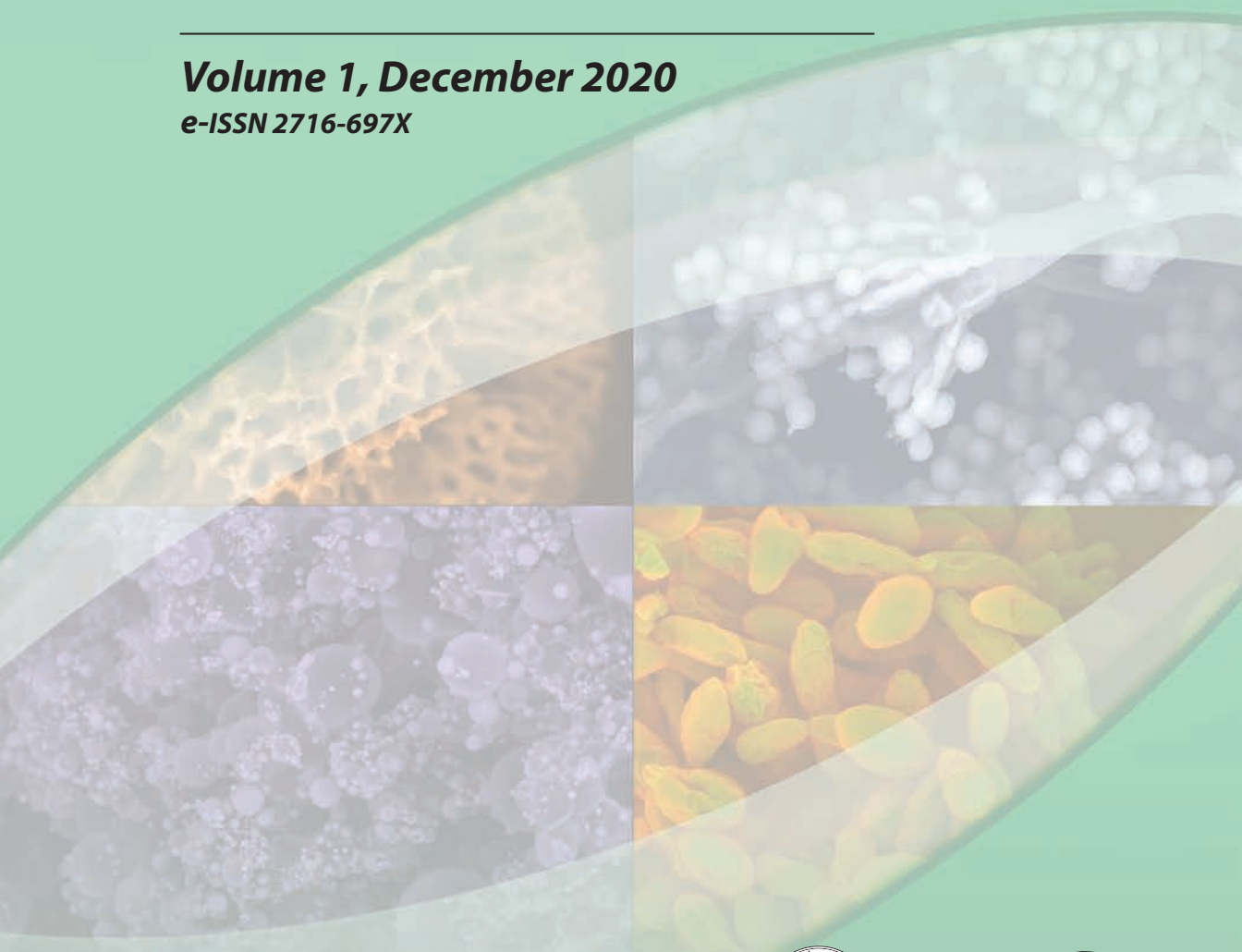

UMS
UNIVERSITI MALAYSIA SABAH

Cover photo credits:	Vijay Kumar, Rolando Robert, Jenny Teo and Teoh Chui Peng
Typeface for text:	Myriad Pro
Text type and leading size:	11/13.2 points
Published by:	Penerbit Universiti Malaysia Sabah Tingkat Bawah, Perpustakaan Universiti Malaysia Sabah Jalan UMS 88400 Kota Kinabalu, Sabah

CONTENTS

PREFACE

We are proud to present the inaugural issue of a new journal, the Borneo International Journal of Biotechnology (BIJB), Volume 1, December 2020. BIJB is initiated by the Biotechnology Research Institute and published by UMS Press. It offers a platform for scientists to share scientific knowledge and discovery in the field of biotechnology. The scopes of this journal cover every aspect of biotechnology, including but not limited to biochemistry, molecular biology, bioprocesses, biosensors, genomics, transcriptomics, proteomics, and metabolomics. BIJB aims to provide readers around the globe with peer-reviewed research articles on a wide variety of biotechnology-related issues.

The editors are committed to maintaining a high ethical standard, and do not tolerate plagiarism, duplicate publication, and other publication frauds and misconducts. While every effort has been taken to ensure compliance with the publication ethics, post-publication articles that are found to breach the BIJB copyright transfer agreement's terms and conditions, or other publication ethics will be retracted from the journal. At least two peer reviewers are assigned to review each manuscript that is submitted to ensure the content has scientific merits and meets the required standard. New members will be added to the editorial board from time to time to include internationally recognized experts from different disciplines of biotechnology. At the same time, the publisher will continue to make the submission to this journal as user friendly as possible. Our vision is to have the BIJB indexed by international databases such as Scopus and Google Scholar within the next five years.

In this inaugural issue, there are nine articles, and these are the highlights of these articles. Obeng et al. in their review paper describe the strategy to enhance the overall functionality of cellulases to produce higher product titer, through the supplementation of cellulases with biological complementation, and chemical additives in their review paper. In another review paper, Nabilah et al. documented several molecular techniques commonly used to assess and determine the genetic diversity of bamboo species. Teoh et al**.** analyze the characteristics of an Antarctic yeast, *Glyciozyma antarctica*. They report that *G. antarctica* PI12 is a bipolar budding and it forms a chain of cells at certain growth stages. They also describe the yeast hydrolytic enzymes. Chong et al. document the steviol glycosides separation from *Stevia rebaudiana* with several aqueous extraction techniques in their first paper, and rebaudioside A separation from *Stevia rebaudiana* using low polarity resin AB-8 in their second paper.

Budiman et al. reported on the reassessment of the catalytic and substrate specificity of Pk-FKBP35 using an alternative method of a protease-free assay. Sugumaran et al. in their paper attribute the antibiotic-resistant profile of *Staphylococcus aureus* and *Escherichia coli* isolated from recreational parks around Kota Kinabalu, Sabah. Simon et al. present the genetic diversity data of Sabah rice cultivars that they have analyzed using the random amplified polymorphic DNA (RAPD) technique. Their article provides insights into the genetic relationships and diversity of Sabah rice. Finally, Gilbert et al. describe the electrochemical sensor optimization for the detection of aluminium ion in drinking water. They indicated that the sensor holds great potentials for rapid on-site detection of heavy metal ions in the drinking water.

As the editors of this inaugural issue, we would like to thank all contributors and reviewers as well as personnel at the Editorial Office of UMS Press.

Clemente Michael Wong Vui Ling
Shafiquzzaman Siddiquee
Chief and Managing Editors

BORNEO INTERNATIONAL JOURNAL OF BIOTECHNOLOGY (BIJB)

EDITORIAL BOARD

Borneo International Journal of Biotechnology (BIJB)
Vol. 1 (December 2020), 1 – 18

e-ISSN 2716-697X

Review Article

ADDITIVES FOR CELLULASE ENHANCEMENT

Eugene M. Obeng[1], Chan Yi Wei[1], Siti Nurul Nadzirah Adam[1] and Clarence M. Ongkudon[1, 2*]

[1]Biotechnology Research Institute, Universiti Malaysia Sabah, Kota Kinabalu, Sabah, Malaysia
[2]Energy Research Institute, Universiti Malaysia Sabah, Kota Kinabalu, Sabah, Malaysia
*Corresponding author's email: clarence@ums.edu.my
Received date: 27 June 2019 | Accepted date: 9 August 2019

ABSTRACT

Cellulases have been vital for the saccharification of lignocellulosic biomass into reduced sugars to produce biofuels and other essential biochemicals. However, the sugar yields achievable for canonical cellulases (i.e. endoglucanases, exoglucanases and β-glucosidases) have not been convincing in support of the highly acclaimed prospects and end-uses heralded. The persistent pursuit of the biochemical industry to obtain high quantities of useful chemicals from lignocellulosic biomass has resulted in the supplementation of cellulose-degrading enzymes with other biological complementation. Also, chemical additives (e.g. salts, surfactants and chelating agents) have been employed to enhance the stability and improve the binding and overall functionality of cellulases to increase product titre. Herein, we report the roadmap of cellulase-additive supplementations and the associated yield performances.

Keywords: cellulases, hemicellulases, laccases, LPMOs, salts, surfactants

INTRODUCTION

Lignocellulose is an important cellulosic feedstock for producing bulk biochemicals and other value-added products due to its abundance, renewability and sustainability (Ramawat & Mérillon, 2015). The use of lignocellulosic biomass has received soaring attention within the last few decades because the ensuing products are believed to be a potential replacement of fossil fuels and fossil-based chemicals. For instance, unlike fossil fuels, (ligno) cellulosic biofuel putatively contribute no net increase in carbon

dioxide concentration in the atmosphere; thus, becoming beneficial in the quest to mitigate climate change and global warming (Balan, Bals, Chundawat, Marshall, & Dale, 2009; Vassilev, Baxter, Andersen, & Vassileva, 2010).

Lignocellulose has a complex structure consisting of inner cellulose (30 – 45%) wrapped by a sheath of hemicellulose (15 – 30%) and lignin (12 – 25%) (Parisutham, Kim, & Lee, 2014), but varies in composition based on the type of species, growth process, growing conditions, age and geographical source of the biomass (Magalhães da Silva, da Costa Lopes, Roseiro, & Bogel-Łukasik, 2013; Vassilev et al., 2010). The holocellulose (hemicellulose plus cellulose) content has been the main source of the substrate to produce vital biochemicals. The process requires a consortium of enzymes, called cellulases, to systematically breakdown the substrate into reduced sugars for specific essential applications (e.g. biofuels) (Chandel & Silvério da Silva, 2013). Specifically, endoglucanases, exoglucanases and β-glucosidases are the three basic cellulases required for cellulose depolymerization.

The cellulase industry has witnessed recommendable improvements in terms of multiplicities in cellulase sources. Different sources, for example, fungi, bacteria, protozoans and even plants and animals, have shown potential for cellulase production (Kim & Kim, 2012). However, the fraternity still faces challenges on stability (thermal and pH) and catalytic efficiency. Remarkably, several attempts have been pursued to enhance the activity of cellulase. Some of these attempts have focused on the pre-treatment of the biomass (Agrawal et al., 2015; Jia et al., 2015; Pandiyan et al., 2014), cellulase engineering (Bommarius, Sohn, Kang, Lee, & Realff, 2014; Ito, Ikeuchi, & Imamura, 2013; Kim, Chokhawala, Nadler, Blanch, & Clark, 2010; Lee, Chang, Jeng, Wang, & Liang, 2012), and the supplementation of the cellulose depolymerization process with additives (biological and non-biological).

Herein, we discuss the roadmap on the enhancement of cellulases for lignocellulose saccharification in the perspective of cellulase supplements and additives. More importantly, we discuss how some of these supplements/additives enhance the functionality of the three basic cellulases toward achieving high titer of reduced sugars to produce essential commodities. To improve comprehensibility, we commence the discussion with a brief description of the structure and nature of the key cellulases. A comprehensive review of these enzymes has been published by Bhat (2000).

CELLULASES

Cellulases are enzymes capable of hydrolysing the β-1,4-glycosidic linkages within the complex cellulose structure to yield reduced sugars such as glucose. The substrate of these enzymes, the cellulose, is a homopolymer which is composed of repeated units of D-glucose monomers linked together by β-1,4-glycosidic bonds. Cellulases

are carbohydrate-degrading enzymes – a type of glycoside hydrolases (GHs) – which commonly possess a carbohydrate-binding module (CBM) to ensure substrate targeting; a catalytic module (CM) to cleave the β-1,4-glycosidic bond; and other types of essential modules such as FN3-like modules (Davies, Gloster, & Henrissat, 2005; Garvey, Klose, Fischer, Lambertz, & Commandeur, 2013; Moraïs et al., 2012). The non-catalytic modules of the multi-modular structure of cellulases frequently assist in protein-protein and protein-carbohydrate interactions (Bommarius et al., 2014).

There are three (3) basic cellulases (namely: endoglucanases, exoglucanase and β-glucosidases) which have been identified to ensure the conversion of cellulose into the glucose monomers. These enzymes differ structurally and functionally, but their catalytic mechanism follow the classical acid-catalyst hydrolysis model, employing two critical glutamate residues which function as a proton donor and a nucleophile, respectively (Garvey et al., 2013; Isorna et al., 2007). The two amino acid residues facilitate the hydrolysis of glycosidic linkages through the retention and/or inversion of the anomeric carbons within the polysaccharide structure (Koshland, 1953).

Endoglucanases (E.C.3.2.1.4) are the most abundant GHs; they are structurally characterized with short loops having well-defined, open active site clefts and show affinity toward amorphous site along cellulose chains (Juturu & Wu, 2014; Wilson, 2015). In contrast to endoglucanases, exoglucanases have long loops that form a tunnel-like structure around the catalytic residue but have an affinity for crystalline sites within the cellulose matrix (Juturu & Wu, 2014). Functional elucidations have led to the discovery and classification of two distinct exoglucanases, namely: the reducing end (E.C.3.2.1.176) and non-reducing ends (E.C. 3.2.1.91) exoglucanases. The classification is based on the portion of the polysaccharide chain (i.e., reducing end or non-reducing end) each enzyme favourably attacks (Wahlström, Rahikainen, Kruus, & Suurnäkki, 2014). However, the two enzymes are complementary and processive. Based on performance, endoglucanases exhibit the most rapid dissociation with the greatest liquefaction that leads to cellulose depolymerization and viscosity reduction (Boyce & Walsh, 2015). The work of endo- and exoglucanases in cellulase cocktails is considered as the rate-determining step ensuring effective cellulose depolymerization (Chandel & Silvério da Silva, 2013). According to Luterbacher, Walker, & Moran-Mirabal (2013), the rate of limiting effect increases the surface area of the substrate and exposes a new binding site for successive enzymes to cleave. Notably, feedback inhibition – a condition where the product of the enzyme impedes the enzyme itself – has been a crucial challenge of endoglucanases and exoglucanases (Van Dyk & Pletschke, 2012); thus, the need to synergize their activity with β-glucosidases.

β-glucosidases (EC 3.2.1.21) have a rigid active site that resides in a large cavity (i.e., the active site pocket) known to permit the entry of disaccharides (Nam, Sung, & Hwang, 2010). Notably, some β-glucosidases are also able to break down soluble cellodextrins with a degree of polymerization ≤ 6 (González-Candelas, Aristoy, Polaina, & Flors, 1989; Zhang & Lynd, 2004). The cavity is surrounded by four hydrophobic loops of different conformations which facilitate substrate binding (Czjzek et al., 2000; Nam et al., 2010). The specificity of β-glucosidases is influenced by the loops, which are potentially stabilized by hydroxyl groups, either from substrate or water (Isorna et al., 2007; Nam et al., 2010). β-glucosidases are categorized into two sub-families, viz. sub-family A (e.g. plant and non-rumen prokaryotic sources) and sub-family B (fungal and rumen bacterial sources) (Park et al., 2011). Similar to endo- and exoglucanases, β-glucosidases also experience glucose feedback inhibition – a challenge that has led to the discovery of glucose tolerant derivatives (Das et al., 2015; Günata & Vallier, 1999; Rajasree, Mathew, Pandey, & Sukumaran, 2013; Riou, Salmon, Vallier, Günata, & Barre, 1998). *Trichoderma* and *Aspergillus* species have been key sources of primary cellulases (endo- and exocellulases) and β-glucosidases, respectively (Brijwani, Oberoi, & Vadlani, 2010; Gottschalk et al., 2010; Gutierrez-Correa, Portal, Moreno, & Tengerdy, 1999; Wang, Bay, Chew, & Geng, 2014).

Functional elucidations have theorized that endoglucanases begin the deconstruction process by hydrolyzing cellulose at amorphous sites into long-chain oligomers (e.g., cellodextrin); exoglucanases attack the long-chain oligomers at the crystalline regions from either reducing or non-reducing ends to yield short-chain oligomers (e.g. cellobiose, cellotriose, cellutetrose, etc.) and β-glucosidases complete the breakdown process by converting cellobiose to D-glucose (Juturu & Wu, 2014; Segato, Damásio, de Lucas, Squina, & Prade, 2014). The overall process involves a series of adsorption and desorption, and it is governed by synergism, cooperativity and substrate channelling (Wilson, 2009).

ADDITIVE EFFECT ON CELLULOSE HYDROLYSIS

The complex structure of lignocellulosic biomass, even after pretreatment, requires a multitude of enzymes in conjunction with the canonical cellulases for effective degradation (Chundawat, Beckham, Himmel, & Dale, 2011). For instance, the supplementation of cellulases with other enzymes of relevant activities and the inclusion of enzyme-activity-enhancing chemicals to ensure most of the saccharides in the biomass are converted to their reduced and fermentable forms are common practices. The supplementary enzymes and accessories play a complementary role in effective biomass bio-depolymerization (Gao et al., 2011). The role and benefits of some of the biological and chemical additives commonly reported in the literature are discussed as follows:

Biological Supplements

Hemicellulases

Hemicellulases are enzymes responsible for the breakdown of the hemicellulose sheath linking core cellulose and the outward lignin of the cell wall of plants. The hemicellulose substrate is the second most abundant plant polymer after cellulose (Peng & She, 2014; Rubin, 2008), and consist of easy-hydrolysable compounds including pentoses (e.g., arabinose and xylose), hexoses (e.g., mannose, galactose and glucose), and sugar acids (Hendriks & Zeeman, 2009; Imman, Arnthong, Burapatana, Laosiripojana, & Champreda, 2013). Generally, hemicellulases share common functionality with cellulases, in that they hydrolyze the β-1,4-glycosidic bonds within hemicellulose (Chang et al., 2011). Hemicellulases are also GHs and possess CMBs and other functional modules which support the functionality of the catalytic domains (CDs). Some CDs exhibit carbohydrate esterase (CE) functionality instead of the common GH-functionality (Shallom & Shoham, 2003). The GH-type catalytic domain hydrolyzes glycosidic linkages whereas CE-type hydrolyzes ferulic acid side groups or ester bonds of acetate (Shallom & Shoham, 2003). Xylanases, xylosidases, and arabinofuranosidases are the most common hemicellulases essential for biomass depolymerization (Ratanakhanokchai, Kyu, & Tanticharoen, 1999). However, mannanases, glucuronidases and esterases are also hemicellulases with distinct activities.

Cellulases and hemicellulases complementarily affect the degree of polymerization of the cellulosic substrate, resulting in a high level of sugar monomers (Pala, Mota, & Gama, 2007). Hemicellulase activity on its feedstock clears the way for cellulases to attack the core cellulose (Doi, 2008). According to Gao et al. (2011), more than 80% of the theoretical glucose yield is achievable using an optimized blend of cellulases and hemicellulases. Gao et al. (2014) compared the yield of reduced sugar (i.e., glucose and xylose) from corn stover (CS) pretreated by ammonium fibre expansion (AFEX), dilute acid (DA) and ionic liquid (IL) with and without hemicellulase supplementation. For IL-CS, they reported 88% glucose and 53% xylose yields in the presence of hemicellulases as against 82% glucose and 12% xylose yields in the absence of hemicellulases within 48 h. The hemicellulase-assisted hydrolysis of AFEX-CS resulted in 99% glucose and 55% xylose yields as against 84% glucose and 10% xylose yields for the hemicellulase-devoid system in 48 h. Lastly, the DA-CS gave close to 97% glucose and 68% xylose yields in the presence of the synergistic hemicellulase supplementation as compared to 88% glucose and 28% xylose yields for raw cellulase cocktail in 48 h. The hemicellulase helped in relieving bound cellulases from the substrate and that led to an improved recovery (Gao et al., 2014). Similar elucidations have been reported for steam-pretreated CS and hybrid poplar (Bura, Chandra, & Saddler, 2009) and barley straw (García-Aparicio et al., 2007). Notably, the glucose released in the presence of hemicellulases has a direct linear relationship with the concurrent release of xylose (Kumar & Wyman, 2009).

Laccases

Laccases (EC 1.10.3.2) are multicopper oxidases responsible for the one-electron oxidation of various feedstocks, including phenolic and non-phenolic subunits of lignin (Chandel, Gonçalves, Strap, & da Silva, 2015; Dwivedi, Singh, Pandey, & Kumar, 2011; Lahtinen et al., 2009). The active sites of laccases have four copper atoms viz. Type-1 (blue copper centre), Type-2 (normal copper) and Type-3 (coupled binuclear copper centres) located at three different centres (Dwivedi et al., 2011). The copper atoms oxidize cellulose substrates at C-1, C-4, and C-6 atoms positions (Segato et al., 2014). It is worth noting that the functionality of laccases is enforced by electron transfer and hydrogen atom mediators. Lignin peroxidase (EC 1.11.1.14) and manganese-dependent peroxidase (EC 1.11.1.13) have also been identified to oxidatively attack phenolic and non-phenolic aromatic lignin moieties (Manavalan, Manavalan, & Heese, 2015; Wan & Li, 2012).

The principal substrate of laccases is lignin, which is a biopolymer composed of mixed phenylpropanoid units (Meyer, Lupoi, & Smith, 2011). For that matter, the supplementation of canonical cellulases with laccases could take care of the lignin residues which remain after the pretreatment lignocellulose. This is necessary because residual lignin in pretreated biomass directly inhibits and impedes the movement of the cellulases along the cellulose chain (Berlin, 2013; Zhang & Lynd, 2004). According to Moilanen, Kellock, Galkin, & Viikari (2011), laccases are capable of liberating trapped cellulases from unproductive adsorption. Moreover, laccases could potentially address phenolic compound inhibition of cellulases during biomass hydrolysis. For instance, Hyeon et al. (2014) obtained a 2.6 fold increase in the reduced sugar yield upon the involvement of laccases in the saccharification of pretreated barley straw. Moilanen et al. (2011) also reported a 12% increase in hydrolysis yield from pretreated spruce, using laccases and commercial cellulases. Furtado, Ribeiro, Lourenzoni, and Ward (2013) and Ribeiro et al. (2011) have also demonstrated the synergy and associated catalytic performance improvement when laccases are fused to other enzymes for biomass hydrolysis.

Lytic Polysaccharide Mono-oxygenases (LPMOs)

Lytic polysaccharide mono-oxygenases (LPMOs) are a recent discovery in the lignocellulose depolymerization pathway. Intriguingly, their inception has been vital in the understanding of how saprophytes breakdown biomass for their energy demands. LPMOs were previously thought of as being endoglucanase due to their ability to exhibit weak endocellulase functionalities (Karkehabadi et al., 2008; Karlsson et al., 2001). However, modern structural and functional elucidations have necessitated their reclassification as auxiliary activity (AA) family enzymes.

Interestingly, the functional insights of LPMOs have challenged and reformed the classical concept of cellulose saccharification by canonical cellulases (Hemsworth, Davies, & Walton, 2013a). Therefore, some research has been geared at fully elucidating their functional distinctions and associated mechanisms to aid in their possible supplementation with cellulases.

Like laccases, LPMOs is also an oxidative enzyme. However, LPMS have a monomeric type II copper ions (Cu^{2+}) in the centre of the active sites for substrate interaction (Hemsworth et al., 2013b; Quinlan et al., 2011). The active site is positioned within an extended flat-face structure which is different from the common tunnel-shaped structures shielding the active sites of cellulases (Hemsworth et al., 2013a; Isaksen et al., 2014). The catalytic activity of LPMOs dwells on the binding of active atmospheric oxygen (O2) to the type II Cu^{2+} ion which then facilitates its interaction with C-1 and C-4 bonds along with the cellulose polymer (Hemsworth et al., 2013a; Walton & Davies, 2016). The presence of molecular oxygen, an external electron donor and possibly CBM is key for LPMO functionality. The external electron donor could be provided by residual lignin present within the cellulose matrix (Westereng et al., 2015).

LPMOs complement cellulases during the breakdown of cellulose by causing chain breaks (via oxidation reactions) in the cellulose matrix thereby improving the accessibility of cleavage sites to cellulases (Horn, Vaaje-Kolstad, Westereng, & Eijsink, 2012; Vaaje-Kolstad et al., 2010). In technical terms, the enzyme causes the abstraction of hydrogen atoms to aid in the cleavage of the bonds between the most accessible and most reactive C-H (i.e. C-1 and C-4) (Obeng et al., 2017). The strong synergism of LPMOs with other cellulases is believed to be due to their ability to attack highly crystalline and recalcitrant spots of cellulose where other enzymes cannot (Harris, Xu, Kreel, Kang, & Fukuyama, 2014). Jung, Song, Kim, and Bae (2015) reported an accelerated synergistic effect of 56 and 174% for the blend of LPMOs and cellulases on pretreated kenaf and oak, respectively. A similar observation (i.e. 60% more glucose) from LPMOs with Celluclast® on dry lignocellulosic biomass has been reported (Müller, Várnai, Johansen, Eijsink, & Horn, 2015).

Non-hydrolytic Accessory Proteins

Expansins and swollenins are the common non-hydrolytic proteins for lignocellulosic biomass deconstruction. They can loosen the cell wall of plants and alter the crystallinity of cellulosic material (Nakashima, Endo, Shibasaki-kitakawa, & Yonemoto, 2014). Expansins are plant proteins whereas swollenins are expansin-derivatives from fungi and bacteria. These proteins disrupt the hydrogen bonds within the cellulose structure to reduce the crystallinity thereby enhancing the cellulose accessibility for enzymatic attacks (Harris et al., 2014). Nakatani, Yamada, Ogino, and Kondo (2013)

reported a 2.9-fold increase in cellulase activity on phosphoric acid swollen cellulose (PASC) by co-displaying cellulase and expansin-like proteins on yeast cells. Also, Nakashima et al. (2014) reported a 35% increase in substrate digestibility by fusing endoglucanase with expansins.

Recently, there is also the practice of using non-enzymatic proteins such as bovine serum albumin (BSA), peptone, yeast extract, soybean protein and processing wastes from the meat, fish and milk industries as lignin blockers (Yang & Wyman, 2013). In simple terms, these proteinaceous materials help to either enhance cellulase adsorption or reduce unproductive adsorption of the cellulases onto lignin by interacting with (or "blocking") lignin. The blocking effect improves the accessibility of cellulases to cellulose to promote efficient cellulose depolymerization. Also, the inclusion of lignin blockers reduces the intensiveness of pre-treatment method (Wang, Kobayashi, & Mochidzuki, 2015), enzyme loading (Luo et al., 2019), and operation time (Brondi, Vasconcellos, Giordano, & Farinas, 2019); thus, improving the economics of biomass saccharification. For instance, Ko, Kim, Ximenes, and Ladisch (2015) supplemented cellulases with BSA for the hydrolysis of hydrothermally pre- treated hardwood. The work reported about a 72% increase in hydrolysis yield compared with 17% for saccharification without BSA. Similarly, Wang et al. (2015) tested the influence of BSA, peptone and yeast extract on the hydrolysis yield of pre-treated rice straw using different commercial enzymes. The work reported 14 – 20% increase in hydrolysis yield upon the inclusion of these blocking agents. Also, Luo et al. (2019) reported the supplementation of pre-treated lignocellulose with soybean protein reported an improved enzymatic conversion 40%, 30%, and 41% for eucalyptus, bamboo, and Masson pine, respectively. The inclusion of soybean protein reduced enzyme loading by 8 times. Similarly, Florencio, Badino, and Farinas (2019) obtained up to 86% improvement sugarcane bagasse hydrolysis. Seki et al. (2015) have also reported about 2.9-fold improvement in saccharification yield due to the effects of non-enzymatic proteins in cattle saliva on cellulose degradation.

Non-biological Additives

The common non-biological additives for enhancing cellulase performance include salts, surfactants and chelating agents. These chemicals provide cellulase activity improvement by either serving as metal cofactors, activators or stabilizers. The associated effects are enzyme, enzyme preparation and concentration dependent.

Salts and Chelating Agent

Many salts have been used in the literature to enhance the activity of cellulases. These salts are dominated by divalent cation-associated salts. However, the anion aspects of the salts have not shown their clear-cut functionality on cellulase enhancement to

date. KCl, $MnCl_2$, $CaCl_2$, $CuCl_2$, $MgCl_2$ and $ZnSO_4$ are some of the common salts being reported in the literature. Each of the metal cations has shown specific affinities for one cellulase compared to another, although the cations may have the same valency number. The discrepancies could have a link with the atomic radius of the cation and dimensions of the active site cavity; however, this is yet to be proved.

Table 1 Impacts of additives in cellulose hydrolysis

Enzyme(s)	Source	Additive	Relative performance	References
Endoglucanase	*Alicyclobacillus vulcanalis*	$CaCl_2$ (10 mM) $MgCl_2$ (10 mM) EDTA (2 mM) Tween 20 (0.1%) Triton X-100 (0.1%)	97% 86% 98% 124 % 124 %	Boyce and Walsh, 2015
Endoglucanase and xylanase fusion protein (Xyl10g GS Cel5B)	*Gloeophyllum trabeum*	$CoCl_2$ (1 mM) $CaCl_2$ (1 mM) $FeCl_3$ (1 mM) KCl (1 mM) LiCl (1 mM) EDTA (1 mM) NaCl (1 mM)	139% (115%) 101% (95%) 100% (115%) 100% (95%) 101% (95%) 91% (88%) 101% (97%)	Kim, Jung, Lee, Song, and Bae, 2015
Exoglucanase	*Rhizopus stolonifera*	$CaCl_2$ (1 mM) KOH (1 mM) $MgSO_4$ (1 mM) $ZnSO_4$ (1 mM) Fe_2Cl_3 (1 mM) NH_4Cl (1 mM) EDTA (1 mM) Tween 20 (1 mM) SDS (1 mM) Triton X 100 (1 mM)	160% 95% 126% 75% 100% 99% 130% 80% 70% 55%	Navya, Bhoite, and Murthy, 2012
β-glycosidase	*Alicyclobacillus acidocaldarius*	Mg^{2+} (5 mM) Mn^{2+} (5 mM) Ca^{2+} (5 mM) Zn^{2+} (5 mM) Co^{2+} (5 mM) Cu^{2+} (5 mM) Ni^{2+} (5 mM) Zn^{2+} (5 mM) Co^{2+} (5 mM) EDTA (5 mM)	Not significant Not significant Not significant 33% 96% Not significant Not significant Not significant Not significant Not significant	Di Lauro, Rossi, and Moracci, 2006

NB: The reported relative performances have been rounded to the nearest whole number. The figures in bracket refer to the concentration of xylose.

One key property of these salts is the ability to dissociate in solution to yield a dielectric strength capable of resisting pH fluctuation, thus preserving/improving the functionality and stability of the enzymes present (Suplatov, Panin, Kirilin, Shcherbakova, & Kudryavtsev, 2014). For instance, Ca^{2+} has been identified as having the ability to improve ligand binding and cellulase stability, and maintain the structural integrity of enzymes (Abou-hachem et al., 2002; Bolam et al., 2004; Jamal, Nurizzo, Boraston, & Davies, 2004). According to Warren and Cheatum (1966), the salts contribute to the enzyme enhancement by modifying the organized structure of the protein macromolecule.

On the other hand, chelating agents improve enzymatic activity by trapping and forming complexes with material (e.g., metal ions). This property may or may not be beneficial since some of these enzymes have inherent metal cations and other chelatable structures. The commonly used chelating agent is ethylenediamine tetraacetic acid (EDTA), and it is known for its metal ion scavenging abilities (Naika & Tiku, 2011). Fontes and Gilbert (2010) opined that EDTA hinders the interaction of dockerins with cohesins (both are facets of most enzyme structures) whereas Ca^{2+} proves essential for dockerin stability and function. Table 1 shows some of the reported impacts of these additives in cellulose hydrolysis.

Surfactants

Surfactants, for example, Tween, Triton and polyethene glycol, have been vital in cellulase enhancement procedures. Similar to lignin blockers, surfactants commonly function by improving the adsorption and desorption catalytic activity of enzymes in a way to improve enzyme mobility and prevent non-specific enzyme attachments (Helle, Duff, & Coopes, 1993; Tu, Zhang, Paice, Mcfarlane, & Saddler, 2009). The amphiphilic surface-active chemical potentially could alter the surface area and composition of cellulosic feedstock to improve the accessibility of cleavage point (Helle et al., 1993). It is worth noting that different surfactants also influence cellulase activity differently and this may be attributed to their polarity (i.e. ionic, non-ionic or zwitterionic), which by extension affects the binding modules of an enzyme. Polyethene glycol (PEG4000), for instance, has been reported to improve the activity of beta-glucosidases and endoglucanase by 20% and 60%, respectively (Rocha-Martín, Martinez-Bernal, Pérez-Cobas, Reyes-Sosa, & García, 2017). However, the associated cost concerns have to be addressed. Table 1 displays some of the reported benefits of common surfactants.

CONCLUSION

Several additives have a pronounced complementary effect on cellulase performance. The successful blend of cellulases, hemicellulases, lignases, accessory proteins and other additives in a way that will promote progressivity, synergism and non-competition are crucial for the cellulose-based industry. The challenge lies in proportionating these enzymes and supplementations in a manner that could function optimally to ensure the complete digestion of lignocellulosic biomass to simple sugars. However, with the current trend of cellulose hydrolysis research, the future of green products form lignocellulose still looks promising.

ACKNOWLEDGEMENTS

The authors wish to acknowledge Autodisplay Biotech GmbH (Germany) for the research fellowship that made the literature review possible.

CONFLICT OF INTEREST

The authors declare that there is no conflict of interest regarding the publication of this work.

REFERENCES

Abou-hachem, M., Karlsson, E. N., Simpson, P. J., Linse, S., Sellers, P., Williamson, M. P., … Holst, O. (2002). Calcium binding and thermostability of carbohydrate binding module CBM4-2 of Xyn10A from rhodothermus marinus ±. *Biochemistry*, *41* (18), 5720 – 5729. DOI: 10.1021/bi012094a

Agrawal, R., Satlewal, A., Gaur, R., Mathur, A., Kumar, R., Gupta, R. P., & Tuli, D. K. (2015). Pilot scale pretreatment of wheat straw and comparative evaluation of commercial enzyme preparations for biomass saccharification and fermentation. *Biochem. Eng. J.*, *102*, 54 – 61. DOI: 10.1016/j.bej.2015.02.018

Balan, V., Bals, B., Chundawat, S. P., Marshall, D., & Dale, B. E. (2009). Lignocellulosic biomass pretreatment using AFEX. In J. R. Mielenz (Ed.), *Biofuels: Methods in molecular biology (Methods and protocols)* (pp. 61 – 77). Totowa, NJ: Humana Press. DOI: 10.1007/978-1-60761-214-8_5

Berlin, A. (2013). No barriers to cellulose breakdown. *Science*, *342* (6165), 1454 – 1456. DOI: 10.1126/science.1247697

Bhat, M. K. (2000). Cellulases and related enzymes in biotechnology. *Biotechnol. Adv.*, *18* (5), 355 – 383. DOI: 10.1016/S0734-9750(00)00041-0

Bolam, D. N., Xie, H., Pell, G., Hogg, D., Galbraith, G., Henrissat, B., & Gilbert, H. J. (2004). X4 modules represent a new family of carbohydrate-binding modules that display novel properties. *J. Biol. Chem*., *279*, 22953 – 22963. DOI: 10.1074/jbc.M313317200

Bommarius, A. S., Sohn, M., Kang, Y., Lee, J. H., & Realff, M. J. (2014). Protein engineering of cellulases. *Curr. Opin. Biotechnol*., *29*, 139 – 145. DOI: 10.1016/j.copbio.2014.04.007

Boyce, A., & Walsh, G. (2015). Characterisation of a novel thermostable endoglucanase from Alicyclobacillus vulcanalis of potential application in bioethanol production. *Appl. Microbiol. Biotechnol*., *99* (18), 7515 – 7525. DOI: 10.1007/s00253-015-6474-8

Brijwani, K., Oberoi, H. S., & Vadlani, P. V. (2010). Production of a cellulolytic enzyme system in mixed-culture solid-state fermentation of soybean hulls supplemented with wheat bran. *Process Biochem*., *45*, 120 – 128. DOI: 10.1016/j.procbio.2009.08.015

Brondi, M. G., Vasconcellos, V. M., Giordano, R. C., & Farinas, C. S. (2019). Alternative low-cost additives to improve the saccharification of lignocellulosic biomass. *Appl. Biochem. Biotechnol*., *187*, 461 – 473. DOI: 10.1007/s12010-018-2834-z

Bura, R., Chandra, R., & Saddler, J. (2009). Influence of xylan on the enzymatic hydrolysis of steam-pretreated corn stover and hybrid poplar. *Biotechnol. Prog*., *25* (2), 315 – 322. DOI: 10.1002/btpr.98

Chandel, A. K., & Silvério da Silva, S. (Eds.). (2013). *Sustainable degradation of lignocellulosic biomass: Techniques, applications and commercialization*. London: InTech Open. DOI: 10.5772/1490

Chandel, A. K., Gonçalves, B. C. M., Strap, J. L., & da Silva, S. S. (2015). Biodelignification of lignocellulose substrates: An intrinsic and sustainable pretreatment strategy for clean energy production. *Crit. Rev. Biotechnol*., *35* (3), 281 – 293. DOI: 10.3109/07388551.2013.841638

Chang, L., Ding, M., Bao, L., Chen, Y., Zhou, J., & Lu, H. (2011). Characterization of a bifunctional xylanase/endoglucanase from yak rumen microorganisms. *Appl. Microbiol. Biotechnol*., *90*, 1933 – 1942. DOI: 10.1007/s00253-011-3182-x

Chundawat, S. P. S., Beckham, G. T., Himmel, M. E., & Dale, B. E. (2011). Deconstruction of lignocellulosic Biomass to fuels and chemicals. *Annu. Rev. Chem. Biomol. Eng*., *2*, 121 – 145. DOI: 10.1146/annurev-chembioeng-061010-114205

Czjzek, M., Cicek, M., Zamboni, V., Bevan, D. R., Henrissat, B., & Esen, A. (2000). The mechanism of substrate (aglycone) specificity in beta-glucosidases is revealed by crystal structures of mutant maize beta -glucosidase-DIMBOA, -DIMBOAGlc, and -dhurrin complexes. *Proc. Natl. Acad. Sci*., *97* (25), 13555 – 13560. DOI: 10.1073/pnas.97.25.13555

Das, A., Paul, T., Ghosh, P., Halder, S. K., Das Mohapatra, P. K., Pati, B.R., & Mondal, K. C. (2015). Kinetic study of a glucose tolerant β-glucosidase from Aspergillus fumigatus ABK9 entrapped into alginate beads. *Waste and Biomass Valorization*, *6*, 53 – 61. DOI: 10.1007/s12649-014-9329-0

Davies, G. J., Gloster, T. M., & Henrissat, B. (2005). Recent structural insights into the expanding world of carbohydrate-active enzymes. *Curr. Opin. Struct. Biol*., *15* (6), 637 – 645. DOI: 10.1016/j.sbi.2005.10.008

Di Lauro, B., Rossi, M., & Moracci, M. (2006). Characterization of a β-glycosidase from the thermoacidophilic bacterium Alicyclobacillus acidocaldarius. *Extremophiles*, *10*, 301 – 310. DOI: 10.1007/s00792-005-0500-1

Doi, R. H. (2008). Cellulases of mesophilic microorganisms: Cellulosome and noncellulosome producers. *Ann. N. Y. Acad. Sci*., *1125*, 267 – 279. DOI: 10.1196/annals.1419.002

Dwivedi, U. N., Singh, P., Pandey, V. P., & Kumar, A. (2011). Structure–function relationship among bacterial, fungal and plant laccases. *J. Mol. Catal. B Enzym*., *68* (2), 117 – 128. DOI: 10.1016/j.molcatb.2010.11.002

Florencio, C., Badino, A. C., & Farinas, C. S. (2019). Addition of soybean protein improves saccharification and ethanol production from hydrothermally pretreated sugarcane bagasse. *BioEnergy Res*., *12* (1), 81 – 93. DOI: 10.1007/s12155-018-9956-6

Fontes, C. M. G. A., & Gilbert, H. J. (2010). Cellulosomes: Highly efficient nanomachines designed to deconstruct plant cell wall complex carbohydrates. *Annu. Rev. Biochem*., *79*, 655 – 681. DOI: 10.1146/annurev-biochem-091208-085603

Furtado, G. P., Ribeiro, L. F., Lourenzoni, M. R., & Ward, R. J. (2013). A designed bifunctional laccase/ -1,3-1,4-glucanase enzyme shows synergistic sugar release from milled sugarcane bagasse. *Protein Eng. Des. Sel*., *26* (1), 15 – 23. DOI: 10.1093/protein/gzs057

Gao, D., Haarmeyer, C., Balan, V., Whitehead, T. A., Dale, B. E., & Chundawat, S. P. (2014). Lignin triggers irreversible cellulase loss during pretreated lignocellulosic biomass saccharification. *Biotechnol. Biofuels*, *7* (1), 175. DOI: 10.1186/s13068-014-0175-x

Gao, D., Uppugundla, N., Chundawat, S. P., Yu, X., Hermanson, S., Gowda, K., … Dale, B. E. (2011). Hemicellulases and auxiliary enzymes for improved conversion of lignocellulosic biomass to monosaccharides. *Biotechnol. Biofuels*, *4*, 5. DOI: 10.1186/1754-6834-4-5

García-Aparicio, M. P., Ballesteros, M., Manzanares, P., Ballesteros, I., González, A., & José Negro, M. (2007). Xylanase contribution to the efficiency of cellulose enzymatic hydrolysis of barley straw. *Appl. Biochem. Biotechnol*., *137 – 140* (1 – 12), 353 – 365. DOI: 10.1007/s12010-007-9064-0

Garvey, M., Klose, H., Fischer, R., Lambertz, C., & Commandeur, U. (2013). Cellulases for biomass degradation: comparing recombinant cellulase expression platforms. *Trends Biotechnol*., *31* (10), 581 – 593. DOI: 10.1016/j.tibtech.2013.06.006

González-Candelas, L., Aristoy, M. C., Polaina, J., & Flors, A. (1989). Cloning and characterization of two genes from Bacillus polymyxa expressing beta-glucosidase activity in Escherichia coli. *Appl. Environ. Microbiol*., *55* (12), 3173 – 3177.

Gottschalk, L. M. F., Oliveira, R. A., & da Silva Bon, E. P. (2010). Cellulases, xylanases, β-glucosidase and ferulic acid esterase produced by Trichoderma and Aspergillus act synergistically in the hydrolysis of sugarcane bagasse. *Biochem. Eng. J*., *51* (1 – 2), 72 – 78. DOI: 10.1016/j.bej.2010.05.003

Günata, Z., & Vallier, M. J. (1999). Production of a highly glucose-tolerant extracellular β-glucosidase by three Aspergillus strains. *Biotechnol. Lett*., *21*, 219 – 223. DOI: 10.1023/A:1005407710806

Gutierrez-Correa, M., Portal, L., Moreno, P., & Tengerdy, R. P. (1999). Mixed culture solid substrate fermentation of Trichoderma reesei with *Aspergillus niger* on sugar cane bagasse. *Bioresour. Technol*., *68* (2), 173 – 178. DOI: 10.1016/S0960-8524(98)00139-4

Harris, P. V., Xu, F., Kreel, N. E., Kang, C., & Fukuyama, S. (2014). New enzyme insights drive advances in commercial ethanol production. *Curr. Opin. Chem. Biol*., *19*, 162 – 170. DOI: 10.1016/j.cbpa.2014.02.015

Helle, S. S., Duff, S. J. B., & Coopes, D. G. (1993). Effect of surfactants on cellulose hydrolysis. *Biotechnol. Bioeng*., *42*, 611 – 617. DOI: 10.1002/bit.260420509

Hemsworth, G. R., Davies, G. J., & Walton, P. H. (2013a). Recent insights into copper-containing lytic polysaccharide mono-oxygenases. *Curr. Opin. Struct. Biol*., *23*, 660 – 668. DOI: 10.1016/j.sbi.2013.05.006

Hemsworth, G. R., Taylor, E. J., Kim, R. Q., Gregory, R. C., Lewis, S. J., Turkenburg, J. P., … Walton, P. H. (2013b). The copper active site of CBM33 polysaccharide oxygenases. *J. Am. Chem. Soc*., *135* (16), 6069 – 6077. DOI: 10.1021/ja402106e

Hendriks, A. T. W. M., & Zeeman, G. (2009). Pretreatments to enhance the digestibility of lignocellulosic biomass. *Bioresour. Technol*., *100* (1), 10 – 18. DOI: 10.1016/j.biortech.2008.05.027

Horn, S., Vaaje-Kolstad, G., Westereng, B., & Eijsink, V. G. (2012). Novel enzymes for the degradation of cellulose. *Biotechnol. Biofuels*, *5*, 45. DOI: 10.1186/1754-6834-5-45

Hyeon, J. E., You, S. K., Kang, D. H., Ryu, S. H., Kim, M., Lee, S. S., & Han, S. O. (2014). Enzymatic degradation of lignocellulosic biomass by continuous process using laccase and cellulases with the aid of scaffoldin for ethanol production. *Process Biochem*., *49*, 1266 – 1273. DOI: 10.1016/j.procbio.2014.05.004

Imman, S., Arnthong, J., Burapatana, V., Laosiripojana, N., & Champreda, V. (2013). Autohydrolysis of tropical agricultural residues by compressed liquid hot water pretreatment. *Appl. Biochem. Biotechnol*., *170* (8), 1982 – 1995. DOI: 10.1007/s12010-013-0320-1

Isaksen, T., Westereng, B., Aachmann, F. L., Agger, J. W., Kracher, D., Kittl, R., … Horn, S. J. (2014). A C4-oxidizing lytic polysaccharide monooxygenase cleaving both cellulose and cello-oligosaccharides. *J. Biol. Chem*., *289*, 2632 – 2642. DOI: 10.1074/jbc.M113.530196

Isorna, P., Polaina, J., Latorre-García, L., Cañada, F. J., González, B., & Sanz-Aparicio, J. (2007). Crystal structures of Paenibacillus polymyxa β-glucosidase B complexes reveal the molecular basis of substrate specificity and give new insights into the catalytic machinery of family I Glycosidases. *J. Mol. Biol*., *371* (5), 1204 – 1218. DOI: 10.1016/j.jmb.2007.05.082

Ito, Y., Ikeuchi, A., & Imamura, C. (2013). Advanced evolutionary molecular engineering to produce thermostable cellulase by using a small but efficient library. *Protein Eng. Des. Sel*., *26* (1), 73 – 79. DOI: 10.1093/protein/gzs072

Jamal, S., Nurizzo, D., Boraston, A. B., & Davies, G. J. (2004). X-ray crystal structure of a non-crystalline cellulose- specific carbohydrate-binding module: CBM28. *J. Mol. Biol*., *339* (2), 253 – 258. DOI: 10.1016/j.jmb.2004.03.069

Jia, L., Gonçalves Budinova, G., Takasugi, Y., Mori, Y., Noda, S., Tanaka, T., … Kamiya, N. (2015). Effect of pretreatment methods on the synergism of cellulase and xylanase during the hydrolysis of bagasse. *Bioresour. Technol*., *185*, 158 – 164. DOI: 10.1016/j.biortech.2015.02.041

Jung, S., Song, Y., Kim, H. M., & Bae, H. J. (2015). Enhanced lignocellulosic biomass hydrolysis by oxidative lytic polysaccharide monooxygenases (LPMOs) GH61 from Gloeophyllum trabeum. *Enzyme Microb. Technol*., *77*, 38 – 45. DOI: 10.1016/j.enzmictec.2015.05.006

Juturu, V., & Wu, J. C. (2014). Microbial cellulases: Engineering, production and applications. *Renew. Sustain. Energy Rev*., *33*, 188 – 203. DOI: 10.1016/j.rser.2014.01.077

Karkehabadi, S., Hansson, H., Kim, S., Piens, K., Mitchinson, C., & Sandgren, M. (2008). The first structure of a glycoside hydrolase family 61 member, Cel61B from Hypocrea jecorina, at 1.6 Å resolution. *J. Mol. Biol*., *383* (1), 144 – 154. DOI: 10.1016/j.jmb.2008.08.016

Karlsson, J., Saloheimo, M., Siika-aho, M., Tenkanen, M., Penttilä, M., & Tjerneld, F. (2001). Homologous expression and characterization of Cel61A (EG IV) of Trichoderma reesei. *Eur. J. Biochem*., *268* (24), 6498 – 6507. DOI: 10.1046/j.0014-2956.2001.02605.x

Kim, H. M., Jung, S., Lee, K. H., Song, Y., & Bae, H. (2015). Improving lignocellulose degradation using xylanase–cellulase fusion protein with a glycine–serine linker. *Int. J. Biol. Macromol*., *73*, 215 – 221. DOI: 10.1016/j.ijbiomac.2014.11.025

Kim, S., & Kim, C. H. (2012). Production of cellulase enzymes during the solid-state fermentation of empty palm fruit bunch fiber. *Bioprocess and Biosystem Engineering*, *35* (2012), 61 – 67. DOI: 10.1007/s00449-011-0595-y

Kim, T. W., Chokhawala, H. A., Nadler, D., Blanch, H. W., & Clark, D. S. (2010). Binding modules alter the activity of chimeric cellulases: Effects of biomass pretreatment and enzyme source. *Biotechnol. Bioeng*., *107*, 601 – 611. DOI: 10.1002/bit.22856

Ko, J. K., Kim, Y., Ximenes, E., & Ladisch, M. R. (2015). Effect of liquid hot water pretreatment severity on properties of hardwood lignin and enzymatic hydrolysis of cellulose. *Biotechnol. Bioeng*., *112* (2), 252 – 262. DOI: 10.1002/bit.25349

Koshland, D. E. (1953). Stereochemistry and the mechanism of enzymatic reactions. *Biol. Rev*., *28*, 416 – 436. DOI: 10.1111/j.1469-185X.1953.tb01386.x

Kumar, R., & Wyman, C. E. (2009). Effects of cellulase and xylanase enzymes on the deconstruction of solids from pretreatment of poplar by leading technologies. *Biotechnol. Prog*., *25* (2), 302 – 314. DOI: 10.1002/btpr.102

Lahtinen, M., Kruus, K., Boer, H., Kemell, M., Andberg, M., Viikari, L., & Sipilä, J. (2009). The effect of lignin model compound structure on the rate of oxidation catalyzed by two different fungal laccases. *J. Mol. Catal. B Enzym*., *57*, 204 – 210. DOI: 10.1016/j.molcatb.2008.09.004

Lee, H. L., Chang, C. K., Jeng, W. Y., Wang, A. H. J., & Liang, P. H. (2012). Mutations in the substrate entrance region of β-glucosidase from Trichoderma reesei improve enzyme activity and thermostability. *Protein Eng. Des. Sel*., *25* (11), 733 – 740. DOI: 10.1093/protein/gzs073

Luo, X., Liu, J., Zheng, P., Li, M., Zhou, Y., Huang, L., … Shuai, L. (2019). Promoting enzymatic hydrolysis of lignocellulosic biomass by inexpensive soy protein. *Biotechnol. Biofuels*, *12*, 51. DOI: 10.1186/s13068-019-1387-x

Luterbacher, J. S., Walker, L. P., & Moran-Mirabal, J. M. (2013). Observing and modeling BMCC degradation by commercial cellulase cocktails with fluorescently labeled Trichoderma reseii Cel7A through confocal microscopy. *Biotechnol. Bioeng*., *110* (1), 108 – 117. DOI: 10.1002/bit.24597

Magalhães da Silva, S.P., da Costa Lopes, A.M., Roseiro, L.B., & Bogel-Łukasik, R. (2013). Novel pre-treatment and fractionation method for lignocellulosic biomass using ionic liquids. *RSC Advances*, *3* (36), 16040 – 16050. DOI: 10.1039/c3ra43091j

Manavalan, T., Manavalan, A., & Heese, K. (2015). Characterization of lignocellulolytic enzymes from white-rot fungi. *Curr. Microbiol*., *70*, 485 – 498. DOI: 10.1007/s00284-014-0743-0

Meyer, M. W., Lupoi, J. S., & Smith, E. A. (2011). 1064nm dispersive multichannel Raman spectroscopy for the analysis of plant lignin. *Anal. Chim. Acta*, *706* (1), 164 – 170. DOI: 10.1016/j.aca.2011.08.031

Moilanen, U., Kellock, M., Galkin, S., & Viikari, L. (2011). The laccase-catalyzed modification of lignin for enzymatic hydrolysis. *Enzyme Microb. Technol*., *49* (6 – 7), 492 – 498. DOI: 10.1016/j.enzmictec.2011.09.012

Moraïs, S., Barak, Y., Lamed, R., Wilson, D. B., Xu, Q., Himmel, M. E., & Bayer, E. A. (2012). Paradigmatic status of an endo- and exoglucanase and its effect on crystalline cellulose degradation. *Biotechnol. Biofuels*, *5* (1), 78. DOI: 10.1186/1754-6834-5-78

Müller, G., Várnai, A., Johansen, K. S., Eijsink, V. G. H., & Horn, S. J. (2015). Harnessing the potential of LPMO-containing cellulase cocktails poses new demands on processing conditions. *Biotechnol. Biofuels*, *8*, 187. DOI: 10.1186/s13068-015-0376-y

Naika, G. S., & Tiku, P. K. (2011). Influence of ethylenediaminetetraacetic acid (EDTA) on the structural stability of endoglucanase from Aspergillus aculeatus. *J. Agric. Food Chem.*, *59* (13), 7341 – 7345. DOI: 10.1021/jf103889m

Nakashima, K., Endo, K., Shibasaki-kitakawa, N., & Yonemoto, T. (2014). A fusion enzyme consisting of bacterial expansin and endoglucanase for the degradation of highly crystalline cellulose. *RSC Adv*., *4* (83), 43815 – 43820. DOI: 10.1039/c4ra05891g

Nakatani, Y., Yamada, R., Ogino, C., & Kondo, A. (2013). Synergetic effect of yeast cell-surface expression of cellulase and expansin-like protein on direct ethanol production from cellulose. *Microb. Cell Fact*., *12*, 66. DOI: 10.1186/1475-2859-12-66

Nam, K. H., Sung, M. W., & Hwang, K. Y. (2010). Structural insights into the substrate recognition properties of β-glucosidase. *Biochem. Biophys. Res. Commun*., *391*, 1131 – 1135. DOI: 10.1016/j.bbrc.2009.12.038

Navya, P. N., Bhoite, R. N., & Murthy, P. S. (2012). Bioconversion of coffee husk cellulose and statistical optimization of process for production of exoglucanase by rhizopus stolonifer. *World Appl. Sci. J*., *20* (6), 781 – 789. DOI: 10.5829/idosi.wasj.2012.20.06.6689

Obeng, E. M., Adam, S. N. N., Budiman, C., Ongkudon, C. M., Maas, R., & Jose, J. (2017). Lignocellulases: A review of emerging and developing enzymes, systems, and practices. Bioresour. *Bioprocess*, *4*, 16. DOI: 10.1186/s40643-017-0146-8

Pala, H., Mota, M., & Gama, F. M. (2007). Enzymatic depolymerisation of cellulose. *Carbohydr. Polym*., *68* (1), 101 – 108. DOI: 10.1016/j.carbpol.2006.07.015

Pandiyan, K., Tiwari, R., Rana, S., Arora, A., Singh, S., Saxena, A. K., & Nain, L. (2014). Comparative efficiency of different pretreatment methods on enzymatic digestibility of *Parthenium* sp. *World J. Microbiol. Biotechnol*., *30*, 55 – 64. DOI: 10.1007/s11274-013-1422-1

Parisutham, V., Kim, T. H., & Lee, S. K. (2014). Feasibilities of consolidated bioprocessing microbes: From pretreatment to biofuel production. *Bioresource Technology*, *161*, 431 – 440. DOI: 10.1016/j.biortech.2014.03.114

Park, S., Ransom, C., Mei, C., Sabzikar, R., Qi, C., Chundawat, S., … Sticklen, M. (2011). The quest for alternatives to microbial cellulase mix production: corn stover-produced heterologous multi-cellulases readily deconstruct lignocellulosic biomass into fermentable sugars. *J. Chem. Technol. Biotechnol.*, *86* (5), 633 – 641. DOI: 10.1002/jctb.2584

Peng, P., & She, D. (2014). Isolation, structural characterization, and potential applications of hemicelluloses from bamboo: A review. *Carbohydr. Polym*., *112*, 701 – 720. DOI: 10.1016/j.carbpol.2014.06.068

Quinlan, R. J., Sweeney, M. D., Lo Leggio, L., Otten, H., Poulsen, J. C. N., Johansen, K. S., … Walton, P. H. (2011). Insights into the oxidative degradation of cellulose by a copper metalloenzyme that exploits biomass components. Proc. Natl. Acad. Sci., 108, 15079 – 15084. DOI: 10.1073/pnas.1105776108

Rajasree, K. P., Mathew, G. M., Pandey, A., & Sukumaran, R. K. (2013). Highly glucose tolerant β-glucosidase from Aspergillus unguis: NII 08123 for enhanced hydrolysis of biomass. *J. Ind. Microbiol. Biotechnol*., *40* (9), 967 – 975. DOI: 10.1007/s10295-013-1291-5

Ramawat, G. K., & Mérillon, J. M. (Eds.). (2015). *Polysaccharides: Bioactivity and biotechnology*. Switzerland, AG: Springer, Cham. DOI: 10.1007/978-3-319-16298-0

Ratanakhanokchai, K., Kyu, K. L., & Tanticharoen, M. (1999). Purification and properties of a xylan-binding endoxylanase from Alkaliphilic bacillus sp. strain K-1. *Appl. Environ. Microbiol*., *65* (2), 694 – 697.

Ribeiro, L. F., Furtado, G. P., Lourenzoni, M. R., Costa-Filho, A. J., Santos, C. R., Peixoto Nogueira, S. C., … Ward, R. J. (2011). Engineering bifunctional laccase-xylanase chimeras for improved catalytic performance. *J. Biol. Chem*., *286* (50), 43026 – 43038. DOI: 10.1074/jbc.M111.253419

Riou, C., Salmon, J. M., Vallier, M. J., Günata, Z., & Barre, P. (1998). Purification, characterization, and substrate specificity of a novel highly glucose-tolerant beta-glucosidase from Aspergillus oryzae. *Appl. Environ. Microbiol*., *64*, 3607 – 3614.

Rocha-Martín, J., Martinez-Bernal, C., Pérez-Cobas, Y., Reyes-Sosa, F. M., & García, B. D. (2017). Additives enhancing enzymatic hydrolysis of lignocellulosic biomass. *Bioresour. Technol*., *244* (1), 48 – 56. DOI: 10.1016/j.biortech.2017.06.132

Rubin, E. M. (2008). Genomics of cellulosic biofuels. *Nature*, *454* (7206), 841 – 845. DOI: 10.1038/nature07190

Segato, F., Damásio, A. R. L., de Lucas, R. C., Squina, F. M., & Prade, R. A. (2014). Genome analyses highlight the different biological roles of cellulases. *Microbiol. Mol. Biol. Rev*., *78*, 588 – 613. DOI: 10.1128/MMBR.00019-14

Seki, Y., Kikuchi, Y., Kimura, Y., Yoshimoto, R., Takahashi, M., Aburai, K., … Sakaguchi, K. (2015). Enhancement of cellulose degradation by cattle saliva. *PLoS One*, *10* (9), e0138902. DOI: 10.1371/journal.pone.0138902

Shallom, D., & Shoham, Y. (2003). Microbial hemicellulases. *Curr. Opin. Microbiol*., *6* (3), 219 – 228. DOI: 10.1016/S1369-5274(03)00056-0

Suplatov, D., Panin, N., Kirilin, E., Shcherbakova, T., & Kudryavtsev, P. (2014). Computational design of a pH stable enzyme: Understanding molecular mechanism of penicillin acylase's adaptation to alkaline conditions. *PLoS One*, *9* (6), e100643. DOI: 10.1371/journal.pone.0100643

Tu, M., Zhang, X., Paice, M., Mcfarlane, P., & Saddler, J. N. (2009). Effect of surfactants on separate hydrolysis fermentation and simultaneous saccharification fermentation of pretreated lodgepole pine. *Biotechnol. Prog*., *25*, 1122 – 1129. DOI: 10.1021/bp.19

U.S. DOE Office of Science. (2014). *Making cellulose more accessible for bioconversion*. Retrieved from https://science.osti.gov/ber/Highlights/2014/BER-2014-07-p

Vaaje-Kolstad, G., Westereng, B., Horn, S. J., Liu, Z., Zhai, H., Sorlie, M., & Eijsink, V. G. H. (2010). An oxidative enzyme boosting the enzymatic conversion of recalcitrant polysaccharides. *Science*, *330* (6001), 219 – 222. DOI: 10.1126/science.1192231

Van Dyk, J. S., & Pletschke, B. I. (2012). A review of lignocellulose bioconversion using enzymatic hydrolysis and synergistic cooperation between enzymes-Factors affecting enzymes, conversion and synergy. *Biotechnol. Adv*., *30* (6), 1458 – 1480. DOI: 10.1016/j.biotechadv.2012.03.002

Vassilev, S. V., Baxter, D., Andersen, L. K., & Vassileva, C. G. (2010). An overview of the chemical composition of biomass. *Fuel*, *89* (5), 913 – 933. DOI: 10.1016/j.fuel.2009.10.022

Wahlström, R., Rahikainen, J., Kruus, K., & Suurnäkki, A. (2014). Cellulose hydrolysis and binding with Trichoderma reesei Cel5A and Cel7A and their core domains in ionic liquid solutions. *Biotechnol. Bioeng*., *111* (4), 726 – 733. DOI: 10.1002/bit.25144

Walton, P. H., & Davies, G. J. (2016). On the catalytic mechanisms of lytic polysaccharide monooxygenases. *Curr. Opin. Chem. Biol*., *31*, 195 – 207. DOI: 10.1016/j.cbpa.2016.04.001

Wan, C., & Li, Y. (2012). Fungal pretreatment of lignocellulosic biomass. *Biotechnol. Adv*., *30* (6), 1447 – 1457. DOI: 10.1016/j.biotechadv.2012.03.003

Wang, H., Kobayashi, S., & Mochidzuki, K. (2015). Effect of non-enzymatic proteins on enzymatic hydrolysis and simultaneous saccharification and fermentation of different lignocellulosic materials. *Bioresour. Technol.*, *190*, 373 – 380. DOI: 10.1016/j.biortech.2015.04.112

Wang, Z., Bay, H., Chew, K., & Geng, A. (2014). High-loading oil palm empty fruit bunch saccharification using cellulases from Trichoderma koningii MF6. *Process Biochem.*, *49*, 673 – 680. DOI: 10.1016/j.procbio.2014.01.024

Warren, J. C., & Cheatum, S. G. (1966). Effect of neutral salts on enzyme activity and structure. *Biochemistry*, *5* (5), 1702 – 1707. DOI: 10.1021/bi00869a036

Westereng, B., Cannella, D., Wittrup Agger, J., Jørgensen, H., Larsen Andersen, M., Eijsink, V. G. H., & Felby, C. (2015). Enzymatic cellulose oxidation is linked to lignin by long-range electron transfer. *Sci. Rep.*, *5*, 18561. DOI: 10.1038/srep18561

Wilson, D. B. (2009). Cellulases and biofuels. *Curr. Opin. Biotechnol.*, *20* (3), 295 – 299. DOI: 10.1016/j.copbio.2009.05.007

Wilson, D. B. (2015). Processive cellulases. In M. E. Himmel (Ed.), *Direct microbial conversion of biomass to advanced biofuels* (pp. 83 – 89). Amsterdam; Oxford; Waltham: Elsevier B.V. DOI: 10.1016/B978-0-444-59592-8.00005-1

Yang, B., & Wyman, C. E. (2013). Lignin blockers and uses thereof. US Patents. Retrieved from https://patents.google.com/patent/US8580541B2/en

Zechel, D. L., & Withers, S. G. (2000). Glycosidase mechanisms: Anatomy of a finely tuned catalyst. *Acc. Chem. Res.*, *33* (1), 11 – 18. DOI: 10.1021/ar970172+

Zhang, Y. H. P., & Lynd, L. R. (2004). Toward an aggregated understanding of enzymatic hydrolysis of cellulose: Noncomplexed cellulase systems. *Biotechnol. Bioeng.*, *88*, 797 – 824. DOI: 10.1002/bit.20282

Borneo International Journal of Biotechnology (BIJB)
Vol. 1 (December 2020), 19 – 33

e-ISSN 2716-697X

A GLANCE AT MOLECULAR IDENTIFICATION OF BAMBOO (*Poaceae: Bambusoideae*)

Nabilah Mohamad Khairi[1], Wilson Thau Lym Yong[1*], Julius Kulip[2], Kenneth Francis Rodrigues[1]

[1]Biotechnology Research Institute, Universiti Malaysia Sabah, Kota Kinabalu, Sabah, Malaysia
[2]Institute for Tropical Biology and Conservation, Universiti Malaysia Sabah, Kota Kinabalu, Sabah, Malaysia
*Corresponding author's email: wilsonyg@ums.edu.my

Received date: 27 October 2020 | Accepted date: 16 November 2020

ABSTRACT

Conservation of plant species plays a vital role in preventing the loss of valuable plant resources. The success of conservation depends on the correct identification and characterization of plant species. Bamboo is one of the most important plants with multiple uses that have contributed to the economy and socio-economy of many people in rural areas. It is under the subfamily of Bambusoideae that includes both woody and herbaceous bamboo. Conventionally, like other plants, bamboo has been classified dependently based on morphological characteristics. However, morphological identification leads to difficulties and misclassification of bamboo species due to their infrequent flowering behaviour and peculiar reproductive biology. Since then, molecular markers have been introduced to overcome the problems associated with bamboo taxonomy and phylogeny. This paper provides an overview of the diverse, predominantly molecular techniques used to assess and determine the genetic diversity of bamboo species.

Keywords: amplified fragment length polymorphism, DNA barcoding, random amplified polymorphic DNA, restriction fragment length polymorphism, sequence characterized amplified region, simple sequence repeat

INTRODUCTION

Bamboo is a plant member of the grass family known as Poaceae and constitutes a single subfamily Bambusoideae. The Bambusoideae subfamily consists of both herbaceous or Olyreae tribe and woody bamboos or the Bambuseae tribe (Ram, Thiruvengadam, & Vinod, 2007). Bamboo comprises approximately 1,290 species, which are naturally distributed worldwide (Hamzah, Hakeem, & Ibrahim, 2016). There is a rich abundance of bamboo species in the Asia-Pacific and South America (Bystriakova, Kapos, Lysenko, & Stapleton, 2003; Das, Bhattacharya, Singh, Filgueiras, & Pal, 2008). The species are mainly classified into three major categories: the pleiotropic woody bamboo, neotropical woody bamboo, and north temperate woody bamboo. The wide variety of species makes bamboo adaptable to many environments and is highly palatable to humans, domestic animals, and wildlife.

Bamboo has emerged as a prospective crop with over 1,500 diversified applications worldwide, ranging from medications to nutrient supplies and from producing toys to aircraft. It is considered the world's best material because of its high tensile strength compared to teak wood and mild steel. It may be a valuable resource for energy because of its fast growth rate (5 – 7 years to mature) and potential fuel characteristics (Bystriakova et al., 2003). The combination of fast-growing, natural vegetative propagation and their adequacy for making several products makes bamboo ideal for various industrial applications to replace other perennials and woody plants (Bonilla, Guarnetti, Almeida, & Giannetti, 2010; Hamzah et al., 2016). The traditional phenotypic approach for identifying bamboo species, however, is very complicated, leading to controversy over the classification based on their peculiar vegetative process and flowering characteristics (Isagi et al., 2004; Ramakrishnan et al., 2020; Sharma et al., 2008). These morphological features are often affected by the environment and are complicated, state-specific, and limited in number, contributing to the misclassification of bamboo at the genus and species level (Wu, 1962; Yeasmin, Ali, Gantait, & Chakraborty, 2015). It is, therefore, essential to have a reliable and precise taxonomic classification and nomenclature system for bamboo to be able to identify and select the best species for growing in the right environment for a purpose that is well suited to it.

TRADITIONAL IDENTIFICATION OF BAMBOO SPECIES

The identification of bamboo is traditionally based on its morphological characteristics, including rhizomes, buds, leaves, branching patterns, inflorescence, flowers, and fruits. This approach has been problematic because there are limited and peculiar morphological characters in bamboo, particularly its flowers, and the flowering period

may vary between 15 – 120 years, and some species have never known to flower (Janzen, 1976). Although traditional taxonomy depends heavily on inflorescence and floral morphology, Usui (1957) revealed the importance of branch and bud characters, and McClure (1973) studied the morphology of the rhizome, branching patterns, and culm sheath for bamboo species identification. Soderstrom and Ellis (1988) also considered leaf morphology characters for subfamilial and subtribal level identification, but they failed to apply it at the generic level.

Vegetative characters are often influenced by the environment, making them less constant for systematic purposes (Yeasmin et al., 2015). Various studies have misclassified bamboo species into different taxonomic groups by considering the morphological features that have not been resolved to date. It is not always easy, for example, to define the inflorescence types in bamboos, and in many cases, several conflicting interpretations have been noticed. Chao and Renvoize (1989) recognized the inflorescence of *Racemobambos* as 'iterauctant', while Dransfield (1992) described it as 'semelauctant'. For its allied genus *Neomicrocalamus*, related confusion has also been observed (Dransfield, 1992; Stapleton, 1994). Furthermore, basic knowledge of bamboo biology and genetics is still severely lacking. Since morphological identification has not proven successful, there is an urgent need to implement alternative techniques to recognize the taxonomic complexities of bamboo.

DNA FINGERPRINTING IN BAMBOOS

The use of molecular markers has increased in many branches and subdisciplines of biology as an alternative method for identifying DNA polymorphisms between individuals, studying genetic diversity, and analyzing the genetic distance between species. Determining the appropriate taxonomic level at which it is most informative and correlating it with morphological taxonomic grouping is the major challenge for molecular markers. The application of molecular techniques for studying genetic diversity in bamboo, however, has still been limited to date. The present study aims to review different molecular tools currently used to assess genetic diversity and infer phylogenetic relationships in the bamboos.

Several generations of molecular markers have become increasingly reliable in the past decades. DNA products such as isozymes and secondary compounds, including phenolics, were initially used to explore the phylogenetic relationship between taxa and assess infraspecific polymorphism for species identification (Alam, Sarker, & Hassan, 1997; Biswas, 1998; Chou & Hwang, 1985; Pattanaik & Hall, 2011). Later on, the focus of the research was on variation in the DNA structure, providing two different types of data, namely restriction fragment data (DNA fingerprinting) and gene sequence data (DNA barcoding). In previous phylogenetic analyses of temperate bamboos, especially *Phyllostachys* and *bambusa*, molecular markers based

on restriction fragment length polymorphism (RFLP), random amplified polymorphic DNA (RAPD), amplified fragment length polymorphism (AFLP), and simple sequence repeat (SSR) were used (Table 1; Barkley, Newman, Wang, Hotchkiss, & Pederson, 2005; Das, Bhattacharya, Basak, & Pal, 2007; Friar & Kochert, 1994; Kobayashi, 1997). More recently, DNA sequences have also been used to deduce bamboo phylogenetic relationships, but only limited sequence variations were found in the genes studied (Attigala, Wysocki, Duvall, & Clark, 2016; Hodkinson, Renvoize, Chonghaile, Stapleton, & Chase, 2000; Ma, Zhang, Zeng, Guo, & Li, 2014; Zhang, 2000).

Table 1 Molecular techniques for classification of bamboo species

Techniques*	Species tested	References
RFLP	*Phyllostachys* spp.	Friar and Kochert (1994)
RAPD	*Bambusa* spp. *Cephalostachyum pergracil* *Chimonobambusa* spp. *Dendrocalamus* spp. *Dinocloa m'Clellandi* *Gigantochloa atroviolacea* *Neosinocalamus affini* *Phyllostachy* spp. *Pseudobambusa kurzii* *Qiongzhuca tumidinoda* *Sasa* sp. *Yushania* sp.	Biradar et al. (2005) Das et al. (2007) Nayak et al. (2003) Zhang et al. (2011)
AFLP	*Bambusa* spp. *Chimonobambusa marmorea* *Dendrocalamus* spp. *Gigantochloa* spp. *Neomicmlamus andropcgonifolius* *Phyllostachys* spp. *Shibataea chinensis* *Sinobambusa tootsik* *Thyrsostachys siamensis*	Hodkinson et al. (2000) Loh et al. (2000)
SCAR	*Bambusa* spp.	Das et al. (2005)
ISSR	*Bambusa* spp. *Dendrocalamus* spp. *Melocanna baccifera* *Oxytenanthera nigrociliata* *Phyllostachys* spp. *Pleioblastus* spp. *Sasa auricoma* *Schizostachyum pergracile* *Thyrsostachys oliveri*	Lin et al. (2010) Mukherjee et al. (2010) Nilkanta et al. (2017) Tian et al. (2012) Yang et al. (2012)

EST-SSR	*Arundinaria* spp. *Bambusa* spp. *Brachystachyum densiflorum* *Dendrocalamus* spp. *Hibanobambusa tranquillans* *Indocalamus* spp. *Melocanna baccifera* *Ochlandra* spp. *Phyllostachys* spp. *Pseudosasa* spp. *Sasa* spp. *Semiarundinaria fastuosa* *Shibataea* spp. *Sinobambusa* spp.	Barkley et al. (2005) Cai et al. (2019) Sharma et al. (2008)

*RFLP = Restriction fragment length polymorphism; RAPD = Random amplified polymorphism DNA; AFLP = Amplified fragment length polymorphism; SCAR = Sequence characterized amplified region; ISSR = Inter-simple sequence repeat; EST-SSR = Expressed sequence tag-simple sequence repeat

Restriction Fragment Length Polymorphism (RFLP)

Friar and Kochert (1994) were the first researchers to use RFLP to identify 61 accessions and 20 species of the genus *Phyllostachys*. RFLP is a polymorphism that results from sequence variation in the genomic DNA recognized by restriction enzymes. The earlier findings of the presence of two distinct sections (*Phyllostachys* and *Heteroclada*) in the *Phyllostachys* species pool were confirmed by RFLP analysis. However, the analysis disagreed with a previous study on putting *Phyllostachys nigra* under the section of *Heteroclada* (Wang et al., 1980). Due to the requirements of a large amount of DNA along with the use of radioactive isotopes, the routine use of RFLP in plant genotyping as well as in bamboo has been limited.

Random Amplified Polymorphism DNA (RAPD)

The RAPD markers are the most straightforward, fastest, and easiest assay to assess the genetic diversity and variation between populations and within them (Kumari & Pande, 2010). The technique has been successfully employed in determining genetic relationships in various plant species. Nayak, Rout, and Das (2003) assessed the genetic variability using RAPD markers in twelve bamboo species and found a wide range of variability among them with ten random primers. Subsequent cluster analysis showed that the twelve taxa belonging to different bamboo genera formed two major clusters based on similarity indices and three minor clusters from each of the major clusters. In

a separate study using 80 random primers on the clones of *Dendrocalamus strictus* and *Bambusa bambos*, a total of 42 and 32 RAPD markers produced polymorphic patterns in *D. strictus* and *B. bambos*, respectively (Biradar, Patil, Kuruvinashetti, Biradar, Patil, & Yaradoni, 2005). Das et al. (2007) showed a phylogenetic relationship between 15 bamboo species using 32 key morphological descriptors and 120 polymorphic loci of the genomic DNA generated by the RAPD primers. The dendrogram and principal component analysis revealed that their phylogenetic relationships were consistent with the commonly referred bamboo classification system. Still, discriminatory was shown by the cluster pattern generated from the similarity matrix of the key morphological characters. More recently, Zhang, Yang, and Liu (2011) had conducted the RAPD analysis using chloroplast DNA of 22 bamboo species to assess the polymorphisms, similarities, and relationships between them. These studies concluded that molecular evidence based on RAPD markers needs to be accompanied by morphological characteristics to confirm the relationships between taxa.

Amplified Fragment Length Polymorphism (AFLP)

The AFLP method involving a combination of restriction digestion and PCR amplification was first developed by Vos et al. (1995) and employed by Loh, Kiew, Set, Gan, and Gan (2000) to identify bamboo species and determine their genetic relationships. The study was carried out using a combination of eight primers on 15 bamboo species belonging to four genera in the subtribe Bambusinae. The results showed that the species were divided into different clusters based on 13 unique banding patterns. Molecular markers of AFLP were also used to compare *Phyllostachys* species (Hodkinson et al., 2000), *Bambusa* species, and their closely related genera (Loh et al., 2000) for phylogenetic analysis. Compared with RAPD, the use of AFLP and RFLP techniques can produce more polymorphic fragments (bands). However, AFLP is often more expensive, time-consuming, complicated in interpretation, and technically demanding than other alternatives.

Sequence Characterized Amplified Region (SCAR)

With higher annealing temperatures, SCAR has been developed as an extension of the RAPD analysis with better reproducibility (Paran & Michelmore, 1993). Later on, two species-specific SCAR markers have been developed for *Bambusa balcooa* and *Bambusa tulda*, the two commercially important species for plantations, to aid the paper and pulp industry in the accurate species diagnosis, especially when key morphological features are indistinguishable during the seedling stage (Das, Bhattacharya, & Pal, 2005). Specifically, the markers were developed from the Bb836

and Bt609 sequences of the respective species, using primers from both flanking ends of the RAPD primers. They successfully amplified the DNA of individuals representing both *B. balcooa* and *B. tulda* species. The findings concluded that the two molecular markers were particularly useful for the regulatory establishment of sovereign rights of the *B. balcooa* and *B. tulda* germplasms.

Inter-Simple Sequence Repeat (ISSR)

The molecular markers of ISSR have been used to identify the genetic diversity of many plant species, including bamboos. Due to their more extended primer sequence and higher annealing temperature, ISSR markers are more efficient and reliable than RAPD, resulting in higher stringency (Tikendra, Amom, & Nongdam, 2019). They have reportedly been used to determine genetic variation and the relationship between various bamboos, including *Phyllostachys* (Lin et al., 2010), *Dendrocalamus* (Tian, Yang, Wong, Liu, & Ruan, 2012; Yang, An, Gu & Tian, 2012), and *Melocanna* (Nilkanta, Amom, Tikendra, Rahaman, & Nongdam, 2017). Lin et al. (2010) crossbred two species of *Phyllostachys* and successfully identified three hybrids produced by the cross with eight ISSR primers. Furthermore, 25 ISSR markers were used by Mukherjee et al. (2010) to investigate genetic diversity among 22 bamboo taxa, of which 12 resulted in reproducible and scorable bands.

Expressed Sequence Tag-Simple Sequence Repeat (EST-SSR)

Combining different molecular markers in identifying the genetic diversity among the population species has also been carried out. Barkley et al. (2005) used 25 EST-SSR markers derived from cereal crops including maize, wheat, sorghum, and rice in evaluating the genetic diversity of 92 bamboos classified under 11 genera and 44 species to find out which markers produced well-resolved polymorphic bands. Considering that grass genomes have co-evolved and share large-scale synteny, Sharma et al. (2008) tested 98 rice SSR primers and 20 sugarcane EST-SSR primers on 23 bamboo species. They reported 44 rice and 15 sugarcane SSR primers for transferability to at least one species of bamboo. More recently, Cai et al. (2019) have developed abundant EST-SSR resources from Lei bamboo transcriptome data useful for genetic diversity analysis and molecular verification of bamboo, suggesting that the markers are more effective and reliable than ISSR and other alternatives.

DNA BARCODING IN BAMBOOS

As reviewed in this section, DNA barcoding or sequence-based methods for phylogenetic analysis on bamboo and grass have been recorded in several studies to date. DNA barcoding is a way of identifying species based on a short sequence of DNA that varies from species to species but is conserved within species (Hebert, Cywinska, Ball, & deWaard, 2003). Two plastid gene regions, *rbcL* and *matK*, were selected as the core DNA barcodes for all land plants (CBOL Plant Working Group 1 et al., 2009). These plastid regions, which played an essential role in the phylogenetic reconstruction of land plants, were used because of their strong phylogenetic signals in both *rbcL* and *matK* (Chase et al., 1993). In previous studies, for both *rbcL* and *matK* barcodes, the success rate of generic and species-level identification was around 70%. With a supplementary marker, the identification success improved to 98%.

Besides, Kress, Wurdack, Zimmer, Weigt, & Janzen (2005) also proposed the nuclear internal transcribed spacer region and plastid *trnH-psbA* intergenic spacer as potentially usable DNA barcodes for flowering plants. In their study, the two plastid genomes of tobacco and deadly nightshade (belladonna) were compared with closely related species in seven plant families and a group of species collected from a local flora comprising 50 plant families, suggesting that the sequences in this pair of loci have the potential to discriminate between the largest number of plant species for barcoding purposes. Although mitochondrial DNA barcoding is well developed in animals using *COI* regions, mitochondrial DNA, however, has low substitution rates and rapidly changing gene content and structure, making it unsuitable for barcoding in plants (Sinha, Kumari, & Singh, 2012).

Chloroplast DNA Barcode

The chloroplast genome has long been used to assess the phylogeny of the grass family and resolve systematic problems at the subfamilial and tribal levels (Hilu & Johnson, 1991). Nadot, Bajon, and Lejeune (1994) used the chloroplast *rps4* gene to construct a phylogenetic tree comprising 28 Poaceae species and resolve the position of Bambusoids with other groups to demonstrate how rice and bamboo were closely related. Meanwhile, the chloroplast *ndhF* gene was also used to address phylogenetic relationships between 45 grass (i.e. the ingroup) and two outgroup taxa (Clark, Zhang, & Wendel, 1995). The analysis resulted in the two neotropical herbaceous bamboo tribes, the Streptochaeteae and Anomochloeae, being resolved as the most basal clade within the family, conforming to the primitive features of their unique inflorescences and spikelets. Other researchers also used chloroplast genes, such as *matK* and *rbcL*, to establish the phylogeny of Poaceae at the subfamilial and tribal levels and study glass systematics and evolution (Cai, Zhang, Zhang, Gao, & Li, 2012; Hilu, Alice, & Liang, 1999; Liang & Hilu, 1996; Yang et al., 2008). Based on a more recent comparative

analysis using 6.7 kb of coding and noncoding sequence data and 37 microstructural characters from the chloroplast genome, four main lineages, i.e., temperate woody, paleotropical woody, neotropical woody, and herbaceous bamboos, were recognized in a phylogeny estimation of bamboo tribes and subtribes (Kelchner & Bamboo Phylogeny Group, 2013).

Nuclear DNA Barcode

In most cases, nuclear DNA barcodes, mainly ITS regions, were used in conjunction with chloroplast DNA for barcoding plants, including bamboo species. Yang et al. (2008) employed the nuclear ITS and GBSSI gene apart from chloroplast *trnL-F* DNA sequences to establish a phylogenetic framework of the paleotropical woody bamboos involving 53 species and 17 genera. Using four woody bamboos of the North Temperate Zone as outgroups, the analysis revealed that the ingroup species clustered into three clades: the Bambusinae clade (including *Thyrsostachys*, *Neosinocalamus*, *Racemobambos*, *Molecalamus*, *Dendrocalamopsis*, *Bambusa*, *Gigantochloa*, *Oxytenanthera* s. str., *Dendrocalamus*, *Bonia* and *Neomicrocalamus*), the Dinochloa clade, and the Melocanninae clade (including *Pseudostachyum*, *Leptocanna*, *Cephalostachyum*, *Melocanna* and *Schizostachyum* s. str.); and further grouped into two monophyletic clades, i.e., the Bambusinae + Dinochloa clade and the Melocanninae clade. Moreover, Cai et al. (2012) suggested that the discriminatory power of the species was substantially enhanced as the nuclear ITS region integrated with a single or combination of plastid markers. Although the ITS alone could identify up to 66.7% of the examined Bambusoideae taxa, combining ITS and chloroplast *rbcL* could exhibit the highest species identification power and serve as a potential DNA barcode for temperate woody bamboos.

Multilocus DNA Barcoding

A combined analysis of multi-gene regions is often useful for improving phylogenetic resolution and support in plant taxonomy. Qiang et al. (2005) compared the genus *Arundinaria* with other related genera, such as *Pleioblastus*, *Pseudosasa*, *Oligostachyum*, *Bashania*, and *Clavinodum*, to determine their phylogenetic relationships by using the nuclear ITS and chloroplast *trnL-F* intergenic spacer. Sungkaew, Stapleton, Salamin, and Hodkinson (2009) reported phylogenetic groupings within Bambusoideae and resolved several previously unrecognized and poorly supported phylogenetic patterns using five chloroplast DNA regions, *trnL* intron, *trnL-F* intergenic spacer, *atpB-rbcL* intergenic spacer, *rps16* intron, and *matK*. Cai et al. (2012) analyzed four barcoding markers, namely *matK, rbcL, trnH-psbA*, and ITS, in species identification of temperate woody bamboos (Bambusoideae) and recommended *rbcL* + ITS as a potential barcode region for species discrimination. Furthermore, Sosa, Mejía-

Saules, Cuéllar, and Vovides (2013) created a DNA barcode library with some leading candidate plastid DNA regions, i.e. *matK*, *rbcL*, and *psbI-K* spacer, as an essential tool for phytosanitary authorities to classify species belonging to groups that command high horticultural trade prices in Mexico. Their study showed that the *psbI-K* spacer retrieved more polymorphic sites in bamboos and suggested *matK* + *psbI-K* as the discriminant barcode loci to identify temperate bamboos to at least their generic level. Lately, in the absence of discriminatory features at the juvenile stage, multiple sequence alignment of *psbA-trnH* barcode has been used to certify planting materials, such as micropropagated plantlets, rhizome transplants, and culm cuttings, of the commercial bamboo species (including *Bambusa*, *Dendrocalamus*, *Melocanna*, *Oxytenanthera*, and *Ochlandra*) in bamboo nurseries in India (Dev, Sijimol, Prathibha, Sreekumar, & Muralidharan, 2020).

CONCLUSION

The bamboo taxonomy is currently in a state of flux, and more phylogenetic studies are required to help resolve the remaining systematic issues. In this paper, we reviewed the availability of numerous molecular-level methods and techniques for achieving bamboo species identification and how the barcoding markers help to provide insights into species-level taxonomy in bamboos. While morphological taxonomy still plays a crucial role in the classification of various bamboo species, molecular markers are undoubtedly valuable tools for addressing phylogenetic questions in the easily confused or cryptic species and can assist traditional approaches in making the identification process more rapid and effective. The availability of the bamboo genome database (http://www.bamboogdb.org/) in the post-genomic era will provide global researchers with a key genomic resource and an extensible analytical platform to better understand the bamboo genome and thus promote future studies based on previous achievements, especially in advanced analysis of phylogenetic and genetic diversity in bamboos.

ACKNOWLEDGEMENTS

This work was supported by the Universiti Malaysia Sabah under a Niche Research Grant Scheme (DN20091). The authors would like to thank the Biotechnology Research Institute for providing the research platform to conduct the review.

REFERENCES

Alam, M. K., Sarker, R. H., & Hassan, M. A. (1997). Chemotaxonomic studies in peroxidase isozyme of bamboos from Bangladesh. *Bangladesh Journal of Botany*, *26*, 99 – 105.

Attigala, L., Wysocki, W. P., Duvall, M. R., & Clark, L. G. (2016). Phylogenetic estimation and morphological evolution of Arundinarieae (Bambusoideae: Poaceae) based on plastome phylogenomic analysis. *Molecular Phylogenetics and Evolution*, *101*, 111 – 121. DOI: https://doi.org/10.1016/j.ympev.2016.05.008

Barkley, N. A., Newman, M. L., Wang, M. L., Hotchkiss, M. W., & Pederson, G. A. (2005). Assessment of the genetic diversity and phylogenetic relationships of a temperate bamboo collection by using transferred EST-SSR markers. *Genome*, *48* (4), 731 – 737. DOI: https://doi.org/10.1139/g05-022

Biradar, D. P., Patil, V. C., Kuruvinashetti, M. S., Biradar, M. D., Patil, S. V., & Yaradoni, S. N. (2005). Characterization of bamboo elite clones from Western ghats of India using RAPD markers. In *Proceedings of the role of biotechnology* (pp. 155 – 156). Villa Gualino, Turin, Italy.

Biswas, S. (1998). Contribution to the isozyme studies on Indian bamboo, *Dendrocalamus strictus* (Roxb.) Nees with emphasis on diversity evaluation. *Annals of Forestry*, *5* (22), 168 – 172.

Bonilla, S. H., Guarnetti, R. L., Almeida, C. M. V. B., & Giannetti, B. F. (2010). Sustainability assessment of a giant bamboo plantation in Brazil: Exploring the influence of labour, time and space. *Journal of Cleaner Production*, *18* (1), 83 – 91.

Bystriakova, N., Kapos, V., Lysenko, I., & Stapleton, C. M. A. (2003). Distribution and conservation status of forest bamboo biodiversity in the Asia-Pacific Region. *Biodiversity & Conservation*, *12*, 1833 – 1841. DOI: https://doi.org/10.1023/A:1024139813651

Cai, K., Zhu, L., Zhang, K., Li, L., Zhao, Z., Zeng, W., & Lin, X. (2019). Development and characterization of EST-SSR markers from RNA-Seq data in *Phyllostachys violascens*. *Frontiers in Plant Science*, *10*, 50. DOI: https://doi.org/10.3389/fpls.2019.00050

Cai, Z. M., Zhang, Y. X., Zhang, L. N., Gao, L. M., & Li, D. Z. (2012). Testing four candidate barcoding markers in temperate woody bamboos (Poaceae: Bambusoideae). *Journal of Systematics and Evolution*, *50* (6), 527 – 539. DOI: https://doi.org/10.1111/j.1759-6831.2012.00216.x

CBOL Plant Working Group 1, Hollingsworth, P. M., Forrest, L. L., Spouge, J. L., Hajibabaei, M., Ratnasingham, … Little, D. P. (2009). A DNA barcode for land plants. *Proceedings of the National Academy of Sciences*, *106* (31), 12794 – 12797. DOI: https://doi.org/10.1073/pnas.0905845106

Chao, C. S., & Renvoize, S. A. (1989). A revision of the species described under *Arundinaria* (Gramineae) in Southeast Asia and Africa. *Kew Bulletin*, *44* (2), 349 – 367. DOI: https://doi.org/10.2307/4110809

Chase, M. W., Soltis, D. E., Olmstead, R. G., Morgan, D., Les, D. H., Mishler, B. D., … Albert, V. A. (1993). Phylogenetics of seed plants: an analysis of nucleotide sequences from the plastid gene *rbcL*. *Annals of the Missouri Botanical Garden*, *80* (3), 528 – 580. DOI: https://doi.org/10.2307/2399846

Chou, C. H., & Hwang, Y. H. (1985). A biochemical aspect of phylogenetic study of Bambusaceae in Taiwan III. The genera *Arthrostylidium*, *Chimonobambusa* and *Dendrocalamus*. *Botanical Bulletin of Academia Sinica*, *26* (22), 155 – 170.

Clark, L. G., Zhang, W., & Wendel, J. F. (1995). A phylogeny of the grass family (Poaceae) based on *ndhF* sequence data. *Systematic Botany*, *20* (4), 436 – 460. DOI: https://doi.org/10.2307/2419803

Das, M., Bhattacharya, S., & Pal, A. (2005). Generation and characterization of SCARs by cloning and sequencing of RAPD products: a strategy for species-specific marker development in bamboo. *Annals of Botany*, *95* (5), 835 – 841. DOI: https://doi.org/10.1093/aob/mci088

Das, M., Bhattacharya, S., Basak, J., & Pal, A. (2007). Phylogenetic relationships among the bamboo species as revealed by morphological characters and polymorphism analyses. *Biologia Plantarum*, *51* (4), 667 – 672.

Das, M., Bhattacharya, S., Singh, P., Filgueiras, T. S., & Pal, A. (2008). Bamboo taxonomy and diversity in the era of molecular markers. Advances in Botanical Research, 47, 225 – 268. DOI: https://doi.org/10.1016/S0065-2296(08)00005-0

Dev, S. A., Sijimol, K., Prathibha, P. S., Sreekumar, V. B., & Muralidharan, E. M. (2020). DNA barcoding as a valuable molecular tool for the certification of planting materials in bamboo. *3 Biotech*, *10*, 59. DOI: https://doi.org/10.1007/s13205-019-2018-8

Dransfield, S. (1992). A new species of *Racemobambos* (Gramineae: Bambusoideae) from Sulawesi with notes on generic delimitation. *Kew Bulletin*, *47* (4), 707 – 711. DOI: https://doi.org/10.2307/4110711

Friar, E., & Kochert, G. (1994). A study of genetic variation and evolution of *Phyllostachys* (Bambusoideae: Poaceae) using nuclear restriction fragment length polymorphisms. *Theoretical and Applied Genetics*, *89*, 265 – 270. DOI: https://doi.org/10.1007/BF00225152

Hamzah, T. N. T., Hakeem, K. R., & Ibrahim, F. H. (2016). Proteomics of bamboo, the fast-growing grass. In K. R. Hakeem, H. Tombuloğlu & G. Tombuloğlu (Eds.), *Plant omics: Trends and applications* (pp. 327 – 349. Cham: Springer International Publishing.

Hebert, P. D. N., Cywinska, A., Ball, S. L., & deWaard, J. R. (2003). Biological identifications through DNA barcodes. Proceedings of the Royal Society of London, Series B: Biological Sciences, *270* (1512), 313 – 321. DOI: https://doi.org/10.1098/rspb.2002.2218

Hilu, K. W., & Johnson, J. L. (1991). Chloroplast DNA reassociation and grass phylogeny. *Plant Systematics and Evolution*, *176*, 21 – 31. DOI: https://doi.org/10.1007/BF00937943

Hilu, K. W., Alice, L. A., & Liang, H. (1999). Phylogeny of Poaceae inferred from *matK* sequences. *Annals of the Missouri Botanical Garden*, *86* (4), 835 – 851. DOI: https://doi.org/10.2307/2666171

Hodkinson, T. R., Renvoize, S. A., Chonghaile, G. N., Stapleton, M. C. A., & Chase, M. W. (2000). A comparison of ITS nuclear rDNA sequence data and AFLP markers for phylogenetic studies in *Phyllostachys* (Bambusoideae, Poaceae). *Journal of Plant Research*, *113*, 259 – 269. DOI: https://doi.org/10.1007/PL00013936

Isagi, Y., Shimada, K., Kushima, H., Tanaka, N., Nagao, A., Ishikawa, T., ... Watanabe, S. (2004). Clonal structure and flowering traits of a bamboo [*Phyllostachys pubescens* (Mazel) Ohwi] stand grown from a simultaneous flowering as revealed by AFLP analysis. *Molecular Ecology*, *13* (7), 2017 – 2021. DOI: https://doi.org/10.1111/j.1365-294X.2004.02197.x

Janzen, D. H. (1976). Why bamboos wait so long to flower. *Annual Review of Ecology and Systematics*, *7*, 347 – 391. DOI: https://doi.org/10.1146/annurev.es.07.110176.002023

Kelchner, S. A., & Bamboo Phylogeny Group. (2013). Higher level phylogenetic relationships within the bamboos (Poaceae: Bambusoideae) based on five plastid markers. *Molecular Phylogenetics and Evolution*, *67* (2), 404 – 413. DOI: https://doi.org/10.1016/j.ympev.2013.02.005

Kobayashi, M. (1997). Phylogeny of world bamboos analysed by restriction fragment length polymorphisms of chloroplast DNA. In G. P. Chapman (Ed.), *The bamboos* (pp. 227 – 234). London: Linnean Society.

Kress, W. J., Wurdack, K. J., Zimmer, E. A., Weigt, L. A., & Janzen, D. H. (2005). Use of DNA barcodes to identify flowering plants. *Proceedings of the National Academy of Sciences*, *102* (23), 8369 – 8374. DOI: https://doi.org/10.1073/pnas.0503123102

Kumari, K., & Pande, A. (2010). Study of genetic diversity in finger millet (*Eleusine coracana* L. Gaertn) using RAPD markers. *African Journal of Biotechnology*, *9* (29), 4542 – 4549.

Liang, H., & Hilu, K. W. (1996). Application of the *matK* gene sequences to grass systematics. *Canadian Journal of Botany*, *74* (1), 125 – 134. DOI: https://doi.org/10.1139/b96-017

Lin, X. C., Lou, Y. F., Liu, J., Peng, J. S., Liao, G. L., & Fang, W. (2010). Crossbreeding of *Phyllostachys* species (Poaceae) and identification of their hybrids using ISSR markers. *Genetics and Molecular Research*, *9* (3), 1398 – 1404. DOI: 10.4238/vol9-3gmr855

Loh, J. P., Kiew, R., Set, O., Gan, L. H., & Gan, Y. Y. (2000). A study of genetic variation and relationships within the bamboo subtribe Bambusinae using amplified fragment length polymorphism. *Annals of Botany*, *85* (5), 607 – 612. DOI: https://doi.org/10.1006/anbo.2000.1109

Ma, P. F., Zhang, Y. X., Zeng, C. X., Guo, Z. H., & Li, D. Z. (2014). Chloroplast phylogenomic analyses resolve deep-level relationships of an intractable bamboo tribe Arundinarieae (Poaceae). *Systematic Biology*, *63* (6), 933 – 950. DOI: https://doi.org/10.1093/sysbio/syu054

McClure, F. A. (1973). *Genera of bamboos native to the new world (Gramineae: Bambusoideae)* (No. 9). T. R. Soderstrom (Ed.). Washington: Smithsonian Institution Press.

Mukherjee, A. K., Ratha, S., Dhar, S., Debata, A. K., Acharya, P. K., Mandal, S., … Mahapatra, A. K. (2010). Genetic relationships among 22 taxa of bamboo revealed by ISSR and EST-based random primers. *Biochemical Genetics*, *48*, 1015 – 1025. DOI: 10.1007/s10528-010-9390-8

Nadot, S., Bajon, R., & Lejeune, B. (1994). The chloroplast gene *rps4* as a tool for the study of Poaceae phylogeny. *Plant Systematics and Evolution*, *191*, 27 – 38. DOI: https://doi.org/10.1007/BF00985340

Nayak, S., Rout, G. R., & Das, P. (2003). Evaluation of the genetic variability in bamboo using RAPD markers. *Plant Soil and Environment*, *49* (10), 24 – 28.

Nilkanta, H., Amom, T., Tikendra, L., Rahaman, H., & Nongdam, P. (2017). ISSR marker based population genetic study of *Melocanna baccifera* (Roxb.) Kurz: a commercially important bamboo of Manipur, North-East India. *Scientifica*, *2017*, 3757238. DOI: https://doi.org/10.1155/2017/3757238

Paran, I., & Michelmore, R. W. (1993). Development of reliable PCR-based markers linked to downy mildew resistance genes in lettuce. *Theoretical and Applied Genetics*, *85*, 985 – 993. DOI: https://doi.org/10.1007/BF00215038

Pattanaik, S., & Hall, J. B. (2011). Molecular evidence for polyphyly in the woody bamboo genus *Dendrocalamus* (subtribe Bambusinae). *Plant Systematics and Evolution*, *291*, 59 – 67. DOI: https://doi.org/10.1007/s00606-010-0380-4

Qiang, Z., Yu-long, D., Chen, X., Hui-yu, Z., Ming-ren, H., & Ming-xiu, W. (2005). A preliminary analysis of phylogenetic relationships of *Arundinaria* and related genera based on nucleotide sequences of nrDNA (ITS region) and cpDNA (*trnL-F* intergenic spacer). *Journal of Forestry Research*, *16*, 5 – 8. DOI: https://doi.org/10.1007/BF02856844

Ram, S. G., Thiruvengadam, V., & Vinod, K. K. (2007). Genetic diversity among cultivars, landraces and wild relatives of rice as revealed by microsatellite markers. *Journal of Applied Genetics*, *48*, 337 – 345.

Ramakrishnan, M., Yrjälä, K., Vinod, K. K., Sharma, A., Cho, J., Sateesh, V., & Zhou, M. (2020). Genetics and genomics of moso bamboo (*Phyllostachys edulis*): Current status, future challenges, and biotechnological opportunities toward a sustainable bamboo industry. *Food and Energy Security*, *9* (4), e229. DOI: https://doi.org/10.1002/fes3.229

Sharma, R. K., Gupta, P., Sharma, V., Sood, A., Mohapatra, T., & Ahuja, T. S. (2008). Evaluation of rice and sugarcane SSR markers for phylogenetic and genetic diversity analyses in bamboo. *Genome*, *51* (2), 91 – 103. DOI: https://doi.org/10.1139/G07-101

Sinha, A., Kumari, K., & Singh, S. (2012). DNA barcoding for species identification in bamboos. *Forestry Bulletin*, *12* (2), 73 – 77.

Soderstrom, T. R., & Ellis, R. P. (1988). The woody bamboos (Poaceae: Bambuseae) of Sri Lanka: A morphological-anatomical study (Vol. 72). Washington: Smithsonian Institution Press.

Sosa, V., Mejía-Saules, T., Cuéllar, M. A., & Vovides, A. P. (2013). DNA barcoding in endangered Mesoamerican groups of plants. *The Botanical Review*, *79*, 469 – 482. DOI: 10.1007/s12229-013-9129-4

Stapleton, C. M. A. (1994). The bamboos of Nepal and Bhutan. Part III: *Drepanostachyum*, *Himalayacalamus*, *Ampelocalamus*, *Neomicrocalamus* and *Chimonobambusa* (Gramineae: Poaceae, Bambusoideae). *Edinburgh Journal of Botany*, *51* (3), 301 – 330.

Sungkaew, S., Stapleton, C. M. A., Salamin, N., & Hodkinson, T. R. (2009). Non-monophyly of the woody bamboos (Bambuseae; Poaceae): a multi-gene region phylogenetic analysis of Bambusoideae s.s. *Journal of Plant Research*, *122*, 95. DOI: https://doi.org/10.1007/s10265-008-0192-6

Tian, B., Yang, H. Q., Wong, K. M., Liu, A. Z., & Ruan, Z. Y. (2012). ISSR analysis shows low genetic diversity versus high genetic differentiation for giant bamboo, *Dendrocalamus giganteus* (Poaceae: Bambusoideae), in China populations. *Genetic Resources and Crop Evolution*, *59*, 901 – 908. DOI: https://doi.org/10.1007/s10722-011-9732-3

Tikendra, L., Amom, T., & Nongdam, P. (2019). Molecular genetic homogeneity assessment of micropropagated *Dendrobium moschatum* Sw. – A rare medicinal orchid, using RAPD and ISSR markers. *Plant Gene*, *19*, 100196. DOI: https://doi.org/10.1016/j.plgene.2019.100196

Usui, H. (1957). Morphological studies on the prophyll of Japanese bamboos. *Botanical Magazine Tokyo*, *70*, 223 – 227.

Vos, P., Hogers, R., Bleeker, M., Reijans, M., van de Lee, T., Hornes, M., … Zabeau, M.(1995). AFLP: A new technique for DNA fingerprinting. *Nucleic Acids Research*, *23* (21), 4407 – 4414. DOI: https://doi.org/10.1093/nar/23.21.4407

Wang, C. P., Yu, T. H., Ye, K. H., Chu, C. T., Chao, C. S., Chen, S. Y., … Chao, H. J. (1980). A taxonomical study of *Phyllostachys*, China (cont.). *Acta Phytotaxonomica Sinica*, *18* (1), 168 – 193.

Wu, M. C. Y. (1962). The classification of Bambuseae based on leaf anatomy. *Botanical Bulletin of Academia Sinica*, *3* (11), 83 – 107.

Yang, H. Q., An, M. Y., Gu, Z. J., & Tian, B. (2012). Genetic diversity and differentiation of *Dendrocalamus membranaceus* (Poaceae: Bambusoideae), a declining bamboo species in Yunnan, China, as based on inter-simple sequence repeat (ISSR) analysis. *International Journal of Molecular Sciences*, *13* (4), 4446 – 4457. https://doi.org/10.3390/ijms13044446

Yang, H. Q., Yang, J. B., Peng, Z. H., Gao, J., Yang, Y. M., Peng, S., & Li, Z. (2008). A molecular phylogenetic and fruit evolutionary analysis of the major groups of the paleotropical woody bamboos (Gramineae: Bambusoideae) based on nuclear ITS, GBSSI gene and plastid *trnL-F* DNA sequences. *Molecular Phylogenetics and Evolution*, *48* (3), 809 – 824. DOI: https://doi.org/10.1016/j.ympev.2008.06.001

Yeasmin, L., Ali, M. N., Gantait, S., & Chakraborty, S. (2015). Bamboo: an overview on its genetic diversity and characterization. *3 Biotech*, *5*, 1 – 11. DOI: https://doi.org/10.1007/s13205-014-0201-5

Zhang, H. Y., Yang, Y. M., & Liu, X. Z. (2011). Bamboo species relations revealed by random amplified polymorphism chloroplast DNA. *African Journal of Agricultural Research*, *6* (5), 1241 – 1245. DOI: https://doi.org/10.5897/AJAR10.794

Zhang, W. (2000). Phylogeny of the grass family (Poaceae) from *rpl16* intron sequence data. *Molecular Phylogenetics and Evolution*, *15* (1), 135 – 146. DOI: https://doi.org/10.1006/mpev.1999.0729

Borneo International Journal of Biotechnology (BIJB)
Vol. 1 (December 2020), 35 – 43

e-ISSN 2716-697X

Research Article

GENETIC DIVERSITY OF SABAH RICE CULTIVARS USING RANDOM AMPLIFIED POLYMORPHIC DNA (RAPD) MARKERS

Alvina Simon[1], Vijay Kumar Subbiah[1], Chee Fong Tyng[2] and Noor Hydayaty Md Yusuf[1*]

[1]Biotechnology Research Institute,
Universiti Malaysia Sabah, Kota Kinabalu, Sabah, Malaysia
[2]Faculty of Sustainable Agriculture,
Universiti Malaysia Sabah, Sandakan, Sabah, Malaysia
*Corresponding author's email: hydayaty@ums.edu.my
Received date: 30 September 2019 | Accepted date: 21 January 2020

ABSTRACT

Rice is the most important staple crop in Malaysia and is cultivated all over the country, including the state of Sabah. The uniqueness of rice cultivation in Sabah lies in the type of rice itself, deriving mainly from local or non-commercial cultivars but with distinctive characteristics including long grains, aromatic properties, and drought tolerance. However, despite having these important agricultural traits, information on the genetic diversity of Sabah rice remains limited. Hence, the purpose of this study was to determine the genetic polymorphisms of Sabah rice using random amplification of polymorphic DNA (RAPD) markers. A total of 101 alleles were profiled, from which 94% were identified as polymorphic. Phylogenetic analysis grouped the rice samples into three clusters, with two clusters classifying the ability of rice to grow under different planting conditions, suitable for growth irrigate and upland condition. The first cluster was dominated by cultivars that could survive in wet (irrigated) areas, while the other featured those that were found in dry (upland) areas. Furthermore, two alleles, OPA-05-B2 and OPA-01-B11, were found to be unique to cultivars within the upland cluster and were thus proposed to be involved in dry environmental adaptation. The results of the present study provide an insight into the genetic relationships and diversity of Sabah rice.

Keywords: rice, upland, irrigated, genetic diversity, RAPD

INTRODUCTION

Rice is a major staple food globally and is consumed by almost 70% of the world's population, especially in Asian countries (Delseny et al., 2001; Razak et al., 2016). According to the Food and Agriculture Organization of the United Nations (FAOSTAT), the total global rice production reached 984 million tons in 2017, higher than that of other staple crops such as potatoes and wheat with a total production of 906 million and 487 million, respectively.

To date, more than 120,000 rice accessions and wild relatives have been identified and deposited to the International Rice GeneBank by the International Rice Research Institute (IRRI). Rice cultivars have different genetic and biochemical properties, and this diversity enables various types of rice to be grown all over the world across different types of geographical area and climate. For example, *Oryza glaberrima* species are widely cultivated in Africa (Vaughan, Lu, & Tomooka, 2008) while *Oryza sativa* species are more versatile, with one subspecies (*Indica*) widely cultivated in temperate, low-latitude and -altitude regions and in warm climates in tropical and sub-tropical countries while the other subspecies (*Japonica*) grows in more temperate regions at high altitude and latitude under cooler climate conditions (Lal et al., 2013; Delseny et al., 2001).

To determine the type of rice for cultivation under different environmental conditions, rice has been categorised into different types including deep-water rice, irrigated rice, rain-feed lowland rice, and upland rice (Poehlman & Sleper, 1995). In Malaysia, a hot and humid climate with variations in rainfall trends often followed by a drier season necessitates that rice is cultivated using irrigation methods (Toriman & Mokhtar, 2012). Therefore, 85.5% of the total rice production in Malaysia is from the states of Peninsular Malaysia, which is dominated by lowland regions suitable for irrigation systems (Vaghefi, Shamsudin, Radam, & Rahim, 2016). In the states of Sabah, however, rice production is lower as the geographical topography with a hilly terrain is unsuitable for large scale cultivation using irrigation systems. Due to this, rice cultivation in Sabah has undertaken upland rice cultivation. However, since both irrigated and upland rice in Sabah is grown on a small scale, limited research has been carried out to profile its genetic diversity. In the present study, the genetic diversity of both irrigated and upland rice in Sabah, from the districts of Kota Belud and Tepulid, was investigated.

MATERIALS AND METHODS

Plant Materials

A total of 29 samples were collected from four cities in the districts of Kota Belud (Tenghilan and Kota Belud towns) and Telupid (Tongod and Telupid towns), including irrigated and upland areas. Samples were collected as peduncles and stored at −20°C until use.

Extraction of DNA from Rice Seeds

DNA was extracted from the rice seeds of all samples following the procedure of Kang, Cho, Yoon and Eun (1998) with modifications. Rice seeds were de-hulled and crushed using a mortar and pestle and DNA was extracted in a buffer [200 mM Tris-HCl (pH 8.0), 200 mM NaCl, 25 mM EDTA, and 0.5% SDS] with the addition of 50 mg of proteinase K. The samples were incubated at 37°C for 1 hour and an equal volume of chloroform was then added. DNA was precipitated from the sample by the addition of two thirds (2/3) of the volume of isopropanol. The DNA pellet was washed with 70% ethanol and suspended in sterilised MiliQ water. Ribonuclease A (RNase; 10 mg) was added to remove RNA from the samples. The quality of DNA was evaluated by gel electrophoresis, and the DNA samples were stored at −20°C until use.

PCR Amplification Using RAPD Markers

DNA extracted from rice samples was used as a template for PCR amplification using a set of 9 decamers of arbitrary oligonucleotide primers. Amplification reactions were carried out in a volume of 25 µl containing 1 × Promega GoTaq® Flexi Buffer, 2.5 mM of $MgCl_2$, 200 µM of each deoxynucleotide triphosphate (dNTP), 10 pmole of primer, 2.5 U of GoTaq® DNA polymerase, and 2 µg of bovine serum albumin (BSA). The PCR reaction protocol modified from Rabbani, Pervaiz, and Masood (2008) and consisted of 1 cycle of 4 minutes at 94°C for initial strand separation followed by 35 cycles of 1 minute at 94°C, 1 minute at 37°C, and 1 minute at 72°C. Finally, 1 cycle of 10 minutes at 72°C was used for the final extension. PCR amplification patterns were profiled based on bands produced following gel electrophoresis in a 2.0% agarose gel stained with ethidium bromide and visualised under UV light in a gel documentation system.

Data Analysis

The banding patterns of agarose gel electropherograms were scored using a binary scoring system where the presence of a band was recorded as "1" and the absence recorded as "0". Only clear bands that were consistently amplified were scored, whereas very faint bands were excluded to avoid false-positive results (REF). The similarity and distance matrices were generated using Nei's (1978) formula in POPGENE 1.31 software based on the shared bands (alleles). The resulting similarity and distance coefficients were subsequently used to evaluate the relationships between samples with a cluster analysis using an unweighted pair-group method with arithmetic averages (UPGMA) software. The POPGENE programme used to construct the dendrograms was an adaptation of the NEIGHBOR of PHYLIP programme, version 3.5c.

RESULTS AND DISCUSSION

Genetic Polymorphism in Sabah Rice

This study was conducted using 29 rice samples collected from two major cultivation area in Sabah, the Kota Belud and Telupid districts. Rice is generally categorised based on the environmental conditions of the cultivation site and can include deep-water rice, irrigated rice, rain-feed lowland rice, and upland rice (Poehlman & Sleper, 1995). In the present study, 24 samples were collected from irrigated paddy fields and grouped under eight cultivars, namely Baragang (4 samples), Pahu (3 samples), Pilit (2 samples), Purak (2 samples), Sarawak (2 samples), Sibor (5 samples), Silia (3 samples), and Sompug (3 samples). Furthermore, five samples were collected from upland fields and locally named as padi wangi (1 sample), upland-1 (1 sample), upland-2 (1 sample), purak-upland (1 sample), and telangkai (1-sample) cultivars. Different cultivars were represented by different numbers of samples, ranging from one to five, with each representative collected from different farms. The number of representatives for each cultivar was by the availability of the cultivars in the area of collection.

The genetic diversity of the study samples was profiled using 11 primers (OPA-01, OPA-02, OPA-03, OPA-05, OPF-09, OPF-17, OPF-19, OPK-12, OPG-17, OPG-18, and OPG-19), of which 2 primers (OPF-17 and OPF-19) showed no amplification in any sample while 9 primers (OPA-01, OPA-02, OPA-03, OPA-05, OPF-09, OPK-12, OPG-17, OPG-18, and OPG-19) showed clear and consistent amplification patterns. The number of alleles identified from each primer ranged from 8 to 17 (see Table 1).

Table 1 The total amplified alleles from nine RAPD markers in Sabah rice

RAPD markers (Name)	Number of alleles amplified
OPA-01	13
OPA-02	17
OPA-03	10
OPA-05	9
OPF-09	7
OPK-12	13
OPG-17	10
OPG-18	8
OPG-19	14
Total	101

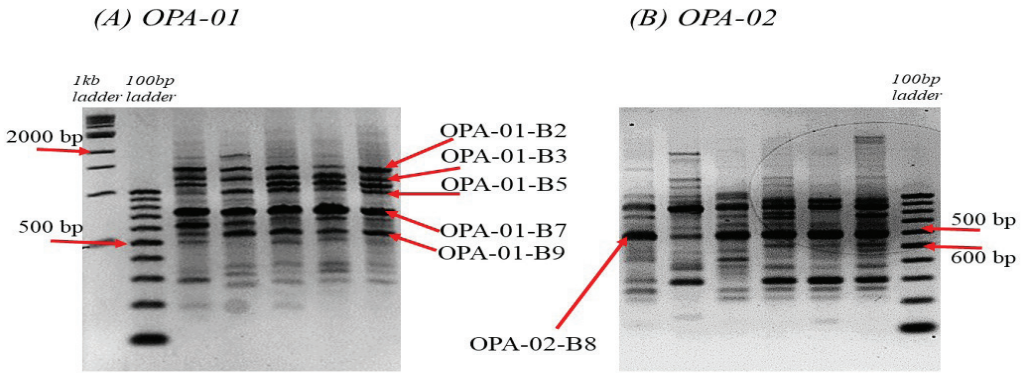

Figure 1 Monomorphic alleles found in all samples (irrigated and upland rice). Alleles OPA-01-B2, OPA-01-B3, OPA-01-B5, OPA-01-B7, OPA-01-B9 were amplified from RAPD marker OPA-01, while allele OPA-02-B8 was amplified from OPA-02.

Using RAPD markers, 101 alleles were identified, from which 94% were polymorphic. Only 6 alleles (out of 101) showed monomorphism, of which five were generated from primer OPA-01 (allele OPA-01-B2, -B3, -B5, -B7, and -B9) and one from OPA-02 (allele OPA-02-B8) (Figure 1). It is suggested that the monomorphic alleles identified in this study may represent beneficial alleles that become fixed during the rice domestication process in Sabah (Payseur & Nachman, 2002). Furthermore, the presence of these common alleles might be attributable to the continuous usage of same-genotype parents for cultivation purposes, which over time may narrow the genetic variation in Sabah rice, as is the case for rice cultivation in Brazil (Rabelo, Guimaraes, Pinheiro, & da Silva, 2015).

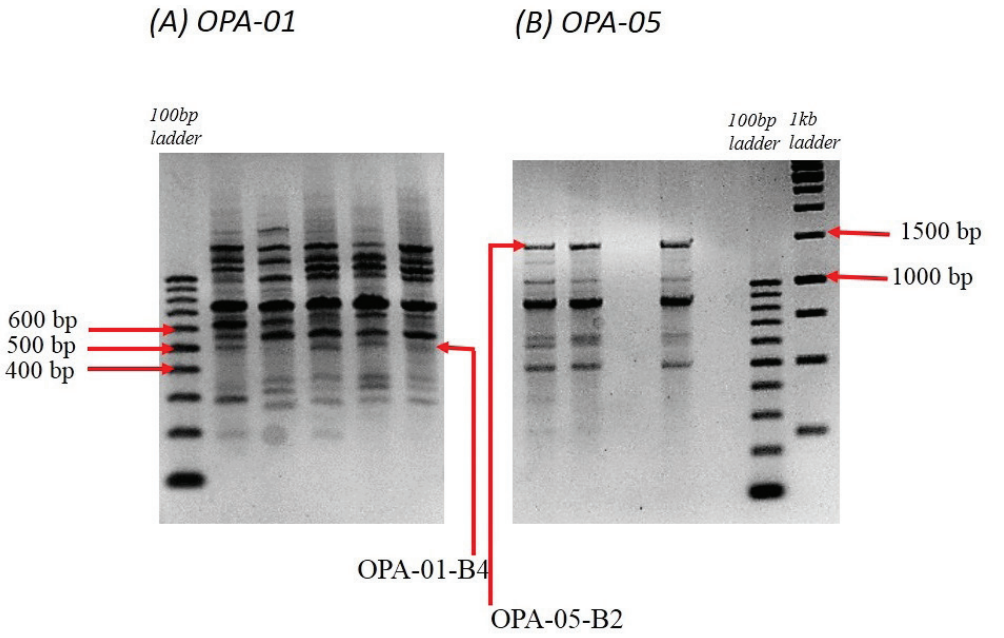

Figure 2 Two alleles unique to upland rice namely OPA-01-B11 and OPA-05-B2 unique to upland rice

RAPD marker analysis also revealed that several alleles were shared between rice cultivars collected from upland areas alone. These alleles were OPA-05-B2 (present in the upland-1, upland-2, and telangkai samples) and OPA-01-B11 (present in the padi wangi, upland-2, purak-upland, and telangkai samples) (Figure 2). Therefore, these alleles are postulated to be unique to upland rice and may be involved in adaptation (drought tolerance), enabling upland rice to survive in upland ecosystems that are exposed to a higher risk of drought (Zhou et al., 2016).

Genetic Diversity of Sabah Rice

In the cluster analysis, the 29 samples were grouped into three main clusters, Cluster I, II, and III (see Figure 3). Cluster I was dominated by samples collected from irrigated areas, as such 22 out of 24 samples were grouped under this cluster. Samples collected from upland areas were found scattered in Clusters II and III. As such, Cluster II comprised upland samples alone, while Cluster III was a mixture of upland and irrigated rice samples. The categorisation of upland and irrigated rice into three clusters was according to a study conducted by Coelho et al. (2017), whereby the genetic diversity of upland and irrigated Brazilian rice was found to be divided into three main clusters. As such, one cluster was formed by irrigated rice, one cluster by upland rice, and a third by a combination of upland and irrigated rice.

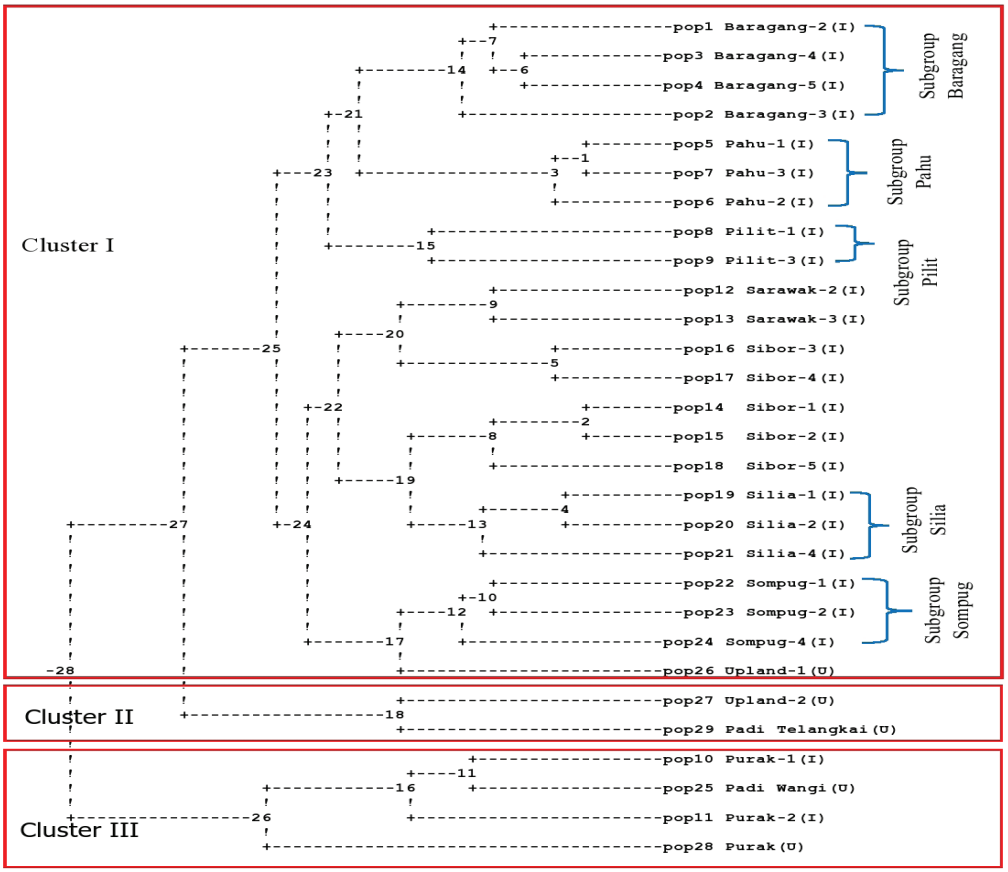

Figure 3 Dendogram based on UPGMA method consisting of 29 Sabah rice. Three boxes represent three cluster namely Cluster I (dominated by irrigated rice), Cluster II (consists of upland rice), and Cluster III (consists of both irrigated and upland rice). Five main subgroups were fund including the Baragang, Pahu, Pilit, Silia, and Sompug subgroup.

Some patterns of clusters indicate various genetic postulation of Sabah rice. As such, the separation between samples collected from irrigated areas into Cluster I and upland areas into Cluster II and III marks the genetic differences of rice of different types; that is, irrigated and upland rice. This separation indicates that Sabah rice may have a polyphyletic origin, whereby rice cultivars may have originated from more than one common ancestor (Wunna et al., 2016). Furthermore, since the clustering of samples in the study pointed towards separation based on cultivation area, the separation of irrigated rice in Cluster I against upland rice suggests that samples under this cluster are of the *Indica* subspecies or are of *Indica* origin. *Indica* rice is mainly cultivated in tropical and subtropical environments at lower latitudes or altitudes (Delseny et al., 2001), similar to the Kota Belud area from which most of the rice from Cluster I originated. Extending from observation, samples grouped under Cluster II and III,

which were dominated by rice collected from upland areas, may be categorised under the *Japonica* subspecies, which are mainly cultivated in more temperate environments at higher latitudes or altitudes (Delseny et al., 2001), similar to the Telupid area from which these samples were collected. Therefore, the distribution of different alleles between irrigated and upland rice cultivars maybe be associated with environment adaptation behaviour, especially with regards to response to drought and water stress conditions (Lyu et al., 2014; Wang, Zhang, Gao, Li, & Li, 2007).

The mixture of samples collected from irrigated and upland areas in Cluster II and III indicates genetic admixture in Sabah rice. Genetic admixture can occur when two or more genetically differentiated plants begin interbreeding, resulting in the introduction of a new genetic lineage (Wang et al., 2017), and may have occurred with the samples in the present study as they were cultivated together in the same area. A similar observation was reported in a study conducted in West Africa, whereby 67% of *Oryza glaberrima* were found to carry some level of admixture with *Oryza sativa* due to natural breeding between these two species, which are frequently grown together or in combination (Chen et al., 2017).

Another observation from this study is that the rice varieties of similar cultivars were clustered under the same subgroup. As such, five distinct subgroups were found, the Baragang, Pahu, Pilit, Silia, Sarawak and Sompug subgroups, indicating that members of these subgroups derive from a common ancestor.

CONCLUSIONS

The results obtained from this study provide additional insight into the genetic polymorphisms, genetic relationships, and diversity of Sabah rice, which has been limited to date. Although rice samples could be classified as irrigated or upland rice, future studies in a larger number of samples collected from the entire state of Sabah and using higher numbers of RAPD markers may obtain more precise information on the genetic polymorphisms and diversity of Sabah rice.

REFERENCES

Chen, C., He, W., Nassirou, T. Y., Nsabiyumva, A., Dong, X., Adedze, Y. M. N., & Jin, D. (2017). Molecular characterization and genetic diversity of different genotypes of *Oryza sativa* and *Oryza glaberrima*. *Electronic Journal of Biotechnology*, *30*, 48 – 57.

Coelho, G. R. C., Brondani, C., Hoffmann, L. V., Valdisser, P. A. M. R., Borba, T. C. R., Mendonca, J. A., … de Menezes, I. P. P. (2017). Genetic diversity of high-performance cultivars of upland and irrigated Brazilian rice. *Genetics and Molecular Research*, *16* (3), 1 – 11.

Delseny, M., Salses, J., Cooke, R., Sallaud, C., Regad, F., Lagoda, P., … Ghesquière, A. (2001). Rice genomics: present and future. *Plant Physiology and Biochemistry*, *39* (3), 323 – 334.

Kang, H. W., Cho, Y. G., Yoon, U. H., & Eun, M. Y. (1998). A rapid DNA extraction method for RFLP and PCR analysis from a single dry seed. *Plant Molecular Biology Reporter*, *16*, 1 – 9.

Lal, B., Nayak, A. K., Gautam, P., Tripathi, R., Singh, T., & Katara, J. (2013). Aerobic rice: A water saving approach for rice production. *Popular Kheti*, *1* (2), 1 – 4.

Lyu, J., Li, B., He, W., Zhang, S., Gou, Z., Zhang, J., … Wang, W. (2014). A genomic perspective on the important genetic mechanisms of upland adaptation of rice. *BMC Plant Biology*, *14*, 1 – 16.

Nei, M. (1978). Estimation of average heterozygosity and genetic distance from a small number of individuals. *Genetics*, *89* (3), 583 – 590.

Payseur, B. A., & Nachman, M. W. (2002). Gene density and human nucleotide polymorphism. *Molecular Biology and Evolution*, *19* (3), 336 – 340.

Poehlman, J., & Sleper, D. (Eds.). (1995). *Breeding field crops*. Oxford, UK: Blackwell Publishing.

Rabbani, M. A., Pervaiz, Z. H., & Masood, M. S. (2008). Genetic diversity analysis of traditional rice cultivars of Pakistani rice (*Oryza sativa* L.) using RAPD markers. *Electronic Journal of Biotechnology*, *11* (3), 1 – 10.

Rabelo, H. O., Guimaraes, J. F. R., Pinheiro, J. B., & da Silva, E. F. (2015). Genetic base of Brazilian irrigated rice cultivars. *Crop Breeding and Applied Biotechnology*, *15* (3), 146 – 153.

Razak, S. Ab., Ismail, S. N., Jaafar, A., Yusof, M. F., Kamaruzaman, R., Rahman, S. N. Ab., … Abdullah, N. (2016). Genetic diversity of Malaysian rice landraces based on single nucleotide polymorphism (SNP) markers. *Int. J. Pure App. Biosci.*, *4* (1), 28 – 34. DOI: http://dx.doi.org/10.18782/2320-7051.2194

Toriman, M. E., & Mokhtar, M. (2012). Irrigation: Types, sources and problems in Malaysia. In S. L. Teang (Ed.), *Irrigation systems and practices in challenging environments* (pp. 361 – 370). Rijeka, Crotia: InTech.

Vaghefi, N., Shamsudin, M. N., Radam, A., & Rahim, K. A. 2016. Impact of climate change on food security in Malaysia: Economic and policy adjustments for rice industry. *Journal of Integrative Environmental Sciences*, *13* (1), 19 – 35.

Vaughan, D. A., Lu, B. R., & Tomooka, N. (2008). Was Asian rice (*Oryza sativa*) domesticated more than once. *Rice*, *1*, 16 – 24.

Wang, H., Zhang, H., Gao, F., Li, J., & Li, Z. (2007). Comparison of gene expression between upland and lowland rice cultivars under water stress using cDNA microarray. *Theoretical and Applied Genetics*, *115* (8), 1109 – 1113.

Wang, W. K., Ho, C. W., Hung, K. H., Wang, K. H., Huang, C. C., Araki, H., … Chiang, T. Y. (2017). Multilocus analysis of genetic divergence between outcrossing Arabidopsis species: Evidence of genome-wide admixture. *New Pathologist*, *188* (2), 488 – 500.

Wunna, Watanabe, K. N., Ohsawa, R., Obara, M., Yanagihara, S., Aung, P. P., & Fukuta, Y. (2016). Genetic variation of rice (*Oryza sativa* L.) germplasm in Myanmar based on genomic compositions of DNA markers. *Breeding Science*, *66* (5), 762 – 767.

Zhou, L., Liu, Z., Liu, Y., Kong, D., Li, T., Yu, S., … Luo, L. (2016). A novel gene OsAHL1 improves both drought avoidance and drought tolerance in rice. *Scientific Reports*, *6*, 1 – 15.

Borneo International Journal of Biotechnology (BIJB)
Vol. 1 (December 2020), 45 – 54

e-ISSN 2716-697X

Research Article

SEPARATION OF REBAUDIOSIDE A FROM *Stevia rebaudiana* EXTRACT USING LOW POLARITY RESIN AB-8

Chong Saw Peng*, Norazlina Noordin, Mustapha Akil and Norellia Bahari

Agrotechnology and Bioscience Division, Malaysian Nuclear Agency (Nuclear Malaysia), Ministry of Energy, Science, Technology, Environment and Climate Change (MESTECC), Bangi, Selangor, Malaysia
*Corresponding author's email: sawpeng@nm.gov.my
Received date: 23 November 2018 | Accepted date: 9 August 2019

ABSTRACT

There are many methods to separate or purify the rebaudioside A compound from *Stevia rebaudiana* extract. However, the ion-exchange chromatography using macroporous resin is still the most popular among those methods. The separation of rebaudioside A from stevia crude extract by macroporous resin AB-8 was optimised in this adsorption separation study. This approach was applied to evaluate the influence of four factors such as the adsorption temperature, desorption time, elution solution ratio, and adsorption volume on rebaudioside A yield of the purified stevia extract. The results showed that the low polarity resin AB-8 is able to separate rebaudioside A from stevia extract with 0.601 in yield compared to the high polarity resin HPD 600 with 0.204 in yield used in Anvari and Khayati study. The best conditions for rebaudioside A separation by macroporous resin AB-8 were at 35°C of adsorption temperature, 30 min of desorption time, elution solution ratio 2:1, and 50 mL of adsorption volume.

Keywords: sweetener, *Stevia rebaudiana*, rebaudioside A, Steviol glycoside, adsorption separation method, macroporous resin

INTRODUCTION

Stevia rebaudiana Bertoni from Asteraceae family is a natural non-caloric sweetener native to Paraguay. This natural sweetener contains 11 main steviol glycosides which give the sweet taste in stevia included stevioside, rebaudioside A to F, rubusoside, steviolmonoside, steviolbioside, and dulcoside A (Geuns, 2003). The chemical structures of stevioside and rebaudioside A are very similar to each other but they showed some differences in sweetness (Wheeler et al., 2008). Stevioside tastes about 150 – 300 times sweeter than sucrose and rebaudioside A tastes about 200 – 400 times sweeter than sucrose. In addition, rebaudioside A has the bitter after taste. Meanwhile, stevioside has no bitterness (Geuns, 2003).

Rebaudioside A and stevioside are the major compounds in steviol glycosides, both of the compounds added up to more than 75% of the total steviol glycosides in stevia extract. Moreover, rebaudioside A has the best quality for sweetness amongst the other steviol glycosides, close to that of glucose (Chatsudthipong & Muanprasat, 2009). Therefore, rebaudioside A is considered to be the major component in stevia, and the demand for rebaudioside A is increasing in the stevia industry.

In the previous study, a few methods have been reported to extract rebaudioside A from *S. rebaudiana* (Zhang, Chen, Shi, & He, 1998; Liu, Li, Xu, & Zhou, 2007). Among all these methods, the adsorption separation technique using macroporous adsorption resin is a relatively new and popular separation method used for rebaudioside A at present. Since this macroporous resin has a special selectivity and good stability, some more low cost and easy regeneration which attracted the industry to use this method in rebaudioside A separation (Babic, Van der Ham, & De Haan, 2006; Liu et al., 2006).

From the previous study, the macroporous resin type HPD 400 and HPD 600 used for the separation of rebaudioside A has previously been studied by Anvari and Khayati (2016). Both resin type HPD 400 and HPD 600 are middle and strong polarity resin, respectively. Based on the results found from the study, the resin HPD 600 has a lower adsorption capacity for rebaudioside A compared to HPD 400. This is because rebaudioside A has higher polar hydrocarbon molecules, therefore, the low polar resin has shown better adsorption capacity than high polar resin for rebaudioside A (Anvari & Khayati, 2016). In this study, resin type AB-8 with low polarity was used to optimise the factors such as desorption time, adsorption volume, elution ratio, and adsorption temperature that affected the efficiency of rebaudioside A separation.

MATERIAL AND METHODS

Materials

New *S. rebaudiana* variety S10A produced through mutation breeding using gamma irradiation in Malaysian Nuclear Agency was planted by Duta Nusajaya Sdn. Bhd. in Penampang, Sabah, Malaysia. The leaves were harvested, washed, and dried at 40°C for 24 h then stored at room temperature. The macroporous resin AB-8 was used in the experiment and its physical properties as listed in Table 1. The resins were pre-treated by dipping them in ethanol for 48 h, then washing with ultrapure water thoroughly to remove the monomers and porogenic agents trapped inside the pores during the synthesis process.

Table 1 Physical properties of the macroporous resin

Resin type	Functional group	Average pore (nm)	Particle diameter (mm)	Polarity
HPD 600	Acylamino polystyrene	7.1	0.3 – 1.25	High polarity
HPD 400	Polydivinyl benzene acrylic ester	8.3	0.3 – 1.20	Middle polarity
AB-8	Polystyrene	13 – 14	0.3 – 1.25	Low polarity

Preparation of Crude Sample

Approximately 40 g of the *S. rebaudiana* leaves were extracted three times, with 1 h for each time in 4 L of boiling water, and all of the clear extracts were combined. The extracts were evaporated in a heating mantle boiler at 100°C to achieve the final volume of 2 L. The concentrated raw solution was used as the feed in all the following experiments.

Experimental Design

Taguchi experimental method with L16 array was used to optimise the separation of steviol glycoside (Sorana & Lorentz, 2007). The factors included desorption time, adsorption volume, elution solution ratio, and adsorption temperature were studied. The experimental factors are given in Table 2. For each experimental trial, the rebaudioside A yield was determined.

Adsorption/Desorption Experiments

The extraction process was conducted on stevia variant produced by Malaysian Nuclear Agency. Different volumes of crude extract solution were added into 5 g of macroporous resin in separate screwed cap bottle and shook in an incubator shaker for 4 h at 35, 40, 45, and 50°C. After that, the resins were washed 5 times with ultrapure water, then desorbed it in 100 mL ethanol-ethyl acetate solution at 30, 60, 90, and 120 min in the incubation shaker (Table 2). Finally, the desorption solution was evaporated and dried in an oven at 100°C to constant weight. All the experiments were carried out in triplicate.

Table 2 L16 array experimental design and the results of rebaudioside A yield

Sample no.	Factor levels				Average rebaudioside A yield
	Adso. temp (°C)	Deso. time (min)	Elu. ratio	Adso. vol. (mL)	
1	35	30	1	50	0.601
2	35	60	2	100	0.711
3	35	90	3	150	0.579
4	35	120	4	200	0.438
5	40	30	2	150	0.595
6	40	60	1	200	0.507
7	40	90	4	50	0.715
8	40	120	3	100	0.661
9	45	30	3	200	0.484
10	45	60	4	150	0.580
11	45	90	1	100	0.645
12	45	120	2	50	0.687
13	50	30	4	100	0.650
14	50	60	3	50	0.667
15	50	90	2	200	0.489
16	50	120	1	150	0.574

The initial concentration of the solution was 1.3 mg/ml.

Analysis of Samples

The amount of rebaudioside A in each sample was analyzed using high-performance liquid chromatography (HPLC). The sample was diluted in 70% (v/v) ethanol-water solution. The rebaudioside A standard was purchased from Sigma-Aldrich and used in this experiment.

$$\text{Rebaudioside A yield (µg/mL)} = \frac{\text{rebaudioside A (purified extract)}}{\text{rebaudioside A (present in the feed)}}$$

RESULTS AND DISCUSSION

The results showed rebaudioside A yield in the range from 0.438 – 0.715 (µg/mL)/(µg/mL) corresponding to the four factors (Table 2). Tables 3 – 6 showed the effects of each factor, which determined the contributions of individual variables on the rebaudioside A yield. Measurement averages were made at the level of each factor.

Table 3 Adsorption temperature effect on the rebaudioside A yield

Sample no.	Adso. temp (°C)	Yield [ug/ug]	Average yield [ug/ug]
1	35	0.601	0.582
2	35	0.711	
3	35	0.579	
4	35	0.438	
5	40	0.595	0.620
6	40	0.507	
7	40	0.715	
8	40	0.661	
9	45	0.484	0.599
10	45	0.580	
11	45	0.645	
12	45	0.687	
13	50	0.650	0.595
14	50	0.667	
15	50	0.489	
16	50	0.574	

Table 4 Desorption time effect on the rebaudioside A yield

Sample no.	Deso. time (min)	Yield [ug/ug]	Average yield [ug/ug]
1	30	0.601	0.583
5	30	0.595	
9	30	0.484	
13	30	0.650	
2	60	0.711	0.616
6	60	0.507	
10	60	0.580	
14	60	0.667	
3	90	0.579	0.607
7	90	0.715	
11	90	0.645	
15	90	0.489	
4	120	0.438	0.590
8	120	0.661	
12	120	0.687	
16	120	0.574	

Table 5 Elution solution ratio effect on the rebaudioside A yield

Sample no.	Elu. ratio	Yield [ug/ug]	Average yield [ug/ug]
1	1:1	0.601	0.582
6	1:1	0.507	
11	1:1	0.645	
16	1:1	0.574	
2	2:1	0.711	0.621
5	2:1	0.595	
12	2:1	0.687	
15	2:1	0.489	
3	3:1	0.579	0.598
8	3:1	0.661	
9	3:1	0.484	
14	3:1	0.667	
4	4:1	0.438	0.596
7	4:1	0.715	
10	4:1	0.580	
13	4:1	0.650	

Table 6 Adsorption volume effect on the rebaudioside A yield

Sample no.	Adso. vol. (mL)	Yield [ug/ug]	Average yield [ug/ug]
1	50	0.601	0.668
7	50	0.715	
12	50	0.687	
14	50	0.667	
2	100	0.711	0.667
8	100	0.661	
11	100	0.645	
13	100	0.650	
3	150	0.579	0.582
5	150	0.595	
10	150	0.580	
16	150	0.574	
4	200	0.438	0.480
6	200	0.507	
9	200	0.484	
15	200	0.489	

The study of adsorption temperatures on the separation of rebaudioside A found that the yield was slightly increased when the adsorption temperature increased from 35°C to 40°C but decreased with the increased of adsorption temperature above 40°C (Table 3). This is because of the macroporous resin adsorption process was an exothermic process. In this experiment, any increasing of temperature more than 40°C was adverse to adsorption (Fu, Shen, & Yao, 1990). The desorption time effect on rebaudioside A yield is shown in Table 4. It showed that rebaudioside A yield increased with the addition of desorption time from 30 min to 60 min and achieved the highest yield at 60 min then started to decrease after 60 min. The results showed an extended time beyond 60 min only caused a reduction in the yield.

The results of elution solution ratios showed no significant differences between the ratios. However, the highest rebaudioside A reading, 0.621 (µg/mL)/(µg/mL) was obtained at the ratio 2:1 (Table 5). A decreased in yield was obtained when the elution solvent ratio was extending the optimum level. This is because macroporous resins did not swell completely in the high ethanol contained a desorption solution. According to the experiment, the increase of elution ratio will cause the increase of ethanol in desorption solution, which made the adsorbed rebaudioside A not easily desorbed from macroporous resins. Table 6 showed the correlation between rebaudioside A yield and adsorption volume. The yield of rebaudioside A decreased with the increase

of adsorption volume. It is probably due to the macroporous resin had a different affinity toward stevia solution. The resin becomes saturated at the volume of 50 to 100 mL, further increase of the adsorption volume caused a significant reduction in yield.

The analysis of variance for the experiment is shown in Table 7. The degree of significance of each factor was represented by its *P*-value. A significance level of 0.05 indicates a 5% risk of concluding that a difference exists when there is no actual difference. In this study, the adsorption volume factor has a *P*-value of less than 0.05. It means the differences between some of the means are statistically significant. However, the other factors showed no significant differences between the means with *P*-value greater than 0.05. The results showed that all factors included adsorption temperature, desorption time and elution solution ratio except adsorption volume were no significant.

Table 7 Analysis of variance of the parameters for the rebaudioside A separation experiment

Source	D.F.	Sum of square	Mean square	*F*-value	*P*-value
Adsorption temperature (°C)	3	0.002	0.001	0.1606	0.9199
Residual error	8	0.036	0.005	–	–
Total	11	0.038			
Desorption time (min)	3	0.002	0.001	0.3563	0.7862
Residual error	8	0.015	0.002	–	–
Total	11	0.018			
Elution solution ratio	3	0.002	0.001	0.4267	0.7394
Residual error	8	0.015	0.002	–	–
Total	11	0.017			
Adsorption volume (mL)	3	0.072	0.024	10.0386	0.0044
Residual error	8	0.019	0.002	–	–
Total	11	0.091			

Based on the results from these four factors, we can determine that the adsorption temperature at 35°C, desorption time at 30 min, elution solution ratio at 2:1 and adsorption volume of 50 ml stevia extract for every 5 g of resin used were the best conditions optimised in this study. Under the optimised conditions, the low polarity resin AB-8 is more efficient to separate rebaudioside A from stevia extract compared

to the high polarity resin HPD 600 used in Anvari and Khayati (2016) study. The rebaudioside A yields were 0.601 and 0.204 in resin AB-8 and HPD 600 respectively. Two of the *S. rebaudiana* marker compounds, rebaudioside A and stevioside were detected and identified in the HPLC chromatogram with comparison to the standard rebaudioside A and stevioside (Figure 1). We ensure that the adsorption separation technique using macroporous resin AB-8 can be applied to separate the rebaudioside A and stevioside from *S. rebaudiana*.

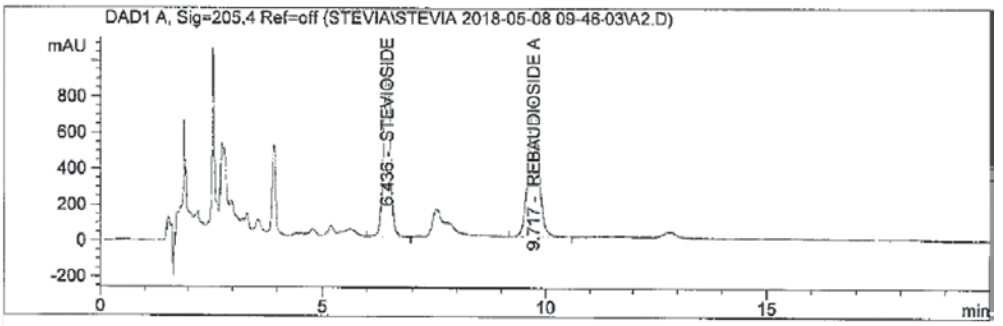

Figure 1 Two of the major marker compounds for *S. rebaudiana*, the rebaudioside A and stevioside were detected in the purified stevia extract in HPLC analysis

CONCLUSIONS

The adsorption separation process of rebaudioside A with macroporous adsorption resin AB-8 was studied and optimised in this work. A low polarity resin AB-8 was used to replace the high polarity resin in this study to see the affinity of steviol glycosides towards different polarity resin. The optimised separation process will be used as the reference for the establishment of a pilot-scale extraction plant for stevia.

ACKNOWLEDGEMENTS

This research was partially supported by research fund (Technofund TF0614D122) granted by the Ministry of Energy, Science, Technology, Environment and Climate Change (MESTECC), Malaysia. We thank our industry collaborator, Duta Nusajaya Sdn. Bhd. for providing the stevia S10A raw material for the experiment.

REFERENCES

Anvari, M., & Khayati, G. (2016). Separation and purification of rebaudioside A from extract of *Stevia Rebaudiana* leaves by macroporous adsorption resins. *Polish Journal of Chemical Technology*, *18* (1), 127 – 132.

Babic, K., Van der Ham, L., & De Haan, A. B. (2006). Recovery of benzaldehyde from aqueous streams using extractant impregnated resins. *Reactive* and *Functional* Polymers, *66*, 1494 – 1505.

Chatsudthipong, V., & Muanprasat, C. (2009). Stevioside and related compounds: Therapeutic benefits beyond sweetness. *Pharmacology* & *Therapeutics*, *21*, 41 – 54.

Fu, X. C., Shen, W. X., & Yao, T. Y. (1990). *Physical chemistry*. Beijing: Higher Education Press, pp 172.

Geuns, J. M. C. (2003). Molecules of interest stevioside. *Phytochemistry*, *64*, 913 – 921.

Liu, C., Li, L. S., Xu, L. L., & Zhou, Z. M. (2007). Separation and identification of stevioside and Rebaudiodside A in Stevia by HPLC. *Chinese Journal* of Medical *Laboratory*, *26*, 23 – 26.

Liu, G. M., Zheng, S. R., Yin, D. Q., Xu, Z. Y., Fan, J., & Jiang, F. (2006). Adsorption of aqueous alkylphenol ethoxylate surfactants by mesoporous carbon CMK-3. *Journal* of *Colloid* and *Interface Science*, *302*, 47– 53.

Sorana, D. B., & Lorentz, J. (2007). Design of experiments: Useful orthogonal arrays for number of experiments from 4 to 16. *Entropy*, *9*, 198 – 232.

Wheeler, A., Boileau, A. C., Winkler, P. C., Compton, J. C., Prakash, I., Jiang, X., & Mandarino, D. A. (2008). Pharmacokinetics of rebaudioside A and stevioside after single oral doses in healthy men. *Food* and *Chemical Toxicology*, *46*, 54 – 60.

Zhang, Y., Chen, T. H., Shi, Z. Q., & He, B. L. (1998). Studies on the separation of rebaudioside A by recrystallization. *Ion Exchange* and *Adsorption*, *14*, 515 – 520.

Borneo International Journal of Biotechnology (BIJB)
Vol. 1 (December 2020), 55 – 75

e-ISSN 2716-697X

Research Article

IDENTIFICATION AND OCCURRENCE OF ANTIBIOTIC RESISTANCE OF *Staphylococcus aureus* AND *Escherichia coli* ISOLATED FROM RECREATIONAL PARKS AROUND KOTA KINABALU, SABAH

Rajeena Sugumaran, Pamela David Jocksing and Nur Athirah Yusof*

Biotechnology Research Institute,
Universiti Malaysia Sabah, Kota Kinabalu, Sabah, Malaysia
*Corresponding author's email: nrathirah.yusof@ums.edu.my
Received date: 11 September 2019 | Accepted date: 21 January 2020

ABSTRACT

Staphylococcus aureus (*S. aureus*) and *Escherichia coli* (*E. coli*) are contributors to infection cases among the Asian population. *S. aureus* is found in the mucous lining of noses and is mainly non-pathogenic while *E. coli*, mostly harmless bacteria, are found in the intestine. Pathogenic strains of both bacteria have adverse effects on the elderly and younger age group of the population. Samples were collected from recreational parks around Kota Kinabalu as they are hotspots frequently visited by families with both age groups. The bacterial samples were isolated and cultured on selective media such as Baird-Parker agar (BPA), Brain Heart Infusion (BHI) agar, MacConkey agar and Eosin-Methylene Blue (EMB) agar. Morphological characteristics of bacterial growth were observed, where *S. aureus* had black-shiny growth in BPA and *E. coli* had a metallic-green sheen in EMB agar. The suspected bacteria samples were then stained and viewed under a light microscope. *S. aureus* was identified as gram-positive, stained violet with a circular shape and clustered appearance. *E. coli* was identified as gram-negative, stained red, rod-shaped with 2 – 3 bacterial alignment. Antibiotic resistance test resulted in *S. aureus* and *E. coli* samples did not display 100% resistance among 4 antibiotics tested (ampicillin, penicillin, tetracycline and chloramphenicol). Most of the bacteria samples were a minimum inhibitory of

0.1 mg/mL of antibiotic concentration. These results provide a foundation for further research on identifying bacterial strains using molecular methods. The findings can then be used to disseminate information to the public to create awareness of potential disease outbreaks in the city.

Keywords: bacteria, recreational parks, antimicrobial resistance, Sabah, community health, infection

INTRODUCTION

Staphylococcus aureus (*S. aureus*) and *Escherichia coli* (*E. coli*) are contributors to cases of infection among the Asian population. Naturally, 30% of bacteria *S. aureus* is found in the mucous membrane lining of noses and are mainly non-pathogenic while *E. coli,* mostly harmless bacteria, are found in the lower intestine of humans and animals (CDC, 2011; WHO, 2018). Humans are the major reservoir for *S. aureus where* it is estimated that up to half of all adults are colonized (Boucher & Corey, 2008; Lowy, 1998). Staphylococci were first observed by Robert Koch in pus in 1878 but were only named "Staphylococcus", a Greek word that meant a bunch of grapes and "coccus" for berry by Alexander Ogston in 1882 (Bhedi, 2016). In 1884, Staphylococci was grown in pure culture for the first time by Friedrich Rosenbach and their characteristics were studied (Bhedi, 2016). *E. coli*, a facultative anaerobic bacteria was first isolated and named by Professor Theodor Escherich in 1885 (Lim, Yoon, & Hovde, 2010).

The main cause of concern of both *S. aureus* and *E. coli* is their pathogenicity; whereby certain strains of the bacteria can cause infection to humans and in extreme cases, may even lead to death. Examples of infection caused by *S. aureus* are bacteremia or sepsis, when the bacteria that are predominantly found in the nose or skin surface, enters the bloodstream (CDC, 2011). Pneumonia occurs when the bacteria attacks patients suffering from weakened lungs, endocarditis, the infection of heart valves and osteomyelitis, infection of the bone (CDC, 2011). The pathogenic strain of *S. aureus* that is resistant to antibiotics are known as Methicillin-resistant *Staphylococcus aureus* (MRSA), Vancomycin-intermediate *Staphylococcus aureus* (VISA), and Vancomycin-resistant *Staphylococcus aureus* (VRSA) (CDC, 2011). Individuals that are susceptible to Staph infection are those with weakened immune systems or have undergone surgeries or have intravenous catheters (CDC, 2011). Over 50% of MRSA infections have been reported in Asia, Malta, North and South America (Sit et al., 2017; Stefani et al., 2012). In Malaysia, MRSA prevalence has increased from 17% in 1986 to 44.1% in 2007 (Sit et al., 2017).

E. coli strains that are pathogenic can cause health problems such as diarrhoea if a human gets infected with the bacteria. Transmission can occur through contact with contaminated food or water, or with come in contact with faeces. Outbreaks of food contamination is a result of Shiga toxin-producing *E. coli* (STEC) or also known as Verocytotoxin-producing *E. coli* (VTEC) or Enterohemorrhagic *E. coli* (EHEC) (CDC, 2016). O157 with the most commonly reported strain in the United States (CDC, 2016). Infection can occur to anyone, however children below the ages of 5, the elderly (above 65 years old) and immunocompromised people are more at risk to develop symptoms such as bloody diarrhoea and kidney failure (haemolytic uremic syndrome) (CDC, 2016). Statistics show that in the United States, around 265,000 cases of STEC infections have been reported yearly with most are caused by O157 strains (Scallan et al., 2011).

The study conducted was aimed to isolate *S. aureus* and *E. coli* bacteria contaminating local recreational parks around Kota Kinabalu, Sabah using selective culture media method. Apart from that, the objective of the research was to identify the occurrence of antibiotic resistance of *S. aureus* and *E. coli*. Although there have been studies conducted on the occurrence of *S. aureus* and *E. coli* in food contamination around Malaysia, this is the first research of its kind to be conducted around recreational parks in Kota Kinabalu. Recreational parks are locations frequently visited by people of all ages and can be a breeding ground for bacteria as the facilities are not cleaned. The lack of proper hygiene habits and sanitation among the community could lead to the outbreak of pathogenic strains of bacteria especially among young children and the elderly. Data from this study lays the foundation for further research, which can be utilised by governmental bodies, non-governmental bodies and the community to raise awareness on public health and prevention measures on the type of bacterial strains and their antibiotic resistance abilities.

MATERIALS AND METHODS

Study Site Description

The sites chosen for this study were public playgrounds or exercise parks located in tourists or residential spots around Kota Kinabalu, Sabah. The sites selected were Tanjung Lipat (P1), Teluk Likas (P2), Perdana Park (P3), Taman Kingfisher (P4), UMS (Universiti Malaysia Sabah) (P5) and City Apartments, Inanam (P6). Tanjung Lipat, Teluk Likas and Perdana Park are popular locations for family outings, tourists' activities with nearby food stalls. These places are extremely crowded especially on weekends and public holidays. The other 3 sampling sites are located in residential areas and university campus grounds and receive slightly lesser crowd.

Sample Collection and Incubation

Sample collection was carried out in September 2018. Sterilised tissue swabs were used to wipe across surfaces of the playgrounds and exercise equipment (horizontally and vertically) especially at hand-held areas. Rusted areas were avoided to prevent contamination in the sample. A total of 12 tissue swab samples were collected from 6 sites. Tissues were then immediately kept in a 10 mL Eppendorf tube that had sterilised. The samples were then incubated at 37°C for 24 to 48 h in 10 mL of 1% sterile peptone broth.

Microbial Analysis

Plating and Isolation of Bacteria

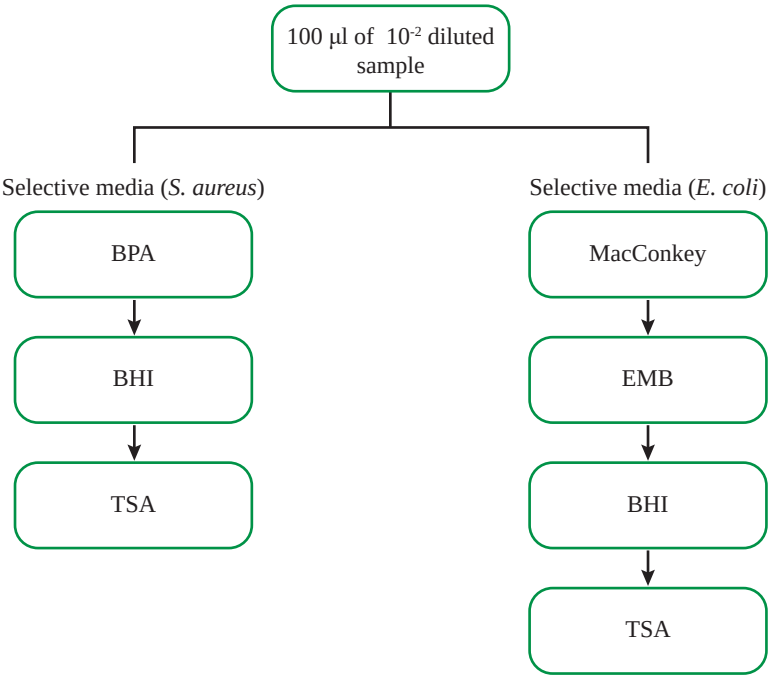

Figure 1 Summary of steps taken to isolate and identify the presence of *S. aureus* and *E. coli* in 6 samples obtained around Kota Kinabalu

For the isolation of *S. aureus*, 0.1 mL of diluted samples was evenly spread on plates of BPA agar (Oxoid, UK) while for the isolation of *E. coli,* 0.1 mL of diluted samples were spread on MacConkey agar (Oxoid, UK). The plates which were inoculated with the samples were incubated for 24 to 48 h at 37°C. For the identification of *S. aureus*, single

colonies with shiny-black growth in BPA agar were selected and then streaked on BHI agar (Oxoid, UK) media. On the other hand, for *E. coli* identification, single colonies with pink growth from the MacConkey media were selected and streaked on EMB agar (Oxoid, UK) plates followed by BHI agar plates for verification. Colour and colony growth were observed and recorded in Table 3 after each stage. Lastly, the samples were streaked on Tryptone Soy Agar (TSA) (Oxoid, UK) plates for storage and kept in 4°C refrigerator. The steps taken to plate and isolate the targeted bacteria were done according to the flow chart shown in Figure 1.

Gram Staining

A drop of saline was introduced on the slide. Next, a bacterial sample was smeared followed by mixing. Heat fixed was done by passing the slide through Bunsen burner. Crystal violet solution was flooded onto the slides and left to react with the specimen for 1 min. The slides were rinsed with distilled water and then flooded with iodine solution for 1 min. Excess iodine is rinsed off; acetone was added to decolourise the specimens for 5 s. The slides were washed off once again using distilled water. Gram-negative bacteria are no longer visible post acetone decolourisation. Next, safranin counterstain was applied to the slides for 30 s. The slide was washed once again with distilled water and viewed under a light microscope (Olympus, USA).

Antimicrobial Susceptibility Tests

Isolates for *S. aureus* and *E. coli* were tested for antibiotic resistance using the Kirby-Bauer disk diffusion susceptibility method. This method complied with the Clinical Laboratory Standard Institute guidelines (Yassin et al., 2017). Antimicrobial susceptibility tests were performed on Mueller Hinton (MH) agar (Oxoid, UK) plates. The concentration gradients of antibiotics were used to determine *S. aureus* and *E. coli*'s sensitivity and resistance are shown in Table 1. A single colony was obtained from each plate and emulsified in 1% sterile buffered peptone water. The solution was mixed thoroughly to ensure that no solid material from the colony was visible in the broth. The inoculated bacterial colonies in the broth were incubated at 37°C for 2 h to reach log phase growth. Next, 100 µL of the bacteria culture were plated on MH agar plates and were evenly spread. The plates were dried for 5 min before the antibiotic discs were placed on the surface of the agar. Sterilised forceps were used. The inoculated plates were inverted and incubated at 37°C for 24 h. Using a ruler, the diameter of the inhibition zones was measured for each disc and compared with the standard table to determine the sensitivity and resistance of bacteria.

Table 1 Concentration of antibiotics used for the susceptibility test of *S. aureus* and *E. coli*

Antibiotics (mg/mL)	Concentration (mg/mL)		
Ampicillin	0.1	1.0	10.0
Ampicillin	0.3	3.0	3.0
Chloramphenicol	0.1	1.0	10.0
Chloramphenicol	0.25	2.5	25
Penicillin	0.1	1.0	10.0
Penicillin	0.3	3.0	3.0
Tetracycline	0.1	1.0	10.0

RESULTS

Isolation and Identification of S. *aureus* in Culture Samples

Based on Figure 2, positive isolation and identification of the bacteria were present in 5 out of the 6 locations which were P1 for Tanjung Lipat, P2 for Teluk Likas, P3 for Perdana Park, P4 for Taman Kingfisher and P6 for City Apartments. The bacteria growth had black colonies in BPA. Only sample P5 obtained from UMS had an absence of *S. aureus*. To validate further the presence of *S. aureus*, single colonies from BPA media were inoculated on BHI media whereby the positive presence of bacteria was seen as pale-yellowish growth as indicated in Figure 3. Yellow colony growth was also observed when single colonies of *S. aureus* obtained from BHI were streaked on TSA for all 5 sites as stated in Figure 4. Summary of colonies observed is described in Table 2.

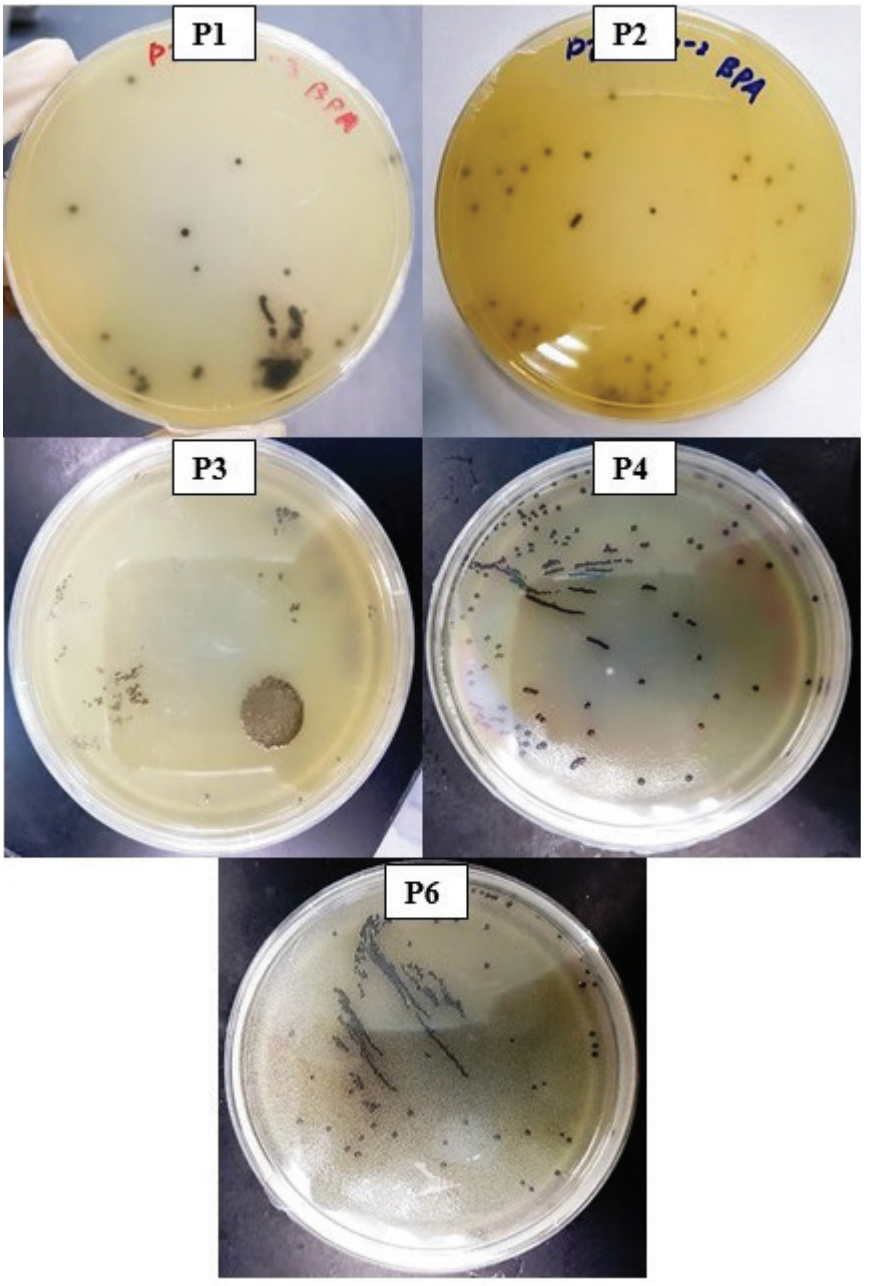

Figure 2 Isolation and identification of *S. aureus* growth on BPA plates. Samples obtained from P1 (Tanjung Lipat), P2 (Teluk Likas), P3 (Perdana Park), P4 (Taman Kingfisher) and P6 (City Apartments, Inanam)

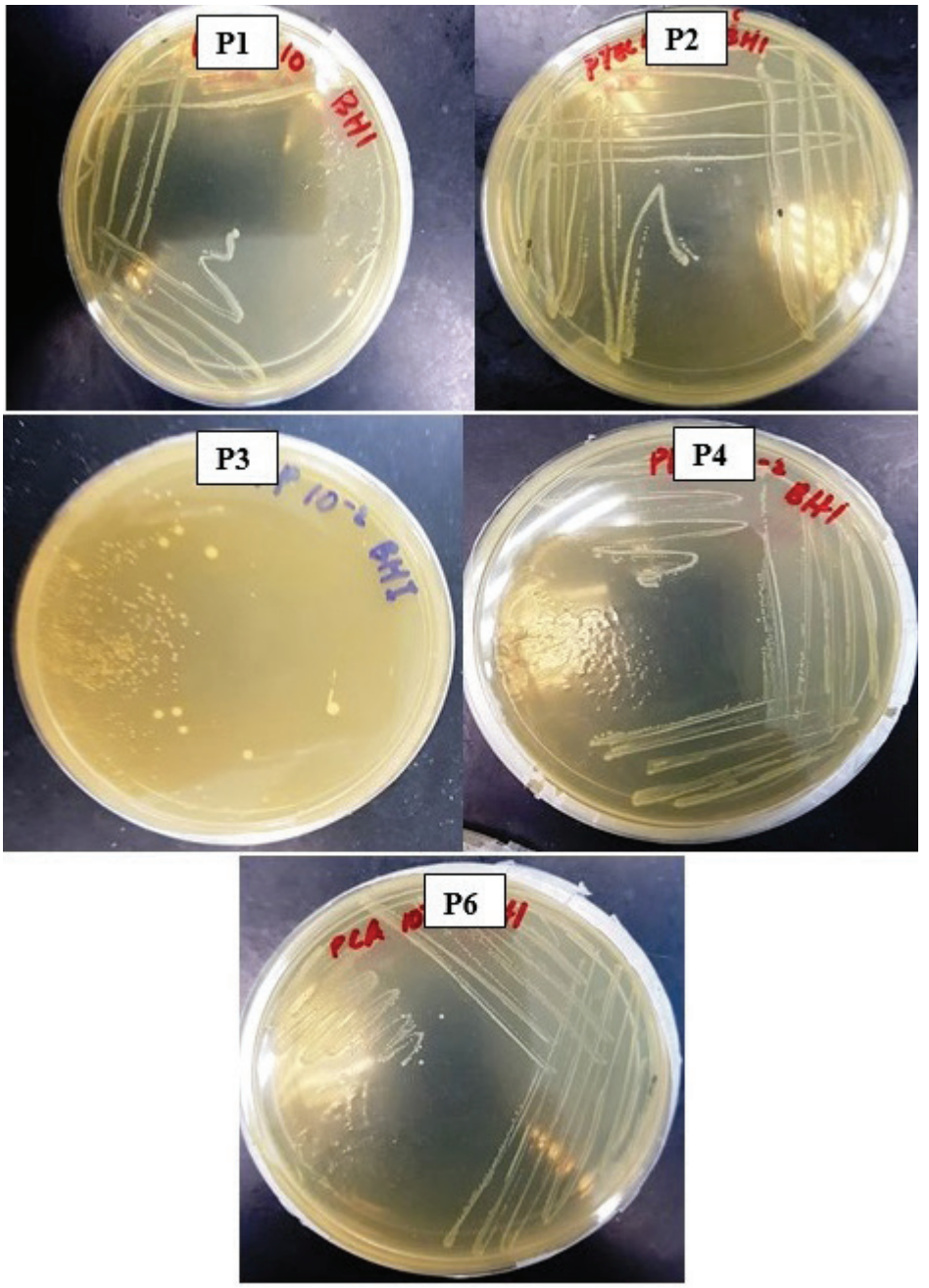

Figure 3 Isolation and identification of *S. aureus* growth on BHI plates labelled as P1 (Tanjung Lipat), P2 (Teluk Likas), P3 (Perdana Park), P4 (Taman Kingfisher) and P6 (City Apartments, Inanam). Samples with black-shiny colonies were selected and streaked on BHI

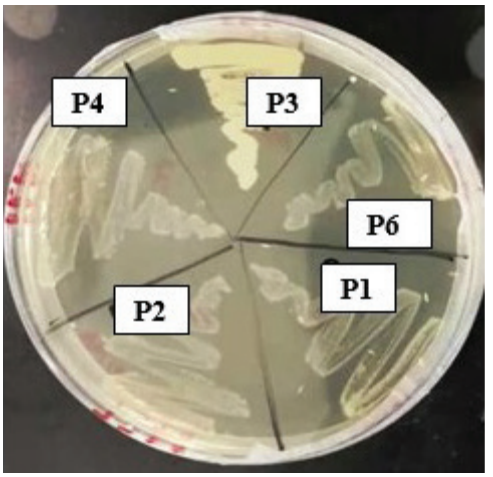

Figure 4 Isolation and identification of *S. aureus* growth on TSA plates. Samples were collected from 6 sampling sites; P1 (Tanjung Lipat), P2 (Teluk Likas), P3 (Perdana Park), P4 (Taman Kingfisher) and P6 (City Apartments, Inanam)

Table 2 Summary of morphological identification and isolation of bacteria using selective media from 6 sampling sites

			Identification of *Staphylococcus aureus*		Identification of *Escherichia coli*				
Sample	**Volume**	**Dilution**	**BPA**	**BHI**	**MacConkey**	**EMB**	**BHI**	**TSA**	**Presumptive isolates**
P1 (Tanjung Lipat)	100 µL	10^{-3}	POS – black, circular and shiny colony growth. No halo zone observed	POS – pale yellowish growth	POS – pink, non-mucoid colonies	NEG. – no metallic green sheen. Mucoid growth		POS – yellowish growth	*Staphylococcus aureus* *Enterobacteria* sp.
P2 (Teluk Likas)	100 µL	10^{-3}	POS – black, circular and shiny growth. No halo zone	POS – pale yellowish growth	POS – pink and colourless, mucoid and non-mucoid colonies	NEG. – pink, mucoid growth		POS – yellowish growth	*Staphylococcus aureus* *Enterobacteria* sp.
P3 (Perdana Park)	100 µL	10^{-2}	POS – circular, black smear	POS – pale yellowish growth	POS – pale pink, mucoid	POS – metallic green sheen	POS – whitish colony growth	POS for both samples – Dominant whitish colony - Pale cream coloured colonies	*Staphylococcus aureus* *Escherichia coli*
P4 (Taman Kingfisher)	100 µL	10^{-3}	POS – black, circular and shiny growth. No halo zone	POS – pale yellowish growth	NEG – no colony growth			POS – yellowish growth	*Staphylococcus aureus*

P5 (Universiti Malaysia Sabah)	100 µL	10^{-2}	NEG – circular, black smear		NEG – pale white colonies				Unidentified species
P6 (City Apartments, Inanam)	100 µL	10^{-3}	POS – black, circular and shiny growth. No halo zone	POS - pale yellowish growth	POS – dark-pink, non-mucoid and mucoid smear	POS – metallic green sheen	POS –white-ish colony growth	POS – yellowish growth	*Staphylococcus aureus* *Escherichia coli*

Note: Bacterial colonies that grew with expected characteristics of *E. coli* and *S. aureus* were labelled as POS, while colonies which did not match the expected characteristics of *E. coli* and *S. aureus* were labelled as NEG.

Isolation and Identification of E. *coli* in Culture Samples

Successful identification of *E. coli* bacterial growth was found in 2 sites; P3 Perdana Park and P6 City Apartments. The bacteria were identified by their pink, mucoid and non-mucoid characteristics when grown in the MacConkey media as seen in Figure 5. Negative results occurred in the remaining sites; P1 Tanjung Lipat, P2 Teluk Likas, P4 Taman Kingfisher and P5 UMS. Validation of the bacteria was conducted by streaking single colonies taken from MacConkey agar onto EMB media and positive *E. coli* was indicated by a metallic sheen appearance in Figure 6. Further isolation and confirmation were done by inoculating the bacteria in BHI and TSA media where a prominent white coloured growth was observed (Figure 7) and a cream-coloured growth was seen in Figure 8. The observed characteristics of *E. coli* isolation were recorded in Table 2.

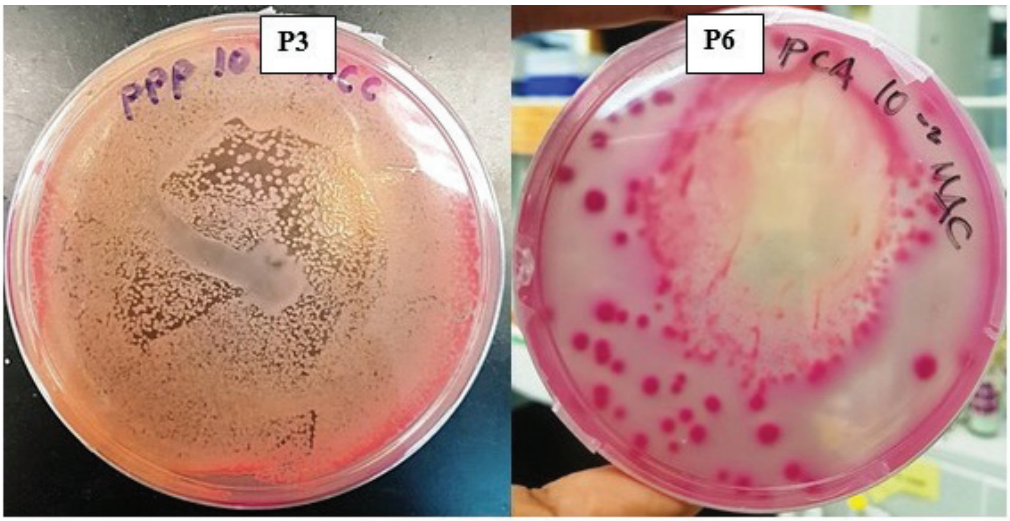

Figure 5 Isolation and identification of *E. coli* growth on MCC plates. Samples obtained from P3 (Perdana Park) and P6 (City Apartments, Inanam)

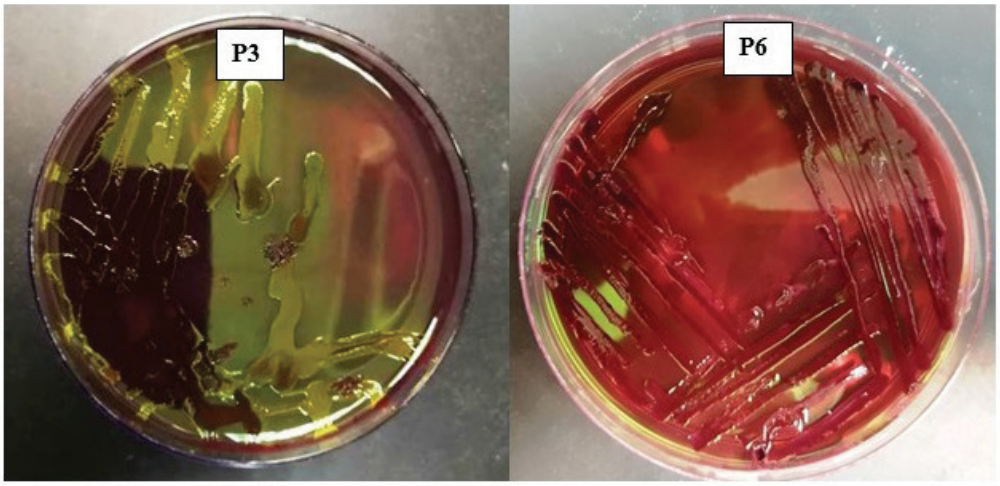

Figure 6 Isolation and identification of *E. coli* growth on EMB plates. Samples obtained from P3 (Perdana Park) and P6 (City Apartments, Inanam)

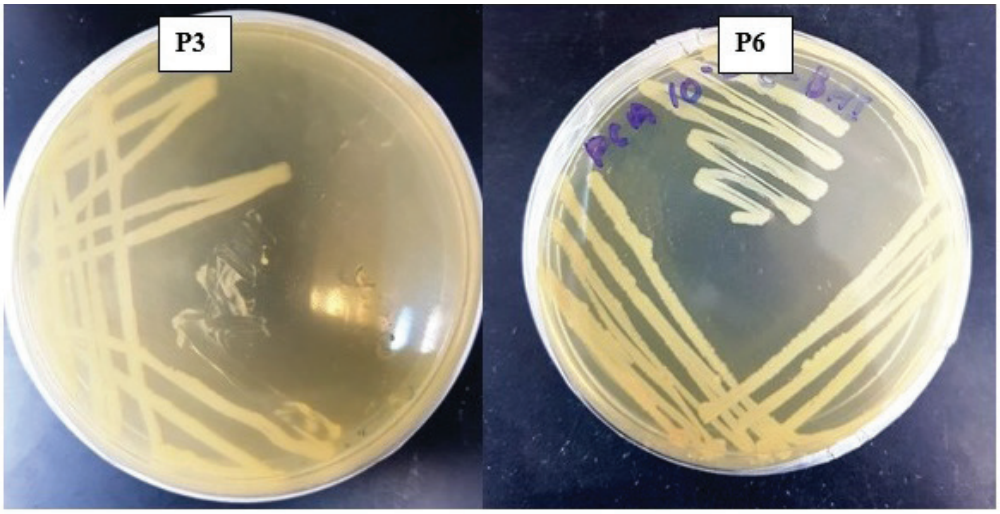

Figure 7 Isolation and identification of *E. coli* growth on BHI plates from P3 (Perdana Park) and P6 (City Apartments, Inanam)

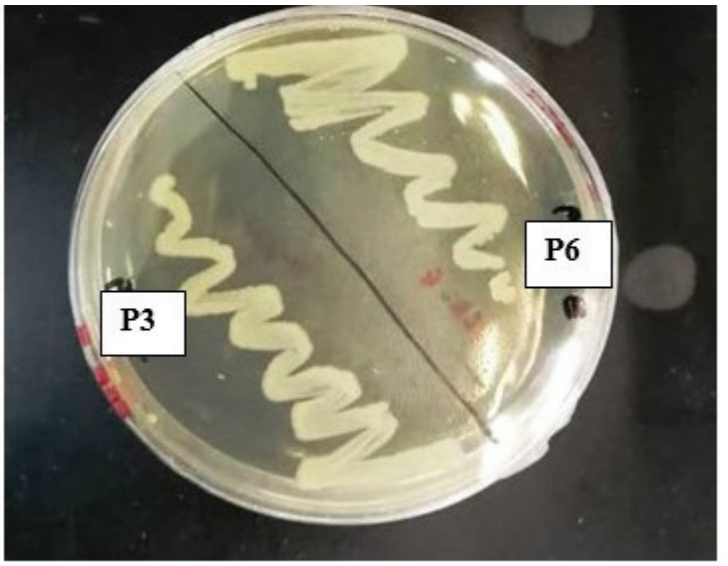

Figure 8 Isolation and identification of *E. coli* growth on TSA plates. Positive samples were identified in P3 (Perdana Park) and P6 (City Apartments, Inanam)

Verification of S. aureus and E. *coli* using Gram Staining

Gram staining was conducted to verify the presence of Gram-positive and Gram-negative bacteria in the isolated colonies obtained from 5 sites positive for *S. aureus* and *E. coli*. This also allowed for the observation of the bacteria's morphological characteristics. As observed in Figure 9, results were positive for the presence of *S. aureus*. The bacteria were stained violet indicating Gram-positive, had grape-like clusters and were circular shaped. Sites verified positive for *S. aureus* are P1 Tanjung Lipat, P2 Teluk Likas, P3 Perdana Park, P4 Taman Kingfisher and P6 City Apartments. Alternatively, *E. coli* is a Gram-negative bacteria where positive colonies are stained red. The results seen in Figure 10 verifies the presence of rod-shaped *E. coli* in P3 Perdana Park and P6 City Apartments. Summary of all verified bacterial colonies is described in Table 3.

Table 3 Summary of the identification and morphological characteristics of Gram-positive and Gram-negative bacteria

Sample	Bacteria	Gram Positive	Gram Negative	Morphology
P1 (Tanjung Lipat)	*Staphylococcus aureus*	X		Stained purple, grape-like clusters (staphylo-). Circular (coccus) shaped
P2 (Teluk Likas)	*Staphylococcus aureus*	X		Stained purple, grape-like clusters (staphylo-). Circular shaped
P3 (Perdana Park)	*Staphylococcus aureus*	X		Stained purple, grape-like clusters (staphylo-). Circular (coccus) shaped
	Escherichia coli		X	Rod-shaped, some aligned 2-3 together, some singular, stained red
P4 (Taman Kingfisher)	*Staphylococcus aureus*	X		Stained purple, grape-like clusters (staphylo-). Circular (coccus) shaped
P6 (City Apartments, Inanam)	*Staphylococcus aureus*	X		Stained purple, grape-like clusters (staphylo-). Circular (coccus) shaped
	Escherichia coli		X	Singular, rod-shaped, stained red.

Antimicrobial Resistance

E. coli and *S. aureus* isolates cultured from P1 Tanjung Lipat, P2 Teluk Likas, P3 Perdana Park, P4 Taman Kingfisher and P6 City Apartments were analysed for their resistance towards a range of antibiotics such as ampicillin, tetracycline, penicillin and chloramphenicol. The results of antimicrobial testing in the present study indicate that all *E. coli* isolates were susceptible to ampicillin. The minimum inhibitory concentration (MIC) of ampicillin which inhibited the visible growth of the bacteria was 0.3 mg/ml. The diameter of the inhibition zone of *E. coli* isolates in all of the ampicillin concentration treated had a variation of ±4 mm. On the other hand, out of the 5 *S. aureus* isolates, only P6 (Perdana Park) did not show any inhibition zone towards ampicillin. The MIC of *S. aureus* against ampicillin was mostly at 0.1 mg/mL except for P1 (Tanjung Lipat) which showed a MIC at 0.3 mg/mL. The summary of the diameter of inhibition zone and MIC is described in Table 4 (a). Table 4 (b) indicates the diameter of inhibition zone for *E. coli* when treated with tetracycline had a variation of ±4 mm between the different antibiotic concentrations. Both *E. coli* and *S. aureus* which were taken from P1 (Tanjung Lipat), P2 (Teluk Likas), P3 (Perdana Park), P4 (Taman Kingfisher) and P6

(City Apartments) were susceptible to the lowest concentration of antibiotic which was 0.1 mg/mL. *S. aureus* isolated from all sites except for P1 has a susceptibility to the lowest concentration of antibiotic, 0.1 mg/mL of Penicillin. The variation in diameter of inhibition zone for *E. coli* between sites P3 and P6 is ±1 mm. All *E. coli* isolates were susceptible to penicillin as found in Table 4 (c). All *E. coli* and *S. aureus* bacteria were susceptible to the lowest concentration of chloramphenicol tested, 0.1 mg/mL. The diameter of inhibition zones increases with the increment of antibiotic concentration where at the highest concentration tested, 25 mg/mL, all isolates of *S. aureus* showed an inhibition zone of 31 mm ±3 mm except for isolates from P4 (Taman Kingfisher). Results are tabulated in Table 4 (d).

Table 4 The diameter of inhibition zones (mm) for *Staphylococcus aureus* and *Escherichia coli* according to 4 types of antibiotics (a) ampicillin, (b) tetracycline, (c) penicillin and (d) chloramphenicol according to their respective concentrations. Locations were P1 (Tanjung Lipat), P2 (Teluk Likas), P3 (Perdana Park), P4 (Taman Kingfisher), P5 (Universiti Malaysia Sabah) and P6 (City Apartments, Inanam)

Ampicillin concentration (mg/mL)	Diameter of inhibition zones (*Staphylococcus aureus*) (mm)					Diameter of inhibition zones (*Escherichia coli*) (mm)	
	P1	P2	P3	P4	P6	P3	P6
0.1	0	11	22	16	No inhibition zone observed	0	0
0.3	12	17	23	20		11	8
1.0	18	23	20	25		15	11
3.0	26	28	19	28		23	24
10	27	32	22	30		27	23
30	28	32	22	30		30	26

(a)

Tetracycline concentration (mg/mL)	Diameter of inhibition zones (*Staphylococcus aureus*) (mm)					Diameter of inhibition zones (*Escherichia coli*) (mm)	
	P1	P2	P3	P4	P6	P3	P6
0.1	20	15	24	10	25	15	19
1.0	27	13	34	12	31	26	24
10	31	13	40	24	36	29	26

(b)

Penicillin concentration (mg/mL)	Diameter of inhibition zones (*Staphylococcus aureus*) (mm)					Diameter of inhibition zones (*Escherichia coli*) (mm)	
	P1	P2	P3	P4	P6	P3	P6
0.1	0	20	17	18	22	6	10
0.3	8	20	16	19	19	6	10
1.0	11	27	22	25	25	9	10
3.0	17	27	22	27	25	10	10
10	20	30	26	25	27	21	22
30	23	36	25	30	30	25	24

(c)

Chloramphenicol concentration (mg/mL)	Diameter of inhibition zones (*Staphylococcus aureus*) (mm)					Diameter of inhibition zones (*Escherichia coli*) (mm)	
	P1	P2	P3	P4	P6	P3	P6
0.1	12	14	14	15	10	6	11
0.25	16	14	16	15	8	11	5
1.0	16	24	22	19	20	23	14
2.5	24	24	20	19	20	27	20
10	30	30	30	21	25	31	35
25	32	34	34	21	31	35	30

(d)

DISCUSSION

Isolation and identification of *S. aureus* and *E. coli* from Recreational Parks

Bacterial isolation was conducted using selective media that enabled the proliferation of target microorganism and suppressed unintended microorganisms on the medium. Based on Table 2, the presence of suspected *S. aureus* can be identified from black colony growth on BPA due to tellurite reduction activity. Some colonies have a clear zone surrounding them due to lecithinase production or an opaque zone of precipitation that is caused by lipase activity by coagulase-positive strains (El-Hadedy & El-Nour, 2012; Ribeiro de Souza da Cunha, 2018). However, there was no indication of halo zone surrounding the bacteria cultures. The components inside the BPA medium are lithium chloride, potassium tellurite and egg yolk (Ribeiro de Souza da Cunha, 2018). Tellurite forming colonies are reduced by the presence of salt and potassium tellurite in the media yolk (Ribeiro de Souza da Cunha, 2018). All samples except for P5 (UMS) that had black, shiny colonies in BPA media were

steaked onto BHI plates to provide enrichment for the bacterial culture (Palilu & Budiarso, 2017). BHI media provided a nutrient-rich environment for Streptococci which is commonly challenging to grow. The results indicated that samples obtained from P1 (Tanjung Lipat), P2 (Teluk Likas), P3 (Perdana Park), P4 (Taman Kingfisher) and P6 (City Apartments, Inanam) were positive for *S. aureus* isolated. This probably happened due to the location of the sites where all except P5 UMS were located in the public areas that were frequently visited by people while P5 UMS was located on university campus grounds that were only accessible to students and lecturers.

Next, identification and isolation of *E. coli* were done in 3 stages, using MacConkey agar where successful growth of bacteria was pink, with mucoid and non-mucoid substances. The MacConkey agar is a differential medium that contains crystal violet and bile salts to inhibit the growth of any Gram-positive bacteria (Black, 2004). The agar also contains sugar lactose and a pH indicator that differentiates Enterobacteria from lactose fermenter colonies as red to non-lactose fermenting bacteria as pale (Black, 2004; Hart & Shears, 2004). In Figure 3, samples P1, P2, P3 and P6 indicate the presence of lactose and non-lactose fermenters. Next, the suspected *E. coli* samples that were cultured in EMB agar displayed a metallic green sheen reflective to light. El-Hadedy & El-Nour (2012) also had the same observation. Some lactose-fermenting bacteria would also produce flat, dark colonies with a green metallic sheen (as shown in P3 of Figure 3) (Acharya, 2013). The growth colonies in P1 and P2 could also be non-lactose fermenters of Gram-negative bacteria as they appear pink (Acharya, 2013). Streaking on BHI agar were only carried out using sample P3 (Perdana Park) and P6 (City Apartments) that had a metallic sheen as an indication of *E. coli*. The presence of *E. coli* bacteria in these 2 locations could be a result of nearby food stalls in the vicinity and the high density of visitors to the area.

Gram staining was conducted to differentiate the components found in the cell wall of bacteria (Bruckner, 2016). Bacteria are categorised into 4 groups; Gram-positive that are stained violet or purple due to the thick peptidoglycan layer (60 – 90%) in the cell wall while Gram-negative bacteria are stained red due to a thinner layer of peptidoglycan in the cell wall (Bruckner, 2016). The other 2 categories are gram variable, where the microorganisms are unevenly stained red and violet, and gram non-reactive where the microorganisms are either poorly stained or not stained at all (Black, 2004). The Gram staining method was devised in 1884 by a Danish physician named Hans Christian Gram (Black, 2004). Observations from Table 3 and Figure 10 showed that P3 (Perdana Park) and P6 (City Apartment) samples were positive for Gram-negative bacteria, *E. coli* based on their rod shape and stain colour red. Gram-negative bacteria are stained red due to the inability of the thin peptidoglycan layer (10 – 20%)

in the cell wall to retain crystal violet colour (Bruckner, 2016; Black, 2004). During the staining process, the crystal violet colour is washed off using a decolouriser (Bruckner, 2016). The decolouriser contains acetone that degrades the outer membrane causing the colour to be washed off. Safarin (red dye) is then added and is easily absorbed by the decolourised Gram-negative bacteria (Bruckner, 2016). Sample P3 was stained violet instead of red possibly due to errors during the decolourization stage, whereby acetone was either washed off too soon before it could degrade the membrane layer or high concentration of crystal violet and iodine was used. Another possibility is that the bacteria become Gram variable if they are cultured longer than 48 h due to the changes in their cell wall components (Black, 2004). Table 3 and Figure 9, on the other hand, showed samples from P1, P2, P3, P4 and P6 containing Gram-positive bacteria, *S. aureus,* in circular, grape-like clusters. The bacteria were stained purple due to the thick peptidoglycan layer with attached teichoic acid polymers (Hart & Shears, 2004). No Gram staining was done on P5 as the colony growth in the selective media did not resemble the morphological characteristics of *S. aureus* or *E. coli*.

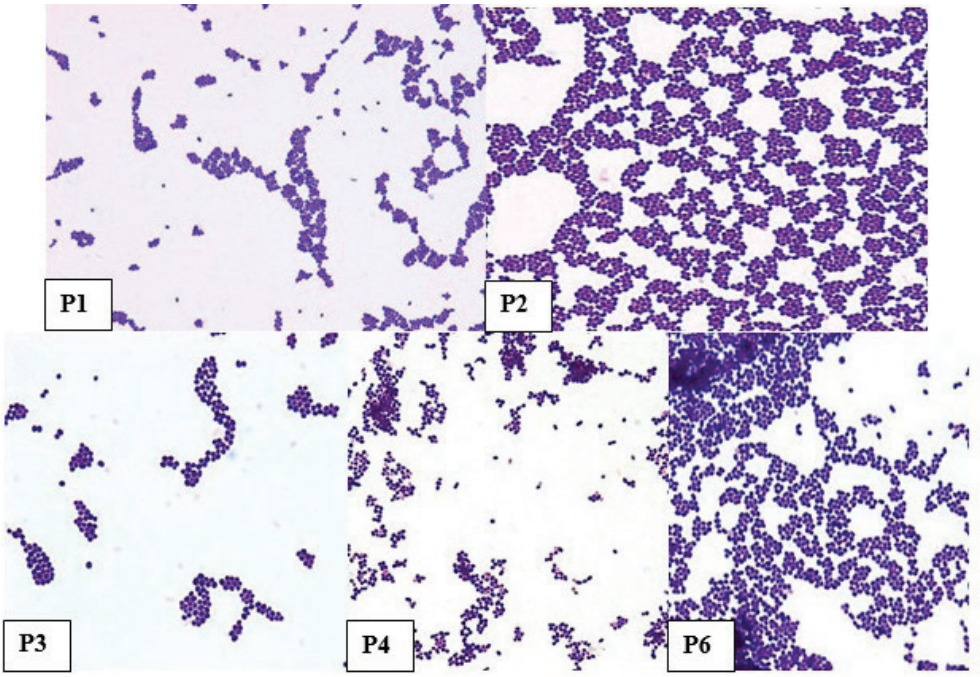

Figure 9 Gram-positive staining for bacteria *S. aureus* in 5 samples P1 (Tanjung Lipat), P2 (Teluk Likas), P3 (Perdana Park), P4 (Taman Kingfisher) and P6 (City Apartments, Inanam). Images were viewed under 1000× total magnification using a compound light microscope

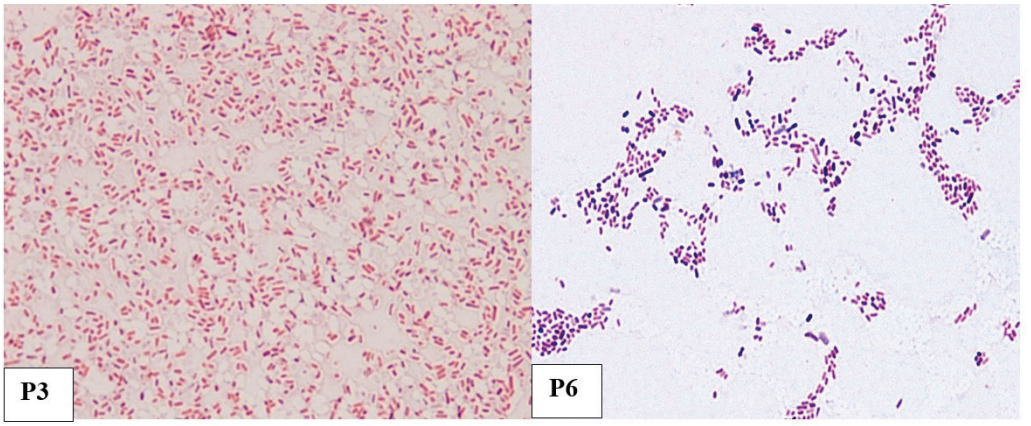

Figure 10 Gram-negative staining for *E. coli* in 2 samples P3 (Perdana Park) and P6 (City Apartments, Inanam). Images were viewed under 1000× total magnification using a compound light microscope

Antimicrobial Susceptibility Test

Minimum inhibitory concentration (MIC) is used to identify the lowest concentration of antibiotic that will inhibit bacterial growth in the culture media (Street, 2014). Analysis of the other antibiotics revealed that all of the *S. aureus* from 4 locations sampled were susceptible to ampicillin, tetracycline, penicillin and chloramphenicol. This data is important as it shows that these parks are safe for children. Dangerous *S. aureus* isolates that are increasing their multi-resistance towards modern-day drugs such as Methicillin-resistant *S. aureus* (MRSA), Vancomycin-Intermediate *S. aureus* (VISA) and Vancomycin-Resistant *S. aureus* (VRSA) have recorded outbreaks globally since the 1970s. Multi-resistance *S. aureus* was once confined largely to hospitals, health care environments, and patients frequenting these facilities, however, since the 1990s, there has been an explosion in the number of infections among the general population with and without exposure to the health care environment (Chambers & Deleo, 2009; David & Daum, 2010). *S. aureus* isolated from P1 (Tanjung Lipat) has already shown resistance towards low doses of ampicillin and penicillin both at 0.1 mg/ml. This is an indicator for the public to be aware and cautious of a potential outbreak of multi-resistant Staphylococcus. Chen and Huang (2014) have reported that Malaysia had 13 cases of MRSA infections from a study period of 2006 – 2007. They have also identified that the increasing rates of MRSA infection in Asian communities have caused an increased usage of glycopeptides as an anti-MRSA agent which has indirectly caused glycopeptide-non-susceptible stains to develop. The densely populated Asian communities also contribute to the infection spreading easily from one infected individual to another.

Results in Table 3 identified *E. coli* isolates from P3 (Perdana Park) and P6 (City Apartments) were resistant to 0.1 mg/mL of ampicillin but were susceptible to tetracycline, penicillin and chloramphenicol at all tested concentrations. Tanih, Sekwadi, Ndip, and Bessong (2015) reported that *S. aureus* and *E. coli* identified in their research showed 100% susceptibility for ampicillin which was not the case for the current study. This goes to show that antibiotic susceptibility varies with time and location (Tanih et al., 2015).

The overall results show that P6 (City Apartments) had both resistant strains of *S. aureus* and *E. coli* towards low dose of antibiotics. This is an important finding as the site is a residential location where children frequently play at the playground. The low hygiene level and awareness at the residential area could have contributed to a mutated strain of bacteria and immediate action needs to be taken by the community or city council to clean the playground facilities.

There are several limitations of the research in identifying the type of *S. aureus* and *E. coli* bacteria found. Observation of phenotypic characteristics alone is insufficient to confirm the presence of bacteria. Further differentiation tests can be carried out using biochemical tests such as catalase and coagulase tests to differentiate Streptococci and Staphylococci, indole or methyl red test to differentiate *E. coli* from other Enterobacteriaceae (Hart & Shears, 2004). DNA sequencing should be carried out to identify the exact species and strain of bacteria present. The results from this research serve only for laboratory reference and to act as a foundation to initiate further research. The identification of bacteria must be conducted as *S. aureus* infection could start with blisters or pus-filled boils on the skin (Kaiser, 2016). The bacteria can spread if anyone comes in contact with the pus, and on rare occasions, further infection such as meningitis, septicaemia, septic arthritis, endocarditis and osteomyelitis could occur (Kaiser, 2016). The test on antibiotic susceptibility would help to identify resistant bacterial strains for the detection and prevention of MRSA. The findings from in-depth research can then be used by the health department and for public awareness on the possibilities of pathogenic bacteria spread amongst children in the playground. The outcome serves as a reminder of the importance of proper hygiene habits to prevent the spread of transmissible diseases.

CONCLUSION

Managing contamination of *S. aureus* and *E. coli* in recreational park facilities is definitely a challenge. Recreational parks are public amenities and the spread of germs and bacteria are highly significant to all users. Awareness needs to be instilled in the community on the importance of personal hygiene not only before and after handling of food but also after using the park facilities. Handwashing or even the usage of hand sanitisers are an effective and inexpensive way to prevent transmission

and infection. In conclusion, further identification and confirmation of bacterial strains via molecular methods by the identification of 16S rRNA is highly recommended before informing the healthcare industry and the community to prevent potential pathogenic outbreaks in the city.

ACKNOWLEDGEMENTS

Gratitude to Biotechnology Research Institute (BRI) for allowing to use their resources and facilities for this experiment.

REFERENCES

Acharya, T. (2013). Eosin Methylene Blue (EMB) agar: Composition, uses and colony characteristics. Retrieved from https://microbeonline.com/eosin-methylene-blue-emb-agar-composition-uses-colony-characteristics/

Bhedi, K. (2016). Isolation and identification of *Staphylococcus aureus* from poultry and poultry house environment with special reference to MRSA (Master Thesis). Department of Veterinary, Public Health and Epidemiology, College of Veterinary Science and Animal Husbandry. Gujarat: Anand Agricultural University.

Black, J. G. (2004). *Microbiology: Principles and explorations* (6th ed.). Virginia, United States of America: John Wiley & Sons, INC.

Boucher, H. W., & Corey, G. R. (2008). Epidemiology of methicillin-resistant *Staphylococcus aureus*. Clinical infectious diseases, 46 (Supplement 5), S344 – S349.

Bruckner, M. Z. (2016). Microbial life: Educational resources. gram staining. Retrieved from https://serc.carleton.edu/microbelife/research_methods/microscopy/gramstain.html

Chambers, H. F., & Deleo, F. R. (2009). Waves of resistance: *Staphylococcus aureus* in the antibiotic era. *Nature reviews. Microbiology*, *7* (9), 629 – 641.

Chen, C. J., & Huang, Y. C. (2014). New epidemiology of *Staphylococcus aureus* infection in Asia. *Clinical Microbiology and Infection*, *20* (7), 605 – 623.

Centre for Disease Control and Prevention (CDC). (2011). *Staphylococcus aureus in healthcare settings*. Retrieved from https://www.cdc.gov/hai/organisms/staph.html

Centre for Disease Control and Prevention (CDC). (2016). *Escherichia coli*. Retrieved from https://www.cdc.gov/ecoli/pdfs/CDC-E.-coli-Factsheet.pdf

David, M. Z., & Daum, R. S. (2010). Community-associated methicillin-resistant *Staphylococcus aureus*: epidemiology and clinical consequences of an emerging epidemic. *Clinical Microbiology Reviews*, *23* (3), 616 – 687.

El-Hadedy, D., & Abu El-Nour, S. (2012). Identification of *Staphylococcus aureus* and *Escherichia coli* isolated from Egyptian food by conventional and molecular methods. *Journal of Genetic Engineering and Biotechnology*, *10* (1), 129 – 135.

Hart, T., & Shears, P. (2004). Colour atlas of medical microbiology (2nd ed.). United Kingdom: Mosby.

Kaiser, G. (2016). Isolation and identification of Staphylococci. Retrieved from https://bio.libretexts.org/Demos%2C_Techniques%2C_and_Experiments/Microbiology_Labs_II/Lab_15%3A_Isolation_and_Identification_of_Staphylococci

Lim, J. Y., Yoon, J., & Hovde, C. J. (2010). A brief overview of *Escherichia coli* O157: H7 and its plasmid O157. *Journal of Microbiology and Biotechnology*, *20* (1), 5 – 14.

Lowy, F. D. (1998) *Staphylococcus aureus* infections. N. Engl. J. Med., 339 (8), 520 – 532.

Palilu, P. T., & Budiarso, T. Y. (2017). Isolation and identification of *Staphylococcus* sp. in powdered infant milk. AIP Conference Proceedings 1844, 020016.

Ribeiro de Souza da Cunha, M. (2018). Chapter 6: Methods for the identification, characterization, and tracking the spread of *Staphylococcus aureus.* In A. Fetsch (Ed.), *Staphylococcus aureus* (pp. 105 – 125). Cambridge, MA: Academic Press.

Scallan, E., Hoekstra, R. M., Angulo, F. J., Tauxe, R. V., Widdowson, M. A., Roy, S. L., ... Griffin, P. M. (2011). Foodborne illness acquired in the United States – major pathogens. *Emerging Infectious Diseases*, *17* (1), 7.

Sit, P. S., Teh, C. S. J., Idris, N., Sam, I. C., Syed Omar, S. F., Sulaiman, H., … Ponnampalavanar, S. (2017). Prevalence of methicillin-resistant *Staphylococcus aureus* (MRSA) infection and the molecular characteristics of MRSA bacteraemia over a two-year period in a tertiary teaching hospital in Malaysia. *BMC Infectious Diseases*, *17* (1), 274.

Stefani, S., Chung, D. R., Lindsay, J. A., Friedrich, A. W., Kearns, A. M., West, H., & Mackenzie, F. M. (2012). Methicillin-resistant *Staphylococcus aureus* (MRSA): Global epidemiology and harmonization of typing methods. *International Journal of Antimicrobial Agents*, *39* (4), 273 – 282.

Street, T. (2014). *Antimicrobial susceptibility*. Retrieved from https://emedicine.medscape.com/article/2103786-overview

Tanih, N. F., Sekwadi, E., Ndip, R. N., & Bessong, P. O. (2015). Detection of pathogenic Escherichia coli and Staphylococcus aureus from cattle and pigs slaughtered in abattoirs in Vhembe District, South Africa. *The Scientific World Journal*.

WHO. (2018). *E. coli.* Retrieved from http://www.who.int/news-room/fact-sheets/detail/e-coli

Yassin, A. K., Gong, J., Kelly, P., Lu, G., Guardabassi, L., Wei, L., … Wang, C. (2017). Antimicrobial resistance in clinical *Escherichia coli* isolates from poultry and livestock, China. *PLoS ONE*, *12* (9): e0185326.

Borneo International Journal of Biotechnology (BIJB)
Vol. 1 (December 2020), 77 – 87

e-ISSN 2716-697X

Research Article

SEPARATION OF STEVIOL GLYCOSIDES FROM *Stevia rebaudiana* USING DIFFERENT AQUEOUS EXTRACTION TECHNIQUES

Chong Saw Peng*, Mustapha bin Akil and Norellia binti Bahari

Agrotechnology and Bioscience Division, Malaysian Nuclear Agency (Nuclear Malaysia), Ministry of Energy, Science, Technology, Environment and Climate Change (MESTECC), Bangi, Selangor, Malaysia
*Corresponding author's email: sawpeng@nm.gov.my
Received date: 14 March 2018 | Accepted date: 16 December 2019

ABSTRACT

Stevia rebaudiana has recently gained the attention of the food industry as one of the natural sweeteners. The sweet flavour is contributed by the glycoside compounds, especially the rebaudioside A and stevioside, which are the stevia main chemical markers. The aim of the work reported here was to compare the different extraction techniques of stevia leaves using different technologies such as the high pressure and ultrasonic on the extraction of steviol glycosides. In this paper, the extraction techniques yielding the highest glycosides from the leaves of *Stevia rebaudiana* were determined using hot water extraction (HWE), pressurised liquid extraction (PLE) and ultrasound-assisted extraction (UAE). The steviol glycoside yields were quantified by two chemical markers, rebaudioside A and stevioside of *Stevia rebaudiana* using high-performance liquid chromatography (HPLC) analysis. The result showed that the HWE managed to obtain 1,110 mg of steviol glycosides. The PLE obtained 294 mg steviol glycosides and the UAE obtained 427.5 mg steviol glycosides. As a conclusion, the results suggested the most efficient technique for stevia extraction in this study was the HWE.

Keywords: hot water extraction, pressurised liquid extraction, ultrasound-assisted extraction, steviol glycosides, rebaudioside A, stevioside

INTRODUCTION

Stevia rebaudiana Bertoni, belonging to the Asteraceae family, is a natural non-caloric sweetener native to Paraguay. Stevia contains 11 main steviol glycosides, namely, stevioside, rebaudioside A to F, rubusoside, steviolmonoside, steviolbioside, and dulcoside A, which are responsible for the typical sweet taste (Geuns, 2003). Although stevioside and rebaudioside A have similar chemical structures, they have significant differences in sweetness and taste quality (Wheeler et al., 2008). Stevioside tastes about 150 – 300 times and rebaudioside A tastes about 200 – 400 times sweeter than sucrose (Geuns, 2003). Stevia products are considered healthy and natural foods and have gained attention in the international markets (Gasmalla, Yang, Musa, Hua, & Ye, 2017) with China, India, Brazil, Korea, Mexico, United States, Indonesia, Tanzania, and Canada as producers (Ahmad, Khan, Hayee, & Nazir, 2014).

In the previous study, many methods such as ultrasonic-assisted extraction, pressurized hot water extraction, and acidified water extraction have been reported to separate steviol glycosides from *S. rebaudiana* (Liu, Li, Xu, & Zhou, 2007; Kootstra & Huurman, 2017; Kovačević et al., 2018). Among all these methods, the aqueous extraction of the stevia leaves was the most indicated choice and presents the highest yields of rebaudoside A and stevioside in the crude extract (Abou-Arab, Abou-Arab, & Abu-Salem, 2010; Chhaya, Mondal, Majumdar, & De, 2012a, 2012b; Mondal & Chhaya, 2012; Rao, Prasad, Sridhar, & Ravikumar, 2012; Periche, Koutsidis, & Escriche, 2014; Sardhara, 2015). This is because water is a universal solvent that can dissolve most substances than any other liquid. This makes water the primary extraction solvent used in most of the extracts.

In this study, we will compare the different aqueous phase extraction methods for the separation of steviol glycosides from stevia. Three commonly used extraction methods like hot water extraction, pressurised extraction and sonication extraction will be studied individually to see their effect on the bioactive molecules, leading to the recovery of glycosides from plant matrices (Roohinejad et al., 2017). We will determine the highest steviol glycosides yield from the leaves of *S. rebaudiana* using hot water extraction (HWE), pressurised liquid extraction (PLE) and ultrasound-assisted extraction (UAE).

The HWE is the most common method used for herbal extraction. In HWE, the stevia leaves are combined with water and are heated to 100°C. When the HWE process is complete, a highly concentrated solution combination of extracted stevia and water will be obtained. The PLE is innovated from HWE to reduce the energy consumption and processing time during extraction. Recently, PLE has become a popular green extraction method for different classes of compounds present in numerous kinds

of matrices such as environmental, food and botanical samples. PLE is an extraction technique that uses water as an extraction solvent at temperatures above the atmospheric boiling point of water (100°C/273 K, 0.1 MPa), but below the critical point of water (374°C/647 K, 22.1 MPa) (Plaza & Turner, 2015).

The ultrasound range used in the UAE is from 20 kHz to 2000 kHz (Handa, Khanuja, Longo, & Rakesh, 2008). Ultrasound creates an effect of acoustic cavitation which will increase the contact between solvents and substrate and permeability of cell walls. During the ultrasound, the plant properties are altered and disrupt the plant cell wall. It helps to release the compounds and increase the mass transport of the solvents into the plant cells (Dhanani, Shah, Gajbhiye, & Kumar, 2013). The UAE's advantages are mainly that it saves time and reduces the use of solvents in extraction. However, when more than 20 kHz of energy used in ultrasound, it will form free radicals that may affect the active phytochemicals in the plant (Handa et al., 2008; Kaufmann & Christen, 2002).

The stevia variety S10A used in the study was produced under the mutation breeding program using gamma irradiation in Gamma Greenhouse at the Malaysian Nuclear Agency in Malaysia. The S10A stevia variety showed significantly increased biomass with shorter internode distance between the leaves compared to the control stevia variety obtained from the Malaysian Agricultural Research and Development Institute (MARDI). Moreover, the S10A variety is more adapts to the local climate compared to the control (Ahmad et al., 2018)

MATERIALS AND METHODS

Materials

Stevia rebaudiana variety S10A produced through mutation breeding using gamma irradiation in the Malaysian Nuclear Agency was planted by Duta Nusajaya Sdn. Bhd. in Penampang, Sabah, Malaysia. The fresh leaves were harvested, washed and dried at 40°C for 24 h then were powdered to 20 – 30 mm mesh size and stored at room temperature for further use (Figure 1).

Macroporous resin AB-8 was purchased from Bengbu Dong Li Chemical Co. Ltd (China). Their physical properties were listed in Table 1. They were pre-treated by dipping them in ethanol for 48 h, then washing with ultrapure water thoroughly to remove the monomers and porogenic agents trapped inside the pores during the synthesis process.

Figure 1 Stevia fresh leaves, dried leaves, and stevia leave powder sieved through 20 – 30 mm mesh size that were used in the study

Table 1 The physical properties of macroporous resin AB-8

Resin type	Functional group	Average pore (nm)	Particle diameter (mm)	Polarity
AB-8	Polystyrene	13 – 14	0.3 – 1.25	Low polarity

Ferrous sulphate and calcium oxide were obtained from Fisher Scientific (UK). Activated charcoal was obtained from Duchefa Biochemie (Netherland). Stevia standard, rebaudioside A and stevioside were purchased from Sigma-Aldrich (Germany).

Methods

Hot Water Extraction (HWE)

The hot water extraction was performed based on Anvari and Khayati (2016) method, with some modification using a heating mantle. Approximately 40 g of stevia leaves were powdered to 20 – 30 mm mesh size and were boiled in 4 L soft water for 1 h. The crude extract was collected after cooled down and the remaining stevia powder was boiled in another 4 L soft water for 1 h. The boiling process was repeated for 3 times, each time 4 L of soft water was added. After the boiling process, the crude extract was concentrated at 100°C to a final volume of 3 L (Anvari & Khayati, 2016). The crude extract was cooled down and pH was adjusted to 10 by adding sodium hydroxide. Approximately 2 g of ferrous sulphate and 1 g of calcium oxide were added to 100 mL of crude extract and mixed for 1 h for the chemical treatment process. The crude extract was allowed to stand for 4 h to fully precipitate the impurities. A yellowish solution was obtained after the flocculation. The solution was filtered through a press filter and adjusted to pH 7 by adding hydrochloric acid. During the decolourisation

process, 10 g of activated charcoal was added to 1 L of crude extract and mixed for 1 h. A transparent solution was obtained by removing the activated charcoal through ultra-filtration (Davis, 2001).

Pressurised Liquid Extraction (PLE)

The pressurised liquid extraction was performed based on Plaza and Turner (2015), with some modification using steriliser HVE-50 (Hirayama). Approximately 40 g stevia leaves were powdered to 20 – 30 mm mesh size. The crude extract was extracted in aqueous solution (1:20) adjusted pH 3 and heated at 60°C with agitation for 6 h. After that, the crude extract was subjected to the pressurised liquid extractor at pressure 100 kPa and temperature 110°C for 10 min (Plaza & Turner, 2015). The crude extract was cooled down and filtered to collect the supernatant. The crude extract was adjusted to pH 10 by adding sodium hydroxide and heated to 60°C for 1 h. Approximately 2 g of ferrous sulphate and 1 g of calcium oxide were added to 100 mL of cooled crude extract and mixed for 1 h for the chemical treatment process. The crude extract was allowed to stand for 4 h to fully precipitate the impurities. A yellowish solution was obtained by removing the precipitates through a press filtration process. The solution was adjusted to pH 7 by adding hydrochloric acid. During the decolorisation process, 10 g of activated charcoal was added to 1 L of crude extract and mixed for 1 h. A transparent solution contained steviol glycosides were obtained by removing the activated charcoal through ultra-filtration (Davis, 2001).

Ultrasound-Assisted Extraction (UAE)

The ultrasound-assisted extraction was performed based on Tang-Bin, Wang, Gan, and Ling (2011), with some modification using Sonicator 4000 (Misomix). Approximately 40 g stevia leaves were powdered to 20 – 30 mm mesh size. The crude extract was extracted in aqueous solution (1:20) adjusted pH 3 and heated at 60°C with agitation for 6 h. After that, the crude extract was sonicated at 68°C, with sonic power (60 W) for 32 min (Tang-Bin et al., 2011). The crude extract was cooled down and filtered to collect the supernatant. The crude extract was adjusted to pH 10 by adding sodium hydroxide and heated to 60°C for 1 h. Approximately 2 g of ferrous sulphate and 1 g of calcium oxide were added to 100 mL of cooled crude extract and mixed for 1 h for the chemical treatment process. The crude extract was allowed to stand for 4 h to fully precipitate the impurities. A yellowish solution was obtained by removing the precipitates through the press filtration process. The solution was adjusted to pH 7 by adding hydrochloric acid. During the decolourization process, 10 g of activated charcoal was added to 1 L of crude extract and mixed for 1 h. A transparent solution contained glycosides was obtained by removing the activated charcoal through ultra-filtration (Davis, 2001).

High-Performance Liquid Chromatography (HPLC)

The transparent solution extracted from each method that contained steviol glycosides was analyzed using HPLC by comparing it to the standard rebaudioside A and stevioside. Rebaudioside A and stevioside were used as the marker compounds in this study. This is because rebaudioside A and stevioside are the major compounds among the 11 steviol glycosides, both of the compounds added up to more than 75% of the total steviol glycosides in stevia extract. Moreover, rebaudioside A has the best quality for sweetness amongst the other steviol glycosides, close to that of glucose (Chatsudthipong & Muanprasat, 2009). The HPLC conditions used in the study is shown in Table 2.

Table 2 HPLC conditions used for the steviol glycosides analysis.

Column	Agilent ZORBAX Carbohydrate Column 4.6 × 250 mm, 5 µm
Mobile Phase A	Water 20%
Mobile Phase B	Acetonitrile 80%
Injection	5 µL volume
Flow rate	1.0 mL/min (isocratic analysis)
Column temperature	30°C temperature
Detector	DAD Detection @ 205 nm, 4 nm BW; Ref: No; PW > 0.25 s (20 Hz)
Equipment	Agilent Technologies Infinity 1260 Quat pump, DAD, TCC, Autosampler.

RESULTS AND DISCUSSION

Water is a universal solvent that can dissolve most of the compounds than other liquid. Besides, water is a polar solvent and their molecules are attracted to other polar molecules, such as those of glycosides. This explains why stevia compounds have such a high solubility in water. In this study, aqueous-based extraction was chosen to investigate the difference between 3 types of extraction technique used for stevia. The results in Figure 2 showed that steviol glycosides were successfully extracted from all 3 aqueous extraction techniques; HWE, PLE, and UAE (Table 3). With 40 g stevia leaves as the extraction material, a total of 1110 mg steviol glycosides containing 887.5 mg rebaudioside A and 222.5 mg stevioside were extracted using the HWE technique (Figure 3). In PLE, 294 mg steviol glycosides contained 247.5 mg rebaudioside A and 46.5 mg stevioside were extracted under pressurised conditions (Figure 4). In UAE, 427.5 mg steviol glycosides containing 380 mg rebaudioside A and 47.5 mg stevioside were extracted under ultrasonic conditions (Figure 5). HWE technique is known as the conventional technique that uses water as the solvent and is carried out generally at

atmospheric pressure. In HWE, stevia leaves were packed in a still compartment and water was added in a sufficient amount and then brought to boil. Hot water acted as the main influential factor in free glycoside compounds of plant tissue (Azmir et al., 2013). During the HWE process, the water moved into the solid plant material and solubilised the glycoside compounds with similar polarity then extracted it from the plant (Amita & Shalini, 2014).

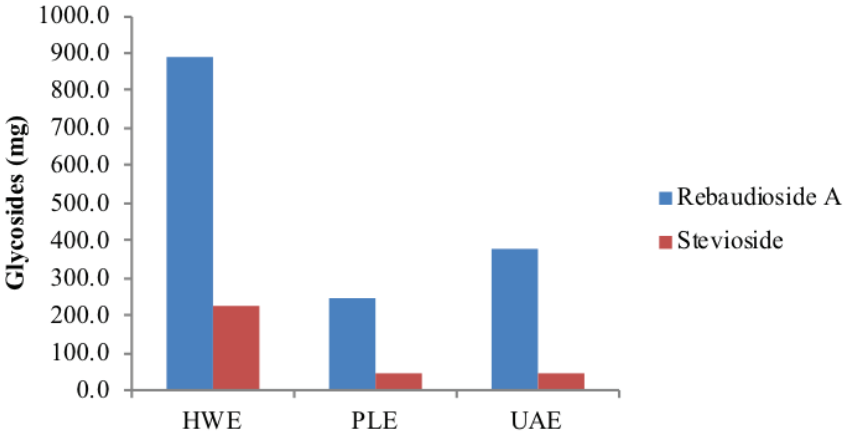

Figure 2 Glycosides yields of *S. rebaudiana* using different extraction techniques

Table 3 Analysis of means and standard deviations of rebaudioside A and stevioside using different extraction techniques

	Rebaudioside A (mg)			Mean	Standard deviation	Stevioside (mg)			Mean	Standard deviation
	1	2	3			1	2	3		
HWE	865.5	910.0	887.0	887.5	22.25	254.0	210.5	203.0	222.5	27.54
PLE	297.0	215.5	230.0	247.5	43.48	45.0	41.0	53.5	46.5	6.38
UAE	352.5	375.5	412.0	380.0	30.00	42.0	48.5	52.0	47.5	5.07

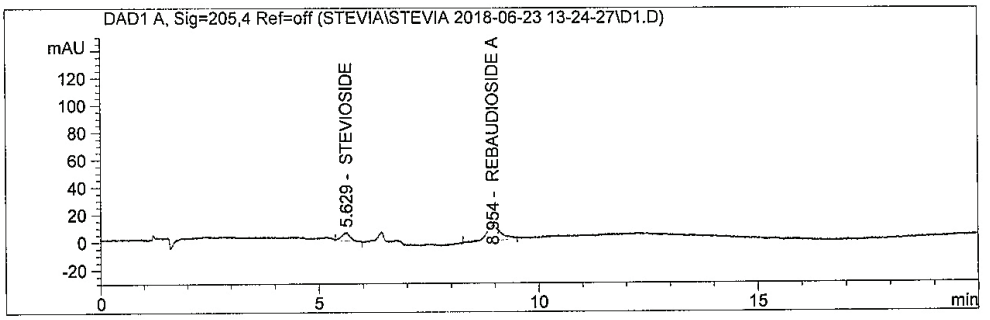

Figure 3 HPLC chromatogram of the rebaudioside A and stevioside extracted using HWE technique

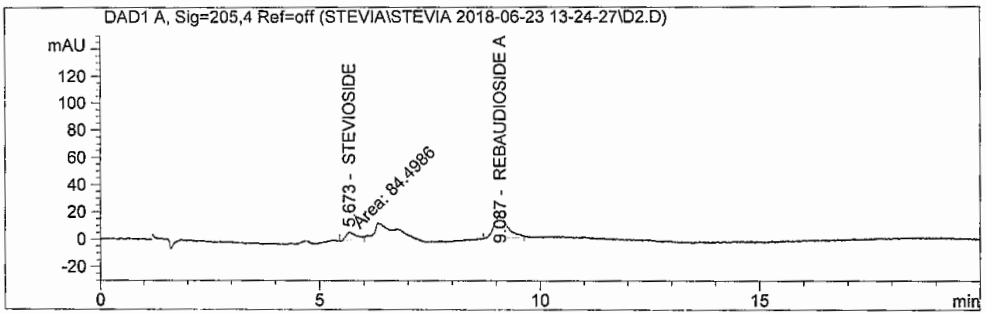

Figure 4 HPLC chromatogram of the rebaudioside A and stevioside extracted using PLE technique

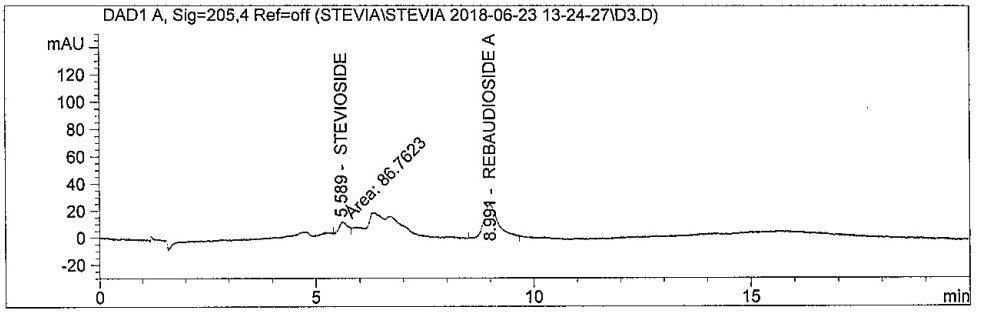

Figure 5 HPLC chromatogram of the rebaudioside A and stevioside extracted using UAE technique

New extraction techniques have been invented due to the need for novel methods of extraction enabling accelerating and shortening extraction times, efficient extraction, automation, and reduction of organic solvent consumption (Rafiee, Jafari, Alami, & Khomeiri, 2011). Two types of new extraction techniques, PLE and UAE were studied and compared to HWE in this study. In the PLE study, water was used as the solvent at elevated temperatures and pressures. During the PLE process, the water condition inside the PLE cell approached the supercritical region which resulted in more efficient extraction. The elevated temperature (110°C) allowed the stevia powder to become more soluble and achieve a higher diffusion rate by increasing the kinetics of the extraction process while the elevated pressure (100 kPa) kept the solvent below its boiling point to maintain the solvent in the liquid state. At elevated pressures and temperatures, water can penetrate stevia powder more efficiently (Raut et al., 2015). UAE is an extraction technique using ultrasound which is attributed to the effect of acoustic cavitation produced in the water by the passage of an ultrasound wave. In this study, ultrasound exerted a mechanical effect through ultrasonic waves that caused the physical and chemical properties of the material subjected to ultrasound were altered and disrupted the plant cell wall. It allowed greater penetration of water into

the tissue and facilitated the release of compounds by increasing the contact surface area between the compounds and water. It enabled the compounds to diffuse quickly from the solid phase to the water (Zhang, Chen, Shi, & He, 1998; Dhanani et al., 2013).

Previous studies always asserted higher yields by PLE and UAE than HWE for bioactive compounds extraction from a plant (Huang & Ning, 2010; Li, Wang, Wang, Walid, & Zhang, 2012). However, our study demonstrated that PLE and UAE can potentially produce lower steviol glycosides yield than HWE. Among the 3 aqueous extraction techniques, HWE showed the highest amount in extracted steviol glycosides (1,110 mg) followed by UAE (427.5 mg) and PLE (247.5 mg) (Figure 2). Although the PLE and UAE techniques have advantages in extracting the compounds at elevated pressure and temperature or altered and disrupted the plant cell wall, it did not show a significant increase in steviol glycosides yield. The HWE with the continuous boiling effect at 100°C had yielded remarkably different on steviol glycosides content compared to PLE and UAE. These phenomena suggested that PLE and UAE likely resulted in the degradation of certain glycosides in stevia. PLE and UAE might degrade these steviol glycosides and thereby change their bioactivities, which deserves further investigation. In other words, the elevated pressure and temperature of PLE and powerful energy input of UAE might collectively contribute to the differences between PLE and UAE-obtained steviol glycosides and those obtained by HWE.

CONCLUSION

The study showed that the most efficient technique for stevia extraction is the HWE compared to PLE and UAE. The conventional HWE technique has been practised for decades with satisfying results and once again proved its efficiency in this study. Moreover, water is a cheap, safe and abundant solvent. Therefore, water is the universal solvent used mostly in bioactive plant compounds extraction.

ACKNOWLEDGEMENTS

This research was partially supported by research fund (Technofund TF0614D122) granted by the Ministry of Energy, Science, Technology, Environment and Climate Change (MESTECC), Malaysia. We thank Norazlina Noordin from Malaysian Nuclear Agency and our industry collaborator, Duta Nusajaya Sdn. Bhd. provided stevia raw material for the experiment.

REFERENCES

Abou-Arab, A. E., Abou-Arab, A. A., & Abu-Salem, M. F. (2010). Physico-chemical assessment of natural sweeteners steviosides produced from Stevia rebaudiana Bertoni plant. *African Journal of Food Science*, *4* (5), 269 – 281.

Ahmad, F., Ahmad, Z., Hassan, A. A., Ariffin, S., Noordin, N., Salleh, S., ... & Rahim, K. A. (2018). A Review on Gamma Greenhouse as a Chronic Gamma Irradiation Facility for Plant Breeding and Improvement Program. *Jurnal Sains Nuklear Malaysia*, *30* (1), 8 – 18.

Ahmad, S., Khan, F. A., Hayee, A., & Nazir, M. S. (2014). A Review on potential toxicity of artificial sweetners vs safety of stevia: A natural bio-sweetner. *Journal of Biology, Agriculture and Healthcare*, *4* (15), 1 – 12.

Amita, P., & Shalini, T. (2014). Concept of standardization, extraction and pre phytochemical screening strategies for herbal drug. *Journal of Pharmacognosy and Phytochemistry*, *2* (5), 115 – 119.

Anvari, M., & Khayati, G. (2016). Separation and purification of rebaudioside A from extract of *Stevia Rebaudiana* leaves by macroporous adsorption resins. *Polish Journal of Chemical Technology*, *18* (1), 127 – 132.

Azmir, J., Zaidul, I. S. M., Rahman, M. M., Sharif, K. M., Mohamed, A., Sahena, F., ... & Omar, A. K. M. (2013). Techniques for extraction of bioactive compounds from plant materials: A review. *Journal of Food Engineering*, *117* (4), 426 – 436.

Chatsudthipong, V., & Muanprasat, C. (2009). Stevioside and related compounds: therapeutic benefits beyond sweetness. *Pharmacology & Therapeutics*, *21*, 41 – 54.

Chhaya, C. S., Mondal, S., Majumdar, G. C., & De, S. (2012a). Clarification of Stevia extract by ultrafiltration: selection criteria of the membrane and effects of operating conditions. *Food and Bioproducts Processing*, *90* (3), 525 – 532.

Chhaya, C. S., Mondal, S., Majumdar, G. C., & De, S. (2012b). Clarification of stevia extract using cross flow ultrafiltration and concentration by nanofiltration. *Separation and Purification Technology*, *89*, 125 – 134.

Davis, S. B. (2001). The chemistry of colour removal: a processing perspective. *Proceedings* of the *South African Sugar Technologists' Association* 75, pp. 328 – 336.

Dhanani, T., Shah, S., Gajbhiye, N. A., & Kumar, S. (2017). Effect of extraction methods on yield, phytochemical constituents and antioxidant activity of Withania somnifera. *Arabian Journal of Chemistry*, *10*, S1193 – S1199.

Gasmalla, M. A. A., Yang, R., Musa, A., Hua, X., & Ye, F. (2017). Influence of sonication process parameters to the state of liquid concentration of extracted rebaudioside A from Stevia (Stevia rebaudiana Bertoni) leaves. *Arabian Journal of Chemistry*, *10* (5), 726 – 731.

Geuns, J.M.C. (2003). Molecules of interest stevioside. Phytochemistry 64, 913–921.

Handa, S. S., Khanuja, S. P. S., Longo, G., & Rakesh, D. D. (Eds.). (2008). *Extraction technologies for medicinal and aromatic plants*. Trieste, Italy: ICS-UNIDO.

Huang, S., & Ning, Z. (2010). Extraction of polysaccharide from *Ganoderma lucidum* and its immune enhancement activity. *International Journal of Biological Macromolecules*, *47*, 336 – 341.

Kaufmann, B., & Christen, P. (2002). Recent extraction techniques for natural products: microwave-assisted extraction and pressurized solvent extraction. *Phytochemical Analysis*, *13*, 105 – 113.

Kootstra, A. M. J., & Huurman, S. (2017). *Extraction of steviol glycosides from fresh Stevia using acidified water; comparison to hot water extraction, including purification* (Pagv-nr.; No. 722). Lelystad: Wageningen UR, PPO/Acrres.

Kovačević, D. B., Barba, F. J., Granato, D., Galanakis, C. M., Herceg, Z., Dragović-Uzelac, V., & Putnik, P. (2018). Pressurized hot water extraction (PHWE) for the green recovery of bioactive compounds and steviol glycosides from Stevia rebaudiana Bertoni leaves. *Food Chemistry*, *254*, 150 – 157.

Li, X., Wang, Z., Wang, L., Walid, E., & Zhang, H. (2012). Ultrasonic-assisted extraction of polysaccharides from Hohenbuehelia serotina by response surface methodology. *International Journal of Biological Macromolecules*, *51* (4), 523 – 530.

Liu, C., Li, L. S., Xu, L. L., & Zhou, Z. M. (2007). Separation and identification of stevioside and Rebaudiodside A in Stevia by HPLC. *Fenxi Shiyanshi (Chinese Journal of Analysis Laboratory)*, *26* (7), 23 – 26.

Mondal, S., & De, S. (2012). Prediction of ultrafiltration performance during clarification of stevia extract. *Journal of Membrane Science*, *396*, 138 – 148.

Periche, A., Koutsidis, G., & Escriche, I. (2014). Composition of antioxidants and amino acids in Stevia leaf infusions. *Plant Foods for Human Nutrition*, *69* (1), 1 – 7.

Plaza, M., & Turner, C. (2015). Pressurized hot water extraction of bioactives. *TrAC Trends in Analytical Chemistry*, *71*, 39 – 54.

Rafiee, Z., Jafari, S. M., Alami, M., & Khomeiri, M. (2011). Microwave-assisted extraction of phenolic compounds from olive leaves; a comparison with maceration. *Journal of Animal & Plant Sciences*, *21* (4), 738 – 745.

Rao, A. B., Prasad, E., Sridhar, G. R. S., & Ravikumar, Y. V. L. (2012). Simple extraction and membrane purification process in isolation of steviosides with improved organoleptic activity. *Advances in Bioscience and Biotechnology*, *3*, 327 – 335.

Raut, P., Bhosle, D., Janghel, A., Deo, S., Verma, C., Kumar, S. S., ... & Tripathi, D. K. (2015). Emerging Pressurized Liquid Extraction (PLE) techniques as an innovative green technologies for the effective extraction of the active phytopharmaceuticals. *Research Journal of Pharmacy and Technology*, *8* (6), 800 – 810.

Roohinejad, S., Nikmaram, N., Brahim, M., Koubaa, M., Khelfa, A., & Greiner, R. (2017). Potential of novel technologies for aqueous extraction of plant bioactives. In H. D. Gonzalez & M. J. G. Munoz (Eds.), *Water extraction of bioactive compounds: From Plants to drug development* (pp. 399 – 419). Amsterdam, Netherlands: Elsevier.

Sardhara, A. M. (2015). *Extraction, purification and formulation of extract from from natural product*. Mumbai, India: Institute of Chemical Technology. pp. 90.

Tang-Bin, Z., Wang, M., Gan, R. Y., & Ling, W. H. (2011). Optimization of ultrasound assisted extraction of anthocyanins from mulberry using response surface methodology. *International Journal of Molecular Sciences*, *12* (2), 3006 – 3017.

Wheeler, A., Boileau, A. C., Winkler, P. C., Compton, J. C., Prakash, I., Jiang, X., & Mandarino, D. A. (2008). Pharmacokinetics of rebaudioside A and stevioside after single oral doses in healthy men. *Food and Chemical Toxicology*, *46* (7), S54 – S60.

Zhang, Y., Chen, T. H., Shi, Z. Q., & He, B. L. (1998). Studies on the separation of Rebaudioside A by recrystallization. *Ion Exchange. Adsorption*, *14*, 515 – 520.

Borneo International Journal of Biotechnology (BIJB)
Vol. 1 (December 2020), 89 – 102

e-ISSN 2716-697X

Research Article

CHARACTERISATION OF AN ANTARCTIC YEAST, *Glaciozyma antarctica* PI12

Teoh Chui Peng, Koh Soon Peng and Clemente Michael Wong Vui Ling*

Biotechnology Research Institute, Universiti Malaysia Sabah, Kota Kinabalu, Sabah, Malaysia
*Corresponding author's email: michaelw@ums.edu.my
Received date: 23 December 2019 | Accepted date: 4 May 2020

ABSTRACT

Glaciozyma antarctica PI12 is a psychrophilic yeast isolated from Antarctica. It has an optimal growth in yeast peptone dextrose (YPD) and yeast mould (YM) broth media but not in potato dextrose (PD) broth medium. Early phase *G. antarctica* PI12 cells had elongated-shape and became oval-shaped as they aged. *G. antarctica* PI12 exhibited bipolar budding and formed a chain of cells during the lag and early exponential phases. The number of chains decreased as the yeast aged. It appeared mainly as a single cell at the stationary phase, and a small number of them still produced buds. Some cells at the stationary phase entered the quiescence state (G_0) as a long-term survival strategy. The *G. antarctica* PI12 cell size decreased when they entered the stationary phase. *G. antarctica* PI12 was found to produce hydrolytic enzymes, chitinase, cellulase, mannanase, and xylanase. A higher glucose concentration of 2% in the PD agar medium inhibited the activities of chitinase but not the cellulase, mananase and xylanase.

Keywords: cell morphologies, bipolar budding, yeast chain, quiescence state, hydrolytic enzyme, Antarctic yeast, *Glaciozyma* spp., enzyme activities, psychrophiles

INTRODUCTION

Psychrophiles live and grow well in extremely cold environments such as the Antarctic. Psychrophiles have attracted much attention due to their abilities to produce a variety of cold-active hydrolytic enzymes (Brenchley, 1996; Ramli et al., 2011; Ramli et al., 2013; Alias, Mazian, Salleh, Basri, & Rahman, 2014). *Glaciozyma antarctica*, previously

known as *Leucosporidium antarcticum* is a psychrophilic yeast isolated from sea-ice in Antarctica (Turchetti et al., 2011; Boo et al., 2013). The first *Glaciozyma* spp. (originally called *Leucosporidium, scottii L. capsuligenum, L. antarcticum, L. frigidum, L. gelidum, L. nivalis* and *L. stokesii*) are isolated from Antarctica and named by Fell, Statzell, Hunter, and Phaff (1969). Subsequently, researchers from Russia and Germany have isolated *L. antarcticum* from Peat bog (Golubev, Blagodatskya, Manukian, & Liss, 1981), and Willow Catkin, northeast Mecklenburg (Kockova-Kratochvilova, Wegener, & Ondrusova, 1972), respectively. In Antarctica, *G. antarctica* is isolated from Moss Cirque, Vestfold Hills, Davis Base (Turchetti et al., 2011), South Victoria Land (Connell et al., 2008), and Admiralty Bay, King George Island (Donachie, 1995).

G. antarctica strain PI12 was previously isolated from the sea ice sample collected in the vicinity of Casey station (Boo et al., 2013). It survived and grew well under extremely cold conditions making it an ideal simple eukaryotic cell for cold adaptation analysis as well as the source to clone cold-active enzymes. The cold-adaptation mechanisms of *G. antarctica* PI12 have been described by some researchers (Firdaus et al., 2018; Koh, Wong, Najimudin, & Mahadi, 2019; Wong, Boo, Voo, Zainuddin, & Najimudin, 2019). Several cold-active hydrolytic enzymes have been cloned from it and characterised (Ramli et al., 2011; Ramli et al., 2013; Alias et al., 2014). Despite being one of the most analysed Antarctic yeasts (Ramli et al., 2011; Ramli et al., 2013; Alias et al., 2014; Firdaus et al., 2018; Koh et al., 2019; Wong et al., 2019), the main general characteristics of *G. antarctica* PI12 such as cell morphologies, growth patterns and metabolic abilities remain unclear. These characteristics are important to compliment all the other scientific research on this Antarctic yeast in the future. Therefore, this study was conducted: (1) to determine the growth rate and performance, and the cell morphology, and (2) to determine its ability to degrade carboxymethyl cellulose (CMC), xylan, chitin and mannan.

MATERIALS AND METHODS

Strain and Culture Conditions

G. antarctica strain PI12 was identified by Boo et al. (2013) based on its large subunit (LSU) rRNA and internal transcribed spacer (ITS) sequences alignment to those in the National Centre for Biotechnology Information (NCBI) GenBank. It was routinely grown in Yeast peptone dextrose (YPD) broth medium and kept in 20% glycerol stock at −80°C for long term storage.

Growth Performance in Different Media

G. antarctica PI12 was grown in YPD, yeast mould (YM), and potato dextrose (PD) broth media at 12°C with shaking at 210 rpm to compare their suitability for growth. Three culture replicates were prepared for medium. The optical density of each culture at 600 nm was measured using a spectrophotometer at an interval of 24 hours until it reached the stationary phase according to the methods described by Boo et al. (2013).

Growth Study

G. antarctica PI12 was grown in YPD broth medium at 12°C with shaking at 210 rpm. Three replicates were prepared. The optical density of each culture at 600 nm was measured from day 0 until day 53. The reading for each replicate was determined by averaging the results of five readings.

Microscopic Analysis

The morphology of *G. antarctica* PI12 was examined using a compound Olympus light microscope and Hitachi scanning electron microscope (SEM). A 10 µL of the culture was transferred to a glass slide and subjected to Gram-staining using standard microbiology protocol. It was viewed under a light microscope under a 400× magnification. In a separate analysis, 20 µL of yeast cell was fixed using 5% glutaraldehyde in 0.1 M phosphate buffer (pH 7.2) at 4°C for 15 minutes. After fixation, the sample was centrifuged at 4,500 rpm for 1 minute. The supernatant was discarded, and the pellet was washed twice with 0.05 M phosphate buffer. The specimen was dehydrated in a series of ethanol (35%, 50%, 95%, and 99.8% (v/v)). The recovered cell pellet was resuspended in 35% (v/v) ethanol and centrifuged at 4,500 rpm for 1 minute. The supernatant was discarded. Dehydration steps were repeated two times with 50, 95, and lastly with 99.8 % (v/v) ethanol. The sample was centrifuged at 4,500 rpm for 1 minute between each dehydration step. The supernatant was discarded, and the pellet was suspended in 1 – 2 mL of hexamethyldisilazane (HMDS) for 5 minutes. HMDS was decanted after centrifugation and the pellet was dried overnight. The dried specimen was mounted onto an SEM specimen metal stub using double-sided sticky tape, coated with gold and viewed under SEM (Pueschel, 2013).

Cell Size Measurement

The length, diameter, and perimeter of *G. antarctica* PI12 measurements were carried out using Cell B software supplied together with the light microscope. Size measurements of 100, 1,800, and 4,000 lag, exponential and stationary phase cells respectively were taken. The average size of the measurements was calculated and recorded.

Metabolic Abilities

The metabolite abilities of *G. antarctica* PI12 were performed using the potato dextrose agar (PDA) and yeast mould agar (YMA) media containing 1 or 2% of glucose. Each of these media was supplemented with different carbon sources, 2.5% of hydrolysate chitin, 0.5% of carboxymethyl cellulose (CMC), 0.5% of guar, 0.2% of starch, or 0.5% of xylan. A 1 µL of yeast cell suspension grown to mid-log phase was inoculated onto the agar medium and incubated at 12°C for 14 days. The colonies were washed off from the agar medium with distilled water. The medium was stained with 1 mg/mL of congo red solution for 15 minutes and de-stained with 1 M sodium chloride (NaCl) for 15 minutes. A halo zone on the agar medium indicated that the substrate had been degraded (Carrasco et al., 2012).

RESULTS

Growth Performance in Different Media

The growth curve revealed that *G. antarctica* PI12 grew optimally in YPD and YM broth media (Figure 1) when compared to the PD broth medium. Nevertheless, YPD broth medium supported better cell growth than YM broth medium from the 72 hours of incubation and beyond.

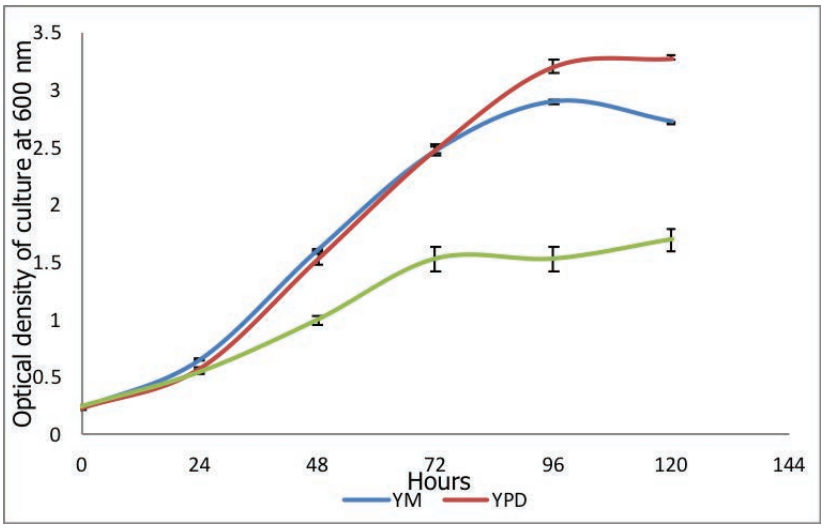

Figure 1 Growth curve of *G. antarctica* PI12 grown in YM, YPD, and PD broth media at 12°C

Growth Study

G. antarctica PI12 had a lag phase of about 3 days and entered the exponential growth phase from the 4th day until the 7th day and had a deceleration phase on the 8th day (Figure 2). The culture entered the stationary phase on the 9th day and remained at the stationary phase after that in the YPD medium.

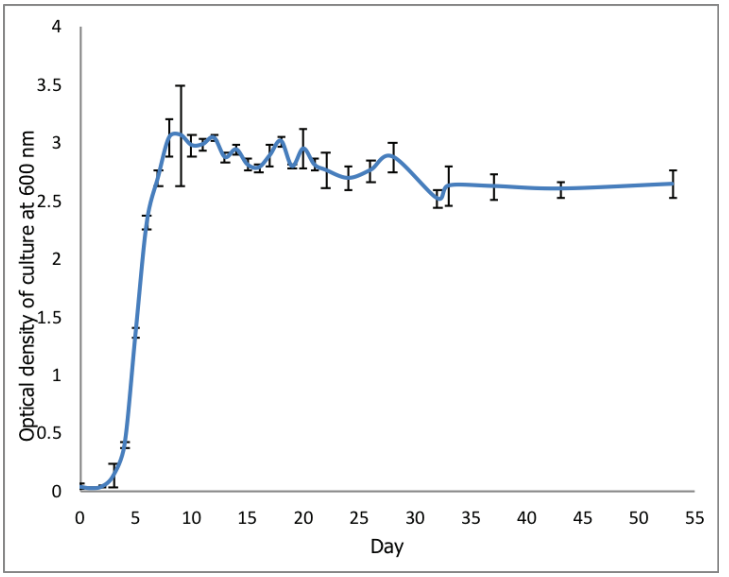

Figure 2 Growth curve of *G. antarctica* PI12 grown in YPD broth medium at 12°C

Microscopic Analysis

G. antarctica PI12 displayed different cell morphology at different growth stages. It formed elongated cells and in chains at the lag (2nd day) and early exponential phases (4th day) (Figure 3; Table 1). The number of yeast cells forming chains decreased as the cells aged. The cells had spherical, and ellipsoidal shapes with most cells having a single daughter cell at the stationary phase (19th day) (Figure 3). The cell surfaces were wrinkled and more obvious on the mother cells. The cells, especially the aged ones, were ellipsoidal (Figure 4). Bud scar was seen on the mother cells (Figure 4). Older cells or cells at the deceleration and stationary phases collapsed (Figure 5). The formation of yeast chains was observed in the SEM photos (Figure 5). *G. antarctica* PI12 exhibited a bipolar budding pattern, where buds were produced at both polar ends of a mother cell.

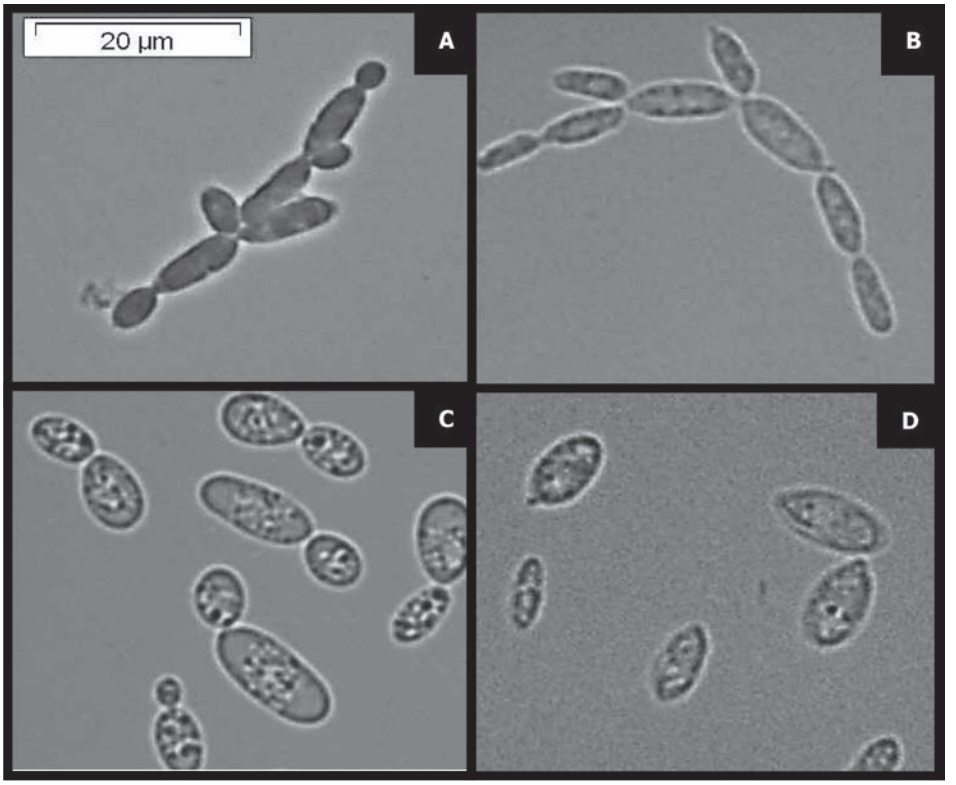

Figure 3 The morphology of *G. antarctica* PI12 was observed under a compound light microscope. Yeast cells were grown in YPD broth. Light microscope image taken at 400 times magnification. (A) Day 2 (lag phase), (B) Day 4 (exponential phase), (C) Day 8 (deceleration phase), and (D) Day 19 (stationary phase)

Table 1 Number of yeast cell chain at different growth phases

Day/ Phase	Number of yeast cell chain present per view under a light microscope (a)	Number of yeast present per view (b)	Ratio (a/b)	Comment
Lag (Day 2)	1	1	1	A small number of cells present, 8 cells yeast chain can be observed.
Exponential				
(Day 3)	5	5	1	As the culture aged, yeast chain formation decreases
(Day 4)	7	9	0.78	
(Day 5)	32	44	0.72	
(Day 6)	20	76	0.26	
(Day 7)	2	273	0.007	
Deceleration				
(Day 8)	1	252	0.004	
Stationary	–		–	No yeast chain was observed

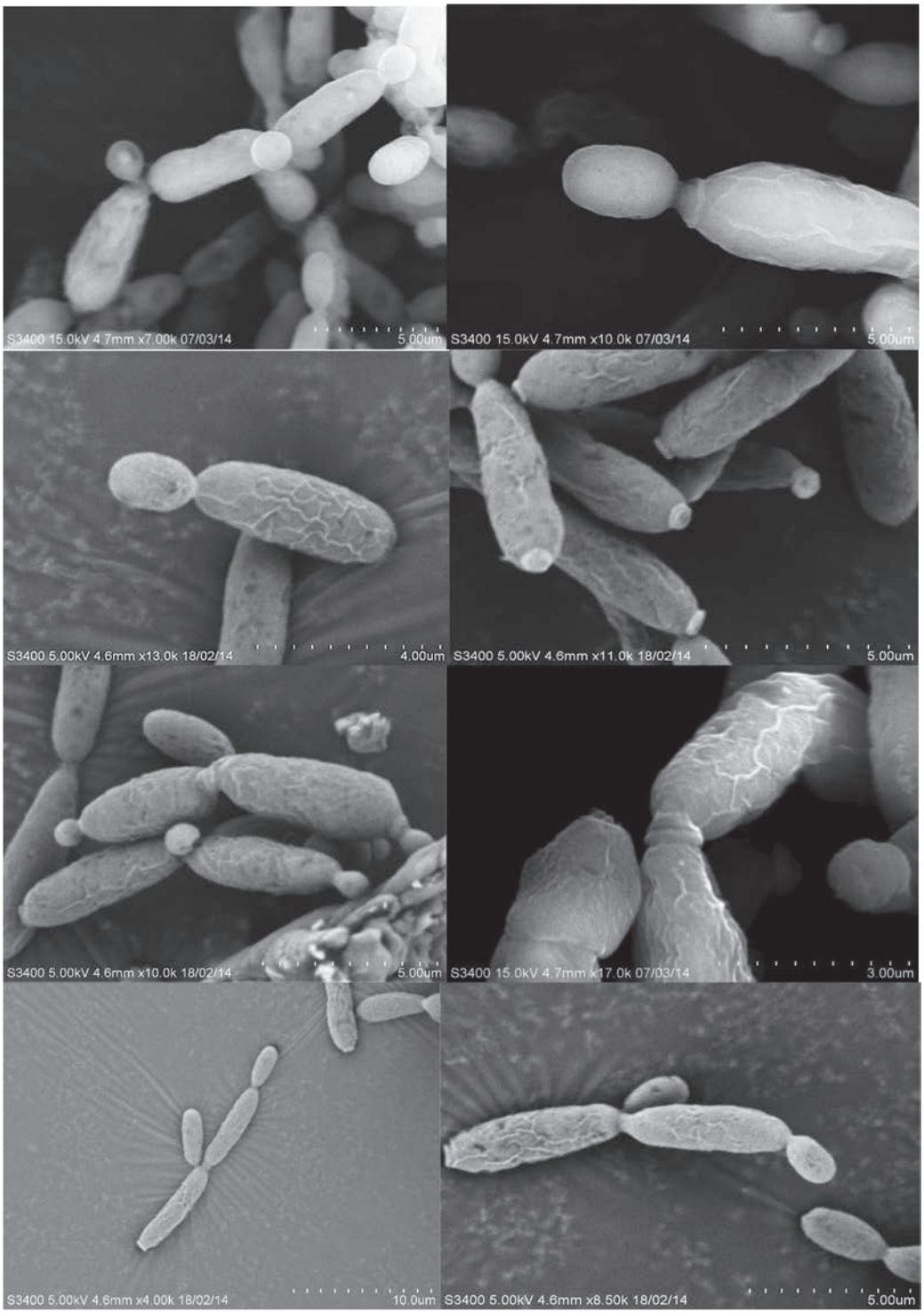

Figure 4 The morphology of *G. antarctica* PI12 at exponential phases under the SEM. *G. antarctica* PI12 was grown in YPD medium. The magnification of SEM is indicated on each photo (Days 3 and 5 yeast cells)

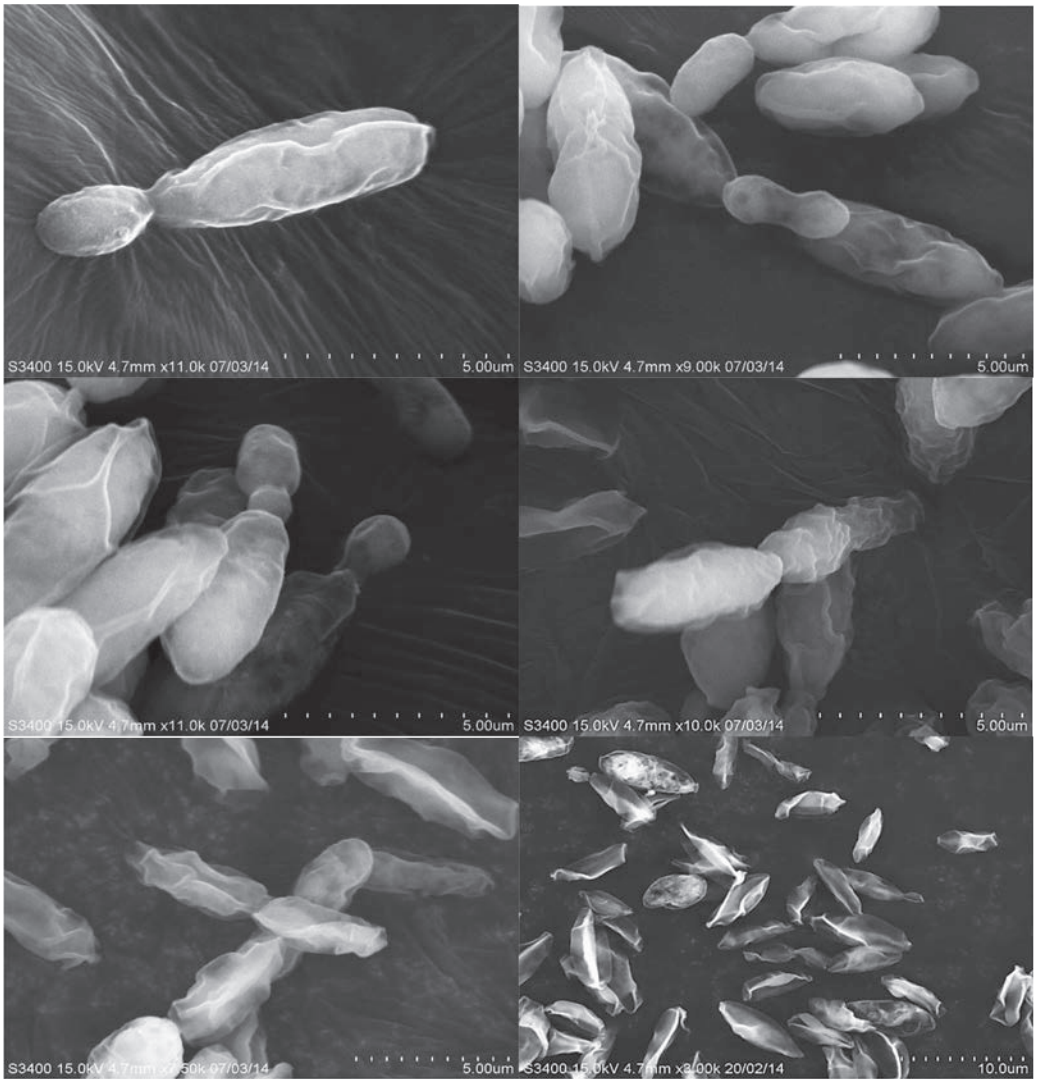

Figure 5 The morphology of *G. antarctica* PI12 at exponential phases under the SEM. *G. antarctica* PI12 was grown in YPD media. The magnification of SEM is indicated on each photo (Days 8, 11 and 32 yeast cells)

Cell Size Measurement

It was found that *G. antarctica* PI12 cell sizes gradually decreased from the lag phase to the stationary phase (Table 2). The average cell length at lag, exponential and stationary phases were 12.5, 11.2 and 10.5 µm, respectively. The average cell diameter at lag, exponential and stationary phases were 5.0, 4.8 4.7 µm respectively (Table 2).

The average bud length of lag, exponential and stationary phase cells ranged from 1.33 to 16.23, 0.99 to 14.7, 1.21 to 12.74, respectively (Table 3). The average bud diameter of lag, exponential and stationary phase cells ranged from 0.99 to 6.41, 0.87 to 7.63, 0.90 to 5.38, respectively (Table 3). Overall, the smallest bud was formed at the exponential phase while the largest bud was formed at the stationary phase (Table 3).

Table 2 Average cell size at different phases

Average mean ± SD / Phase	Length (µm)	Diameter (µm)	Area (µm²)	Perimeter (µm)
Lag phase	12.47±5.04	5.00±1.43	57.12±32.14	31.99±11.03
Exponential phase	11.21±4.65	4.78±1.73	48.54±28.98	28.96±10.14
Stationary phase	10.57±3.36	4.72±1.56	47.94±23.74	28.52±7.96

Table 3 Average range of bud size at different phases

Average range of bud size (µm) / Phase	Length	Diameter	Area
Lag Phase	1.33 – 16.23	0.99 – 6.41	3.84 – 76.82
Exponential Phase	0.99 – 14.72	0.87 – 7.63	1.11 – 79.55
Stationary Phase	1.21 – 12.74	0.90 – 5.38	1.67 – 54.15

Metabolic Abilities

G. antarctica PI12 exhibited chitinase, carboxymethyl cellulase (cellulase), mannanase, and xylanase activities by the formation of halos on chitin, CMC, guar gum and xylan media, respectively (Table 4). Similar results were observed in yeast grown on PDA containing 1% and 2% glucose and the assay substrates, except that mannanase activity was not detected. Also, the chitinase activity was suppressed when 2% of glucose was present in the PDA medium.

Table 4 Summary of the chitinase, CMCase (cellulase), mannanase, and xylanase activity of *G. antarctica* PI12. (+) = with activity; (–) = no activity; (±) = mild to low activity

Polysaccharides / Media	Chitin	CMC	Guar	Xylan
PDA (+1% glucose)	+	±	–	+
PDA (+2% glucose)	±	±	–	+
YMA (+1% glucose)	+	±	+	±
YMA (+2% glucose)	+	±	+	+

DISCUSSION

It is important to ensure that the yeast is growing in the most suitable medium when conducting experiments. According to Lodish et al. (2000), yeast can grow in a minimal broth medium containing glucose or dextrose as a carbon source, nitrogen, phosphorus, and trace metals. This was observed in the current study whereby *G. antarctica* PI12 was able to grow on PD, YPD and YM media (Figure 1). Nevertheless, it grew better in YPD and YM media when compared to the PD medium (Figure 1). YPD and YM media contained yeast extract and bacto-peptone that are richer in nutrient contents when compared to the potato dextrose medium ingredients. Overall, YPD is still a better growth medium for *G. antarctica* PI12 when compared to YM medium. Hence, YPD was used in several subsequent experiments to grow *G. antarctica* PI12.

G. antarctica PI12 is a relatively slow-growing yeast despite being incubated at its optimal growth temperature of 12°C (Boo et al., 2013), requiring 3 days exit lag phase. The overall slower growth rate was most probably due to the lower chemical reaction rates to maintain adequate metabolic fluxes at 12°C (Feller & Gerday, 1997). After the exponential stage, yeast cells usually enter the death phase, which is indicated by a decline in the OD readings. However, the OD_{600nm} readings of *G. antarctica* PI12 at the stationary phase remained almost constant until day 53 (Fig. 2). The extended stationary phase of *G. antarctica* PI12 suggested that the cells remained viable and intact. According to Gray et al. (2004), a long period of stationary phase suggests that *Saccharomyces cerevisiae* has probably entered an alternative (G_0) or resting state, where the cells entered non-proliferating state or exited from the normal cell cycle. This resting state is known as quiescence or G_0. Yeast is reported to enter quiescence or G_0 when growth conditions are unfavourable such as during starvation due to depleting nutrients (Wei, Nurse, & Broek, 1993) and the accumulation of toxic metabolites (Galdieri, Mehrotra, Yu, & Vancura, 2010). This implied that the long stationary phase exhibited by *G. antarctica* is very similar to other yeasts such as *Saccharomyces cerevisiae*.

Although *G. antarctica* PI12 shared some of the model yeast, *S. cerevisiae* growth properties, and produced off-springs through budding, their morphologies differed slightly. Unlike *S. cerevisiae* that is usually ellipsoidal and spherical, *G. antarctica* PI12 formed elongated cell, apart from the ellipsoidal and spherical cell. The production of daughter cells was almost always at the polar ends in *G. Antarctica* PI12 while *S. cerevisiae* budding sites are axial, polar and random (Saito et al., 2004; Vopálenská, Hůlková, Janderová, & Palková, 2015). *G. antarctica* PI12 exhibited bipolar budding, whereby the daughter cells arose at both ends of the elongated cell. According to Walker (1998), bipolar budding gives rise to the buds which are restricted at the ends or poles of the elongated cells along the longitudinal axis of the mother cells. Also, bipolar budding is not restricted to one cell at the end, which means that two or more buds may arise from the same pole at the same time.

Chain *G. antarctica* PI12 cell formation was observed at both lag and exponential phases. But the frequency gradually decreased as the culture aged in the late exponential phase from day 6 onwards. The formation of chain *G. antarctica* PI12 cells was not observed in the stationary phase (Figure 2; Table 1). According to Powell, Zandcyke, Quain, and Smart (2000), chain formation is a characteristic phenotype of some brewing yeast strain and the formation occurred due to ineffective separation between mother and daughter cells. Besides, complete separation between the mother-daughter cells is not necessary to continue reproduction (Powell et al., 2000). Chain of *G. antarctica* PI12 cells formation frequency decreased as the cells aged. This was due to the culture cell density increment, and the availability of the nutrient deceased. As a result, it was not able to support the cells to reproduce or divide. Additionally, cells do not actively reproduce or divide when culture entered stationary phase. The SEM electron micrograph showed similar structures to those taken using a light microscope but with more details. Wrinkled mother cells were observed under the SEM and this could be caused by the chemical used during the sample preparation steps, or it could be a normal morphology of the cell, but the latter possibility is higher. Figure 4 shows that the buds did not wrinkle even though they were exposed to the same sample preparation steps. According to Powell et al. (2000), as the cells age, the wrinkling on the cell surface increases to compensate for the decrease in the surface area.

The *G. antarctica* PI12 cell sizes were larger at lag and exponential phases than those at the stationary phase (Table 2 and Table 3). According to Turner, Ewald, and Skotheim (2012), budding and fission yeasts are coordinated to reach a certain size threshold during the cell-cycle before the cells can move to the next phase. In *Schizosaccharomyces pombe,* cell cycle arrest takes place at the G2-M phase transition while in *S. cerevisiae,* cell cycle arrest takes place at G1-S phase (Johnston, Pringle, & Hartwell, 1977). As a result, the arrested cell size increased to achieve the size threshold. Hence, the larger *G. antarctica* PI12 cell size at the lag phase was likely to be controlled similarly. Generally, cells grow rapidly on rich media divide at a larger

size when compared to cells growing slowly under poor nutrient conditions (Turner et al., 2012) such as *G. antarctica* PI12 which had larger cells initially at the lag and exponential phases. When nutrients in the medium were depleted at the stationary phase, smaller cells were formed.

G. antarctica PI12 lives in an environment with limited nutrient and carbon source. Hence, an organism with the ability to use a wider source of carbon will have an advantage to survive and grow when compared to others that do not. Interestingly, *G. antarctica* PI12 produced hydrolytic enzymes that degraded chitin, CMC, guar gum and xylan, indicating that it can utilize those substrates as carbon sources. However, the production of mannanase by *G. antarctica* PI12 occurred in the YMA medium but not in the PDA medium (Table 3). This indicated the starch in PDA medium suppressed mannanase but not the chitinase, carboxymethyl cellulase (cellulose), and xylanase production in *G. antarctica* PI12. Stoll, Stalbrand, and Warren (1999) reported the production of proteins with endo mannanase activity of *Cellulomonas fimi* decreases when glucose is present. However, this did not happen to *G. antarctica* PI12, although the inclusion of 2% of glucose into the PDA medium did reduce chitinase enzyme production. The overall results show that *G. antarctica* PI12 produced several hydrolytic enzymes to allow the cells to utilize complex types of the substrates, and glucose was not necessary the only primary source of carbon for its metabolism and energy.

CONCLUSION

Overall, we found that *G. antarctica* PI12 shared some of the characteristics of other yeasts, and at the same time has its unique properties such as its cell morphology and sizes at different phases of growth. These are probably the reasons why *Glaciozyma* spp. and *G. antarctica* PI12 specifically are so successful in inhibiting various low nutrient habitats such as Antarctica.

ACKNOWLEDGEMENTS

The funding support from the Ministry of Science, Technology, and Innovation (MOSTI), Malaysia, under the Antarctica Flagship Programme (Sub-Project 1: FP1213E036) is gratefully acknowledged.

REFERENCES

Alias, N., Mazian, A., Salleh, A. B., Basri, M., & Rahman, R. N. Z. R. A. (2014). Molecular cloning and optimization for high level expression of cold-adapted serine protease from Antarctic yeast *Glaciozyma antarctica* PI12. *Enzyme Research*, (2014), 1 – 20.

Boo, S. Y., Wong, C. M. V. L., Rodrigeus, K. F., Najimudin, N., Murad, A. M. A., & Mahadi, N. M. (2013). Thermal stress responses in Antarctica yeasts, *Glaciozyma antarctica* PI12, characterized by real-time quantitative PCR. *Polar Biology*, *36*, 381 – 389.

Brenchley, J. E. (1996). Psychrophilic microorganisms and their cold-active enzymes. *Journal of Industrial Microbiology*, *17* (5 – 6), 432 – 437.

Carrasco, M., Rozas, J. M., Baahona, S., Alcalno, J., Cifuentes, V., & Beaze, M. (2012). Diversity and extracellular enzymatic activities of yeasts isolated from King George Island, the sub-Antarctic region. *BMC Microbiology*, *12*, 251.

Connell, L., Redman, R., Craig, S., Scorzetti, G., Iszard, M., & Rodriguez, R. (2008). Diversity of soil yeasts isolated from South Victoria Land, Antarctica. *Microbial Ecology*, *56* (3), 448 – 459.

Donachie, S. P. (1995). *Ecophysiological description of marine bacteria from Admiralty Bay (Antarctica), and the digestive tracts of selected Euphausiidae* (Doctoral Thesis). Polish Academy Sciences, Warsaw.

Fell, J. W., Statzell, A. C., Hunter, I. L., & Phaff, H. J. (1969). *Leucosporidium* gen. n., the heterobasidiomycetous stage of several yeasts of the genus *Candida*. *Antonie van Leeuwenhoek*, *35* (1), 433 – 462.

Feller, G., & Gerday, C. (1997). Psychrophilic enzymes: Molecular basis of cold adaptation. *Cellular and Molecular Life Sciences CMLS*, *53* (10), 830 – 841.

Firdaus, R. M., Hashim, N. H. F., Bharudin, I., Bakar, M. F. A., Huang, K. K., Alias, H., … Tay, L. J. (2018). The *Glaciozyma antarctica* genome reveals an array of systems that provide sustained responses towards temperature variations in a persistently cold habitat. *PloS One*, *13* (1).

Galdieri, L., Mehrotra, S., Yu, S., & Vancura, A. (2010). Transcriptional regulation in yeast during diauxic shift and stationary phase. *Omics: A Journal of Integrative Biology*, *14* (6), 629 – 638.

Golubev, V. I., Blagodatskya, V. M., Manukian, A. R., & Liss, O. L. (1981). The yeast floras of peat (in Russia). *Izvestila Akademii Nauk SSSR, Serila Biologicheskaia*, 181 – 187.

Gray J. V., Petsko, G. A., Johnston, G. C., Ringe, D., Singer, R. A., & Werner-Washburne, M. (2004). "Sleeping Beauty": Quiescence in *Saccharomyces cerevisiae*. *Microbiology and Molecular Biology Review*, *68* (2), 187 – 206.

Johnston, G. C., Pringle, J. R., & Hartwell, L. H. (1977). Coordination of growth with cell division in the yeast *Saccharomyces cerevisiae*. *Experimental Cell Research*, *105* (1) 79 – 98.

Koh, J. S. P., Wong, C. M. V. L., Najimudin, N., & Mahadi, N. M. (2019). Gene expression patterns of *Glaciozyma antarctica* PI12 in response to cold, and freeze stress. *Polar Science*, *20*, 45 – 54.

Kockova-Kratochvilova, A., Wegener, K. A., & Ondrusova, D. (1972). Ein-Beitrag zur okologie der Hefen aus Nordost-Mecklenburg. *Mycopathologia Et Mycologia Applicata*, *48*, 191 – 212.

Lodish, H., Berk, A., Zipursky, S. L., Matsudaira, P., Baltimore, D., & Darnell, J. (2000). *Molecular cell biology* (4th edition). New York: W. H. Freeman.

Powell, C. D., Zandcyke, S. M. V., Quain, D. E., & Smart, K. A. (2000). Replicative ageing and senescence in *Saccharomyces cerevisiae* and the impact on brewing fermentations. *Microbiology*, *146*, 1023 – 1034.

Pueschel, M. (2013). SEM-Specimen preparation and techniques. Retrieved from http://australianmuseum.net.au/Specimen-preparation-and-techniques.

Ramli, A. N., Mahadi, N. M., Rabu, A., Murad, A. M., Bakar, F. D., & Illias, R. M. (2011). Molecular cloning, expression and biochemical characterisation of a cold-adapted novel recombinant chitinase from Gla*ciozyma antarctica* PI12. *Microbial Cell Factories*, *10* (1), 94.

Ramli, A. N., Azhar, M. A., Shamsir, M. S., Rabu, A., Murad, A. M. A., Mahadi, N. M., & Illias, R. M. (2013). Sequence and structural investigation of a novel psychrophilic α-amylase from *Glaciozyma antarctica* PI12 for cold-adaptation analysis. *Journal of Molecular Modeling*, *19* (8), 3369 – 3383.

Saito, T. L., Ohtani, M., Sawai, H., Sano, F., Saka, A., Watanabe, D., … Morishita, S. (2004). SCMD: *Saccharomyces cerevisiae* morphological database. *Nucleic Acids Research*, *32*, 319 – 322.

Stoll, D., Stalbrand, H., & Warren, R. A. J. (1999). Mannan-degrading enzyme from *Cellulomonas fimi*. *Applied and Environmental Microbiology*, *65* (6), 2598 – 2605.

Turchetti, B., Hall, S. R. T., Connell, L. B., Branda, E., Buzzini, P., Theelen, B., … Boekhout, T. (2011). Psychrophilic yeasts from Antarctica and European glaciers: Description of *Glaciozyma* gen. *nov.*, *Glaciozyma martinii sp. nov.* and *Glaciozyma watsonii sp. nov. Extremophiles*, *15* (5), 573 – 586.

Turner, J. J., Ewald, J. C., & Skotheim, J. M. (2012). Cell size control in yeast. *Current Biology*, *22* (9), 350 – 359.

Vopálenská, I., Hůlková, M., Janderová, B., & Palková, Z. (2005). The morphology of *Saccharomyces cerevisiae* colonies is affected by cell adhesion and the budding pattern. *Research in Microbiology*, *156* (9), 921 – 931.

Walker, M. (1998). *Yeasts physiology and biotechnology*. Chichester, UK: John Wiley and Son Ltd.

Wei, W., Nurse, P., & Broek, D. (1993). Yeast cells can enter a quiescent state through G1, S, G2, or M phase of the cell cycle. *Cancer Research*, *53* (8), 1867 – 1870.

Wong, C. M. V. L., Boo, S. Y., Voo, C. L. Y., Zainuddin, N., & Najimudin, N. (2019). A comparative transcriptomic analysis provides insights into the cold-adaptation mechanisms of a psychrophilic yeast, Glaciozyma antarctica PI12. Polar Biology, *42* (3), 541 – 553.

Borneo International Journal of Biotechnology (BIJB)
Vol. 1 (December 2020), 103 – 123

e-ISSN 2716-697X

Research Article

OPTIMISATION OF AN ELECTROCHEMICAL SENSOR BASED ON BARE GOLD ELECTRODE FOR DETECTION OF ALUMINIUM ION

Gilbert Ringgit[1], Shafiquzzaman Siddiquee[1*], Suryani Saallah[1] and Mohammad Tamrin Mohamad Lal[2]

[1]Biotechnology Research Institute, Universiti Malaysia Sabah, Kota Kinabalu, Sabah, Malaysia
[2]Borneo Research Marine Institute, Universiti Malaysia Sabah, Kota Kinabalu, Sabah, Malaysia
*Corresponding author's email: shafiqpab@ums.edu.my
Received date: 2 January 2020 | Accepted date: 22 May 2020

ABSTRACT

In this work, an electrochemical method for detection of trace amount of aluminium (Al^{3+}), a heavy metal ion, based on a bare gold electrode (AuE) was developed. Current responses of the AuE under various type of electrolytes, redox indicators, pH, scan rate and accumulation time were investigated using cyclic voltammetry (CV) method to obtain the optimum conditions for Al^{3+} detection. The sensing properties of the AuE towards the target ion with different concentrations were investigated using differential pulse voltammetry (DPV) method. From the CV results, the optimal conditions for the detection of Al^{3+} were Tris-HCl buffer (0.1 M, pH 2) supported by 5 mM Prussian blue with scan rate and accumulation time respectively of 100 mVs^{-1} and 15 s. Under the optimum conditions, the DPV method was detected with different concentrations of aluminium ion ranging from 0.2 to 1.0 ppm resulted in a good linear regression r^2 = 0.9806. This result suggests that the optimisation of the basic parameters in electrochemical detection using AuE is crucial before further modification of the Au-electrode to improve the sensitivity and selectivity especially for the low concentration of ion detection. The developed method has a great potential for rapid detection of heavy metal ion (Al^{3+}) in drinking water samples.

Keywords: electrochemical sensor, heavy metal, aluminium, cyclic voltammetry, differential pulse voltammetry

INTRODUCTION

Aluminium is the most abundant metal in the Earth's crust that can be found in a wide variety of chemical forms throughout the environment. Aluminium has been used tremendously in industrial applications for fabrication of electrical appliances, automobiles, building constructions, packaging materials, cooking utensils as well as for the development of vaccines (Mergu, Singh, & Gupta, 2015; Soni, White, Flamm, & Burdock, 2001; Baylor, Egan, & Richman, 2002). Besides, aluminium is a well-known flocculant in the water treatment system. The high amount of aluminium from human daily activities could be changed the amount of aluminium in the environment. The concentrated aluminium is entering the environment through the raining process. The pH of the rain is changed more to the acidic condition as aluminium high released into the air. As a result, acidic raining condition high amount of aluminium is saturated in natural water and biological systems (Tripathi et al., 2014; Manjumeena, Duraibabu, Rajamuthuramalingam, Venkatesan, & Kalaichelvan, 2015).

Excessive exposure to this metal element has been linked to serious health problems related to neurodegenerative and neurological disorders such as Alzheimer's disease (Rastogi, Dash, & Ballal, 2017), Parkinson's disease and dementia (Ramezani, Jahani, Mashhadizadeh, Shahbazi, & Jalilian, 2018), breast cancer (Kim, Angupillai, & Son, 2016) and other diseases like osteomalacia (Kim et al., 2016; Sarkar, Ghosh, Gharami, Mondal, & Murmu, 2017). Therefore, accurate determination and efficient monitoring of aluminium level in the food chain, especially the drinking water system has become increasingly important. An average safety level of weekly human body dietary intake of aluminium is 7 mg kg^{-1} body weight while the permissible level in drinking water is 0.2 ppm as per WHO guidelines (Diao et al., 2016; Fu et al., 2014; Barceló & Poschenrieder, 2002; WHO, 2008).

Several analytical methods for the aluminium detection in different matrices are available such as fluorescence method (Manjumeena et al., 2015), flame atomic absorption spectrometry (Altunay, Yıldırım, & Gürkan, 2018), graphite furnace atomic absorption spectrometry (Dravecz, Bencs, Beke, & Gali, 2016), flow injection/sequential injection analysis (Khanhuathon, Siriangkhawut, Chantiratikul, & Grudpan, 2015), inductively coupled plasma mass spectrometry (Silva et al., 2015), near-field enhanced atomic emission spectroscopy (Wang et al., 2018), inductively coupled plasma dynamic reaction cell mass spectroscopy (Skalny et al., 2018), UV-vis spectroscopy (Lima, Papai, & Gaubeur, 2018; Elečková, Alexovič, Kuchár, Balogh, & Andruch, 2015), neutron activation analysis (Mohseni et al., 2016) and high-performance liquid chromatography (Zioła-Frankowska, Kuta, & Frankowski, 2015). However, most of these methods are complicated, time-consuming, and required skilled operators to perform the *ex-situ* analysis (Ma, Yuan, Chai, & Liu, 2010; Rana, Mittal, Singh, Singh, & Banks, 2017; Suherman et al., 2018).

In recent years, electrochemical techniques for determination of aluminium are a subject of immense interest by researchers worldwide as a simple and rapid alternative to the aforementioned conventional methods. On top of that, an advanced method allowed for the fabrication of portable device via *in situ* analysis (Suherman et al., 2018; Ramezani et al., 2018). In electrochemical sensing, selection of suitable working electrode is important as it has a direct impact on the current formation. Among the various type of working electrodes for electrochemical sensing applications, gold electrode offers favourable characteristics in terms of electrocatalytic and conductive properties, good selectivity, high signal to noise ratio, and have been widely used for detection of varying heavy metal ions including ions of hexavalent chromium (Wu et al., 2019), arsenite (Wen, Wang, Yuan, Liang, & Qui, 2018), mercury (Yang et al., 2015), cadmium and lead (Xuan & Park, 2018; Gumpu, Veerapandian, Krishnan, & Rayappan, 2017) as well as zinc and manganese ions (Gilbert et al., 2018, Gilbert, Siddiquee, Saallah, & Tamrin, 2019). However, in most cases of electrochemical sensing based on Au-electrode, the electrode is simply used, modify and functionalised for detection of the target ion. As the current response obtained during the electrochemical measurement is highly influenced by various factors such as types of the electrolytic solution, redox indicators, pH, scan rates and accumulation times, investigation of the effect of these factors towards the current response is of great importance to obtain the optimum conditions that can give a good current response. To the best of our knowledge, there is no paper published on the optimisation of the electrochemical method for aluminium ion detection using a bare gold electrode.

MATERIALS AND METHODS

Chemicals for preparation of buffer including potassium hydrogen phosphate, potassium dihydrogen phosphate, sodium citrate dihydrate and sodium chloride were purchased from Systerm while sodium citrate dihydrate and citric acid anhydrous were obtained from Nacalai Tesque. The other buffer materials including hydrochloric acid, ammonium acetate and Tris-HCl were purchased respectively from J. T. Baker, Ajax Chemical and FIRST Base. The chemicals of redox indicator were obtained from Nacalai Tesque (potassium hexacyanoferrate (III) and potassium ferrocyanide (II) trihydrate), Systerm (methylene blue) and Sigma-Aldrich (iron (III) chloride). Aluminium sulphate as a target ion was obtained from Systerm.

Instrumentation

All electrochemical measurements were carried out using a potentiostat/galvanostat (PGSTAT) electrochemical workstation (Metrohm-Autolab B.V) with a standard three-electrode system consisting of a bare gold electrode, platinum wire and silver chloride as the working, counter and reference electrodes, respectively. Voltammograms obtained from the CV and DPV methods were analysed with NOVA Autolab 1.11 software. All experiments were conducted at a room temperature condition of 20 ± 2°C.

Pre-treatment of the Bare Gold Electrode

The bare AuE pre-treatment was conducted according to the method previously described by Siddiquee, Yusof, Salleh, Tan, and Bakar (2010). First, the working electrode (gold) was polished with alumina slurry (0.3 – 0.5 µm in diameter) for 2 minutes followed by subsequent cleaning and rinsing with distilled water. Then, the electrode was dried using nitrogen gas before submerged together with the counter electrode (platinum) and the reference electrode (silver chloride) in 3 M potassium chloride (KCl) solution. These three electrodes were used to measure the current flows through the electrolytic solution after applying the potential (external current).

Preparation of the Electrolytic Solutions

Five types of electrolytic buffer solutions were studied including acetate buffer (Chaiyo et al., 2016; Honeychurch, Rymansaib, & Iravani, 2018), phosphate buffer saline (Gholivand, Akbari, Faizi, & Jafari, 2017; Trachioti, Hrbac, & Prodromidis, 2018), citrate buffer (Gumpu et al., 2017), ammonium buffer (Ferancová, Hattuniemi, Sesay, Räty, & Virtanen, 2016) and Tris-HCl buffer (Ensafi, Amini, & Rezaei, 2013). The mentioned buffers were prepared in 0.1 M concentration. These buffers were widely used for the detection of heavy metal ions.

Preparation of the Redox Indicators

Three redox indicators including plusferocyanide ($[Fe(CN_6)]^{4-}$) (Peng et al., 2016), methylene blue (MB) (Ensafi et al., 2013) and Prussian blue (PB) (Wen et al., 2018) were investigated to 'boost' the current response and improve the performance of the bare AuE. These redox indicators were dropped onto the surface of the electrode and left for 2 minutes to allow attachment on the surface of the electrode. The concentrations of

all redox indicators were standardised to 5 mM for 10 µL. Then, these redox indicators were applied for the detection of aluminium ions. The combination of the matched buffer with redox indicator is shown in Scheme 1 with the current response.

Preparation of the Al^{3+} Analyte

The concentration of Al^{3+} was set at 0.2 ppm according to the standard drinking water quality by WHO (2008) and Engineering Service Division, Ministry of Health, Malaysia (2016). A 0.2 ppm of aluminium sulphate ($Al_2(SO_4)_3$) was diluted directly into 10 mL of buffer solution under 100 mVs^{-1} with potential volt ranging from 0.0 to 1.7 V for CV measurements. Five different buffers were tested at 0.2 ppm of Al in the presence of three redox indicators. For the DPV procedure, different concentrations of aluminium ion were detected from 0.2 to 1.0 ppm.

A 10 µL of (5 mM) redox indicator was dropped onto the surface of the Au electrode and left for 2 minutes. Then, the electrode was cleaned with Tris-HCl buffer solution before the electrochemical measurement. In this procedure, all electrodes (working electrode, the counter electrode and reference electrode) were submerged into 10 mL of buffer solution containing 0.2 ppm of aluminium ion. The setting of optimal electrochemical measurements such as the potential range from 0.0 V to 1.7 V; stop and start potential = 0.8 V; scan rate = 100 mVs^{-1} under 15 s of accumulation time. These measurements were determined through optimisation step using the CV method. The DPV method was performed at different concentrations of Al^{3+}.

RESULTS AND DISCUSSION

To obtain the best results for Al^{3+} detection using bare AuE, selection of electrochemical conditions including types of buffer and redox indicators, pH, scan rates and accumulation times are crucial as these conditions have a direct impact to the current signals during electrochemical measurement. Therefore, in this study, these parameters were studied and optimised using the CV method and applied for detection with different concentrations of Al^{3+} using the DPV method.

Selection of Buffer and Redox Indicator

Electrolytic solutions consisted of both the positively-charged (cation) and negatively-charged (anion) ions. Generally, the positive charge ion attracts to the negative terminal while the negative charge ion moves to a different direction (positive terminal). When an external force is applied in the form of potential, the current travels into different medium known as an electrolytic solution. The medium with the presence of the charged ions capable to conduct the electricity and exhibited the formation of current in the form of voltammogram graph.

In this study, five types of buffer were tested as electrolytic solution as these buffers have been used by other researchers for detecting varying heavy metal ions such as zinc (Honeychurch et al., 2018), cadmium (Trachioti et al., 2018; Gumpu et al., 2017), arsenite (Gumpu et al., 2017), lead (Tarley et al., 2017), mercury (Gumpu et al., 2017), nickel (Ferancová et al., 2016). Effect of the buffer towards the electrochemical detection of aluminium ion is depicted in cyclic voltammograms as shown in Figure 1. Tris-HCl buffer supported by 5 mM Prussian blue (PB) showed the highest peak current responses as compared to other buffers and redox indicators. The magnitude of oxidation almost twice was higher than that of the reduction which indicated that the two ion radicals were diffused onto the surface-active area by competition process (Rana et al., 2017).

The oxidation peak formed at 1.6130 V (3.6907 mA) while the reduction was formed at 0.4704 V with the current response of –0.9821 mA. The formations of the peak for all buffers are not in a position of potential range. All the peaks were shifting from one to another. This shifting of current responses was due to the diffusion of the aluminium ion on the surface of the bare AuE. Based on the current responses, Tris-HCl buffer supported by 5 mM Prussian blue was selected as an electrolytic solution for detection of Al^{3+}.

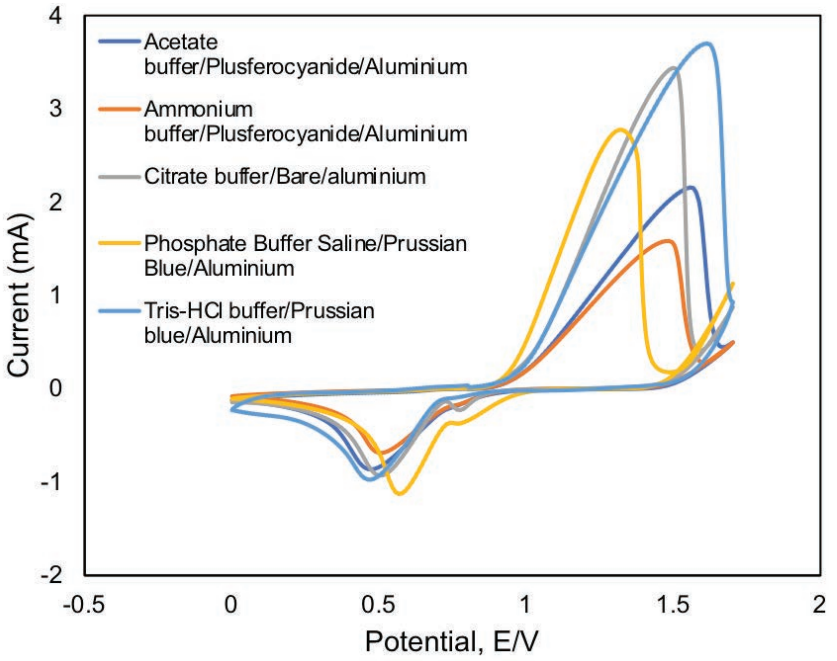

Figure 1 CV analysis of different buffers (0.1 M, pH 2) in the presence of 5 mM redox indicators. The buffers such as acetate buffer, ammonium buffer, citrate buffer, phosphate buffer saline and Tris-HCl buffer tested with potential range from 0.0 V to 1.7 V and 100 mVs^{-1} scan rates. The experimental work was repeated at least three times (n>3)

Effects of the Different pH Ranges

The influence of the pH of the electrolytic solutions on the detection of Al^{3+} was studied by CV in the presence of 0.2 ppm of Al^{3+} in 0.1 M Tris-HCl buffer supported by 5 mM Prussian blue, with pH values ranging from 2.0 to 9.0 (Figure 2A). The pH value was calibrated using either 1 M hydrochloric acid (HCl) or 1 M potassium hydroxide (KOH). The cyclic voltammograms were obtained under the potential ranged from 0.0 to 1.7 V.

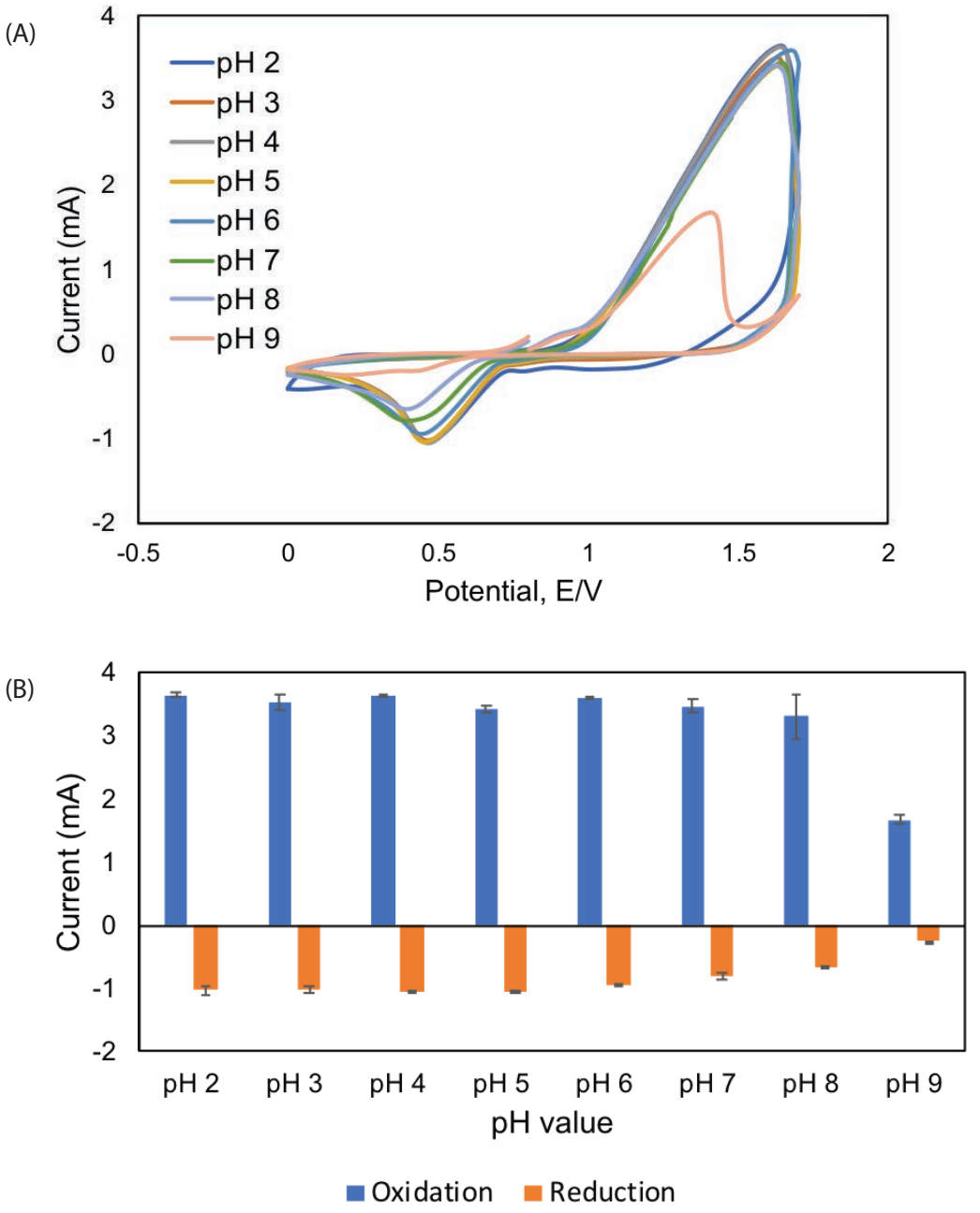

Figure 2 CV analysis for optimisation of the pH values for pH 2 to 9. The optimisation of pH was applied to 0.1 M Tris-HCl buffer supported by 5 mM Prussian blue in the presence of 0.2 ppm Al^{3+}. The graph of different pH values 2(A) and the comparison of oxidation and reduction peaks for every peak point formed on 2(B). The repetition of the experiment was conducted more than three times (n>3)

Based on Figure 2(A), there was no much different on the current response on oxidation and reduction reactions. Therefore, the comparison of the current response was evaluated based on the peak current responses by oxidation and reduction peak current signals in Figure 2(B). Oxidation and reduction peaks were formed with different potential ranged of 0.0 V to 1.7 V. Oxidation peaks were formed at more positive potential point at 1.6227 V to 1.6768 V while reduction closed to 0.0 V specifically potential point between 0.3947 V to 0.4655 V. At this potential, electron flowed at the highest potential rate as indicated by the highest peak signal before its declining to form a horizontal line where the equilibrium state of both oxidation and reduction current located. Overall, the oxidation peaks were always higher than the reduction peaks for all the pH value assay. At the reduction peak, pH 2 until pH 5, almost similar current responses were obtained. Above pH 5, the current responses were gradually decreased. As for the oxidation peak, at pH 2 to pH 8, the current responses were fluctuated and rapidly declining at pH 9. The pH 2 (Tris-HCl buffer) was selected as the optimal pH as both oxidation and reduction peak currents obtained maximum value.

Effects of Scan Rate

The effects of scan rate were evaluated using the CV method by adjusting the rate of current flow in the system in the electrochemical measurement. Electrochemical measurement for scan rate analysis was performed as 50 mVs^{-1}, 100 mVs^{-1}, 150 mVs^{-1} and 200 mVs^{-1} as shown in Figure 3(A). Based on Figure 3, the current signal getting higher as the scan rate adjusted at a higher value.

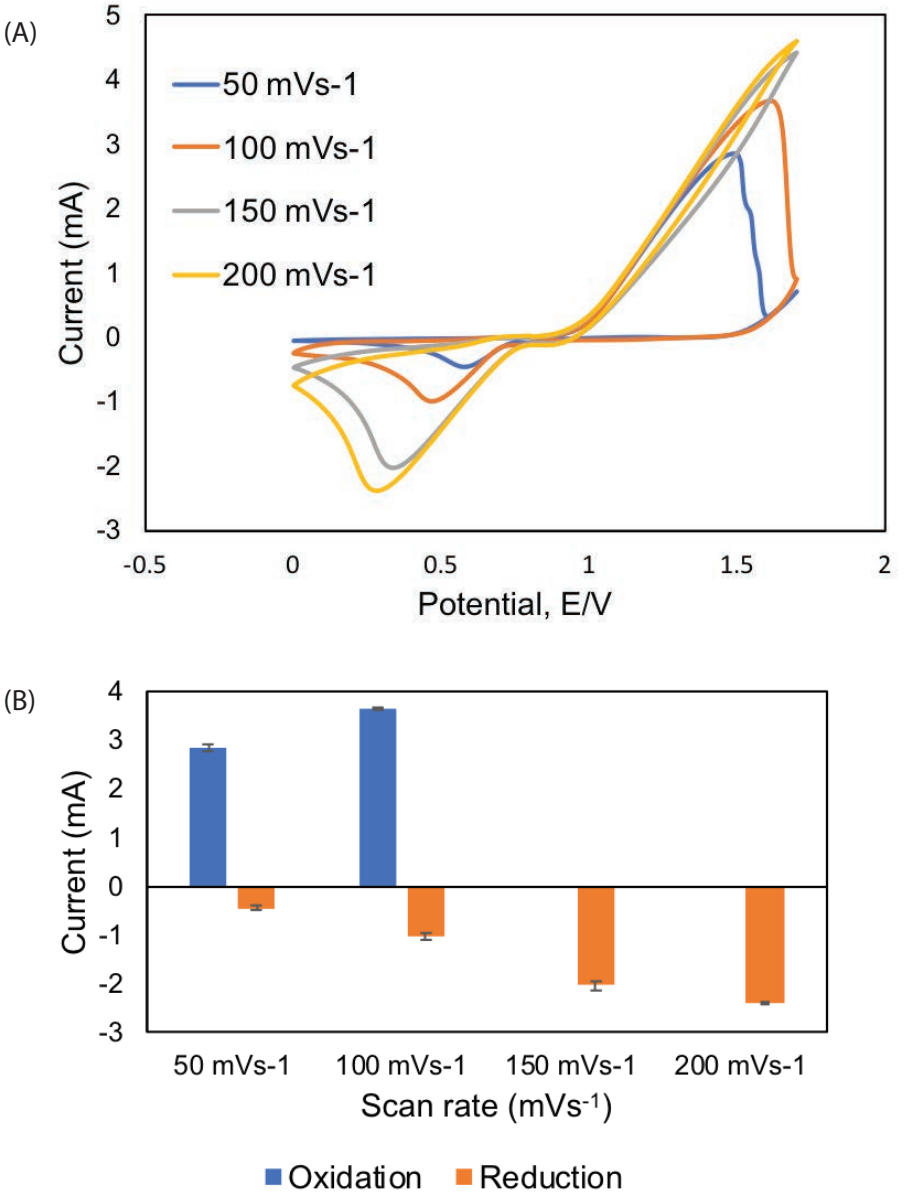

Figure 3 CV analysis for optimisation of scan rate from 50, 100, 150 and 200 mVs^{-1} for (0.1 M, pH 2) Tris-HCl buffer supported by 5 mM Prussian blue with the presence of 0.2 ppm Al^{3+}. The graph for different scan rates (A) and line graph of the comparison between oxidation and reduction potential peaks current response (B). This experiment was conducted more than three times (n>3)

This indicated that scan rate proportions to peak current signal. According to Suherman et al. (2018), this formation was due to surface controlled of bare AuE to aluminium ion based on the shifted graph. Absorption of the aluminium ion was depending on the speed of the current flow promoted by the scan rate. The faster the current flow, the higher the current response as shown by the 100 mVs^{-1} scan rate until overoxidation occurred when the scan rate above 100 mVs^{-1} was applied. Oxidation peaks with a scan rate of 150 mVs^{-1} and 200 mVs^{-1} were invalid due to the flat current response as the speed of the current increased. Despite the validity, the scan rate of 50 mVs^{-1} and 100 mVs^{-1} were left to compare. From Figure 3(B), it was seen that the 100 mVs^{-1} scan rate has higher oxidation and reduction peaks compared to the 50 mVs^{-1} scan rate. Therefore, 100 mVs^{-1} was chosen as the optimal scan rate for this study.

Effects of Accumulation Time

The effects of accumulation time on electrochemical detection of Al^{3+} was investigated using the CV method. Before analysis began, the accumulation time was applied to allow the current flow into the system first by generating the current to breakdown the chemical compounds into single radial ions such as cation and anion. These ions were transferred into the cathode and anode as a result of oxidation and reduction peaks current as shown in Figure 4(A). The range of accumulation was selected from 5 – 40 s. All the accumulation times showed not many different responses except for the 10 s, where the current response dropped drastically (Figure 4(B)).

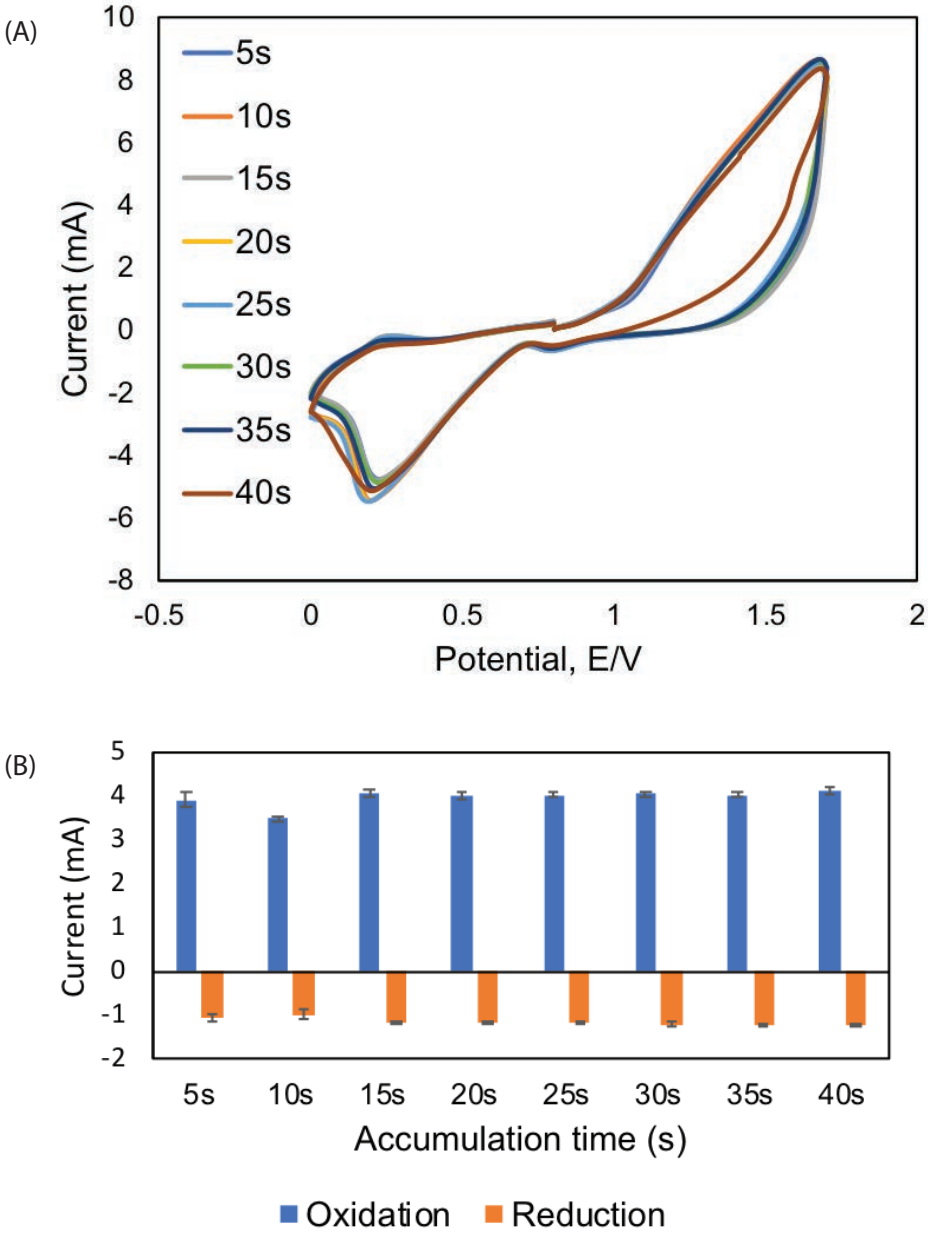

Figure 4 CV analysis for optimisation of the accumulation time from 5, 10, 15, 20, 25, 30 and 40 s for (0.1 M, pH 2) Tris-HCl buffer supported by 5 mM Prussian blue at the presence of 0.2 ppm aluminium under 100 mVs^{-1} of scan rate. The graph of different accumulation times (A) and the line graph for oxidation and reduction peaks formed by cyclic voltammogram. This experiment was conducted at least three times (n> 3)

At this accumulation time, the lowest current response at oxidation and reduction peaks were obtained as compared to the other accumulation times. Theoretically, this factor might be due to the net charge concentration and surface-active site. According to the Nernst-Planck equation:

$$\frac{\partial C_i}{C_t} + \vec{\mu} \cdot \nabla C_i \left(\nabla \cdot \vec{\mu}_i\right) = D_i \nabla^2_{C_i}$$

Where is the electric current, is the diffusion coefficient, gradient concentration and is ionic strength. When the current as experiencing momentum due to diffusion coefficient and gradient concentration of the current (, it is expressed as:

$$i = -D \nabla C_i$$

Based on the equation, Al^{3+} experienced the repulsion force as it approaches the surface of the electrode due to the similar positive charge of both the ion and the electrode. This statement leads to the second condition, as aluminium ion experienced momentum, has convicted its electrons. As aluminium lost 3 electrons, aluminium oxidized into Al^{3+}. The 3 electrons are forced transferring to the bare AuE which Au^{3+} under 100 mVs^{-1} of scan rate. Its force against the electromagnetic force produced by different terminal charges with the presence of external force such as current for a non-spontaneous chemical reaction to occur. The concentration of its current, then, expressed as:

$$i_{con} = \mu_i C_i$$

Where is ionic strength and is the concentration of the aluminium (Wang, 2001). The second factor might be happened was due to surface active site. The current signal was depending on the absorption site capacity according to Langmuir isotherm as shown below:

$$\emptyset = \frac{KP_A}{1 + KP_A} = \frac{\text{No. adsorption site occupied}}{\text{No. adsorption site available}}$$

As the rate of adsorption was while the rate desorption was . The equilibrium reaction between the rate of adsorption and the rate of desorption leads to the stability of the system (Wang, 2001). Therefore, 10 s showed the reaction was not fully complete in term of electron transfer and the surface-active area was still available. When the accumulation time was above 15 s, the peak of the current became stable until reaching 40 s. For the oxidation peaks, the highest current responses were observed

at a potential between 1.5 to 1.6 V due to the saturation of the ion on the electrode surface (Rana et al., 2017). A similar trend was observed at the reduction peaks where the highest current response formed at potential applied between 0.4 to 0.5 V. The selection of the 15 s was compared to other accumulation times due to sharp peak form between 10 to 15 s. This is the strong evidence of the electron transfer on the system (Rana et al., 2017). The formation of the peak from 10 to 15 s almost twice as compared the interval between the accumulation times. Therefore, 15 s was selected as an optimal accumulation time.

Detection of Different Concentration of Al^{3+}

Differential pulse voltammetry (DPV) is widely used for detection with different concentrations of Al^{3+} ranged from 0.2 to 1.0 ppm (Figure 5). After optimisation using CV analysis, DPV analysis was performed to test the current response related to different concentrations of Al^{3+} under the optimum conditions (Table 1).

Table 1 Optimum conditions applied for DPV analysis

Parameter	Optimum condition
Buffer	Tris-HCl buffer (0.1 M, pH 2)
Redox indicator	5 mM Prussian Blue
Scan rate	100 mVs^{-1}
Accumulation time	15 s
Reduction range	0.2 V to 0.8 V

The reduction range of 0.2 to 0.8 V was selected due to the stability of the current response as shown in Figure 5(A). As mentioned previously, the concentration of aluminium ion was set at 0.2 ppm according to the safety level of Al^{3+} in the drinking water standardised by Ministry of Health, Malaysia (2010) following the WHO guideline. The formation of reduction peak was observed from 0.55 to 0.75 V. The sensitivity of the bare AuE was about −0.0382 mA.

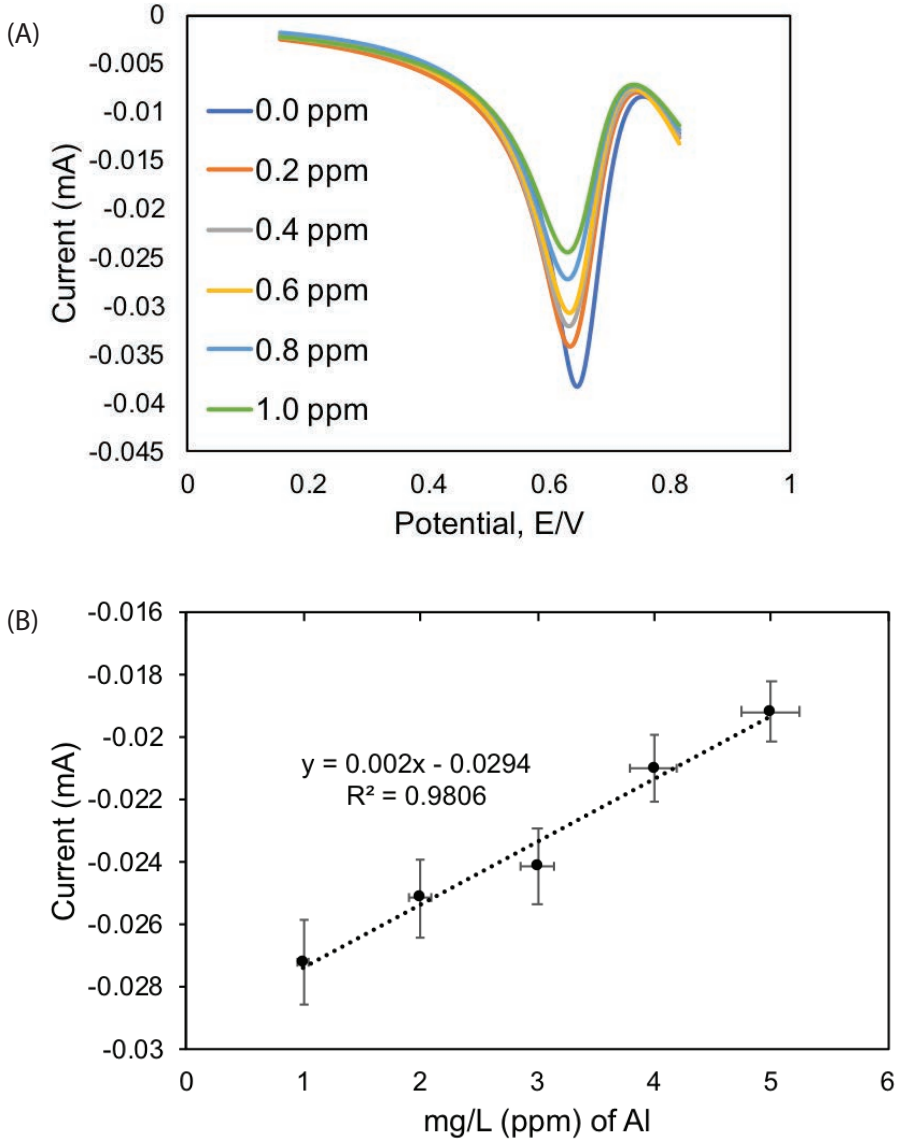

Figure 5 DPV analysis for different concentrations of aluminium in (0.1 M, pH 2) Tris-HCl buffer solution fixed as 0.2, 0.4, 0.6, 0.8 and 1.0 ppm with range potential 0.55 – 0.75 V under 100 mVs^{-1} of scan rate. DPV results of different concentrations aluminium ion (A) and the line graph for reduction peaks among the different concentrations (B). This experiment was repeated more than three times ($n > 3$)

Based on Figure 5 (A), the current is shifted to the left as the increasing amount of the aluminium added (from 0.6526 V to 0.6375 V) indicating the presence of Al^{3+} in the electrolytic solution. Also, the peak current response was proportional to the concentrations of aluminium as its approaching positive current. The peaks of the current response formed at reduction potential as the amount of the aluminium increasing. This is the strong evidence that aluminium is a strong reducing agent as its formed high peak at negative current axis according to standard reduction potential.

Determination of the reactions between the target ion and the surface of the bare AuE was conducted by analysing the data using a line graph as shown in Figure 5(B). The peak points among the concentrations were collected and the linear regression equation was obtained as $y = 0.002x - 0.0294$, where y stands for the peak of the current (mA) while x is the different concentrations of the aluminium ion (ppm) with a good linear correlation of $r^2 = 0.9806$. The peaks of the current response were closer to positive current as the high amount of aluminium added as mentioned before.

The possible electrochemical mechanism of these findings might be due to the affinity of target ion to the surface of the electrode. In the electrolytic solution, the cation produced by the buffer itself. Based on the chemical composition of Tris-HCl buffer ($C_4H_{11}NO_3$), it might produce complex compound $NH_2NaC(CH_2OH)_3.HCl$ due to the addition of sodium chloride (NaCl) into the solution. The possible chemical reaction by the formation of buffer in the electrolytic solution is as below:

$$NaCl + NH_2C(CH2OH)_3.HCl \longrightarrow NH_2NaC(CH2OH)3.HCl + Cl^-$$

Based on Alfred Werner's coordination theory, 1 HCl bound directly onto N in the form of $NH_2C(CH2OH)_3.HCl$. When the NaCl was added, the $NH_2NaC(CH2OH)_3.HCl$ was formed and it released Cl^- to bind with H^+ from water molecules (Berke, 2014). The other possible reaction was the formation of Na^+ which was possible cation that competed with Al^{3+}. This formation happened during the electrolysis process when the Na^+ breaks into the single radical ion from Tris-HCl buffer's chemical structure. The chemical reaction is shown below:

$$NH_2NaC(CH_2OH)_3.HCl \longrightarrow NH_2C(CH_2OH)_3.HCl + Na^+$$

The mixture was directly dissolved in the distilled water which was containing the cation identified as H^+. Therefore, the possible ions that might present in the solution are Na^+ are H^+ including the target ion (Al^{3+}). These ions chemically competed to attach on the cathode terminal by chemical affinity order. Theoretically, the more

positive radical ion compared to other cations, the higher chance of the ion to attach on the surface of the electrode. The affinity of Al^{3+} is stronger than H^+, while Na^+ is lower than Al^{3+} and H^+. This order might be affecting the accumulation of the ion on the surface of the bare AuE. Based on the affinity order, Al^{3+} was expected to attach on the surface of the electrode but at the same time, the Na^+ and H^+ competed on the same site which shows the unstable peak formation of different concentrations. Also, Al^{3+} was expected to attach on the surface of the electrode when the current response shifted to the left as shown in Figure 5(A). The other consideration the line graph was not linear as expected due to the charge of the electrode itself. Bare AuE has positive one ion (could be 2+ and 3+) based on it electron configuration ($5d^{10}$ $6s^1$). The repulsion force might happen between two elements with identical charges due to magnetic force. Some Al^{3+} might be repelled away from the bare AuE (positive charge) which indicated by the current responses in Figure 5(A) with less amount of aluminium shows the highest peak current response. However, the characteristic of the electrode itself as a good conductor enhanced the current flow through the system as well as increasing the current intensity cannot be denied. Therefore, the detection of Al^{3+} using AuE is successfully sensing through optimisation of all the important parameters.

CONCLUSION

This research paper reported the rapid detection of Al^{3+} using electrochemical methods through comprehensive optimisation of the important parameters such as buffer, redox indicator, pH value, scan rate, accumulation time and concentration window. The current response showed a good linear correlation (R^2 = 0.9806) with reversed current reaction, indicated by the reduction peaks when different concentrations of aluminium are applied into the DPV method. The proposed method can detect aluminium ion in 15 s. Finally, this optimised conditions, an electrochemical sensor is successfully detected of aluminium ion on the ranged of 0.2 to 1.0 ppm with high sensitivity (–0.0381663 mA). Therefore, the proposed method holds great potential for simple, rapid and in situ analysis of aluminium in drinking water and other sources.

ACKNOWLEDGEMENTS

This research was supported by UMSgreat (GUG0236-1/2018).

REFERENCES

Altunay, N., Yıldırım, E., & Gürkan, R. (2018). Extraction and preconcentration of trace Al and Cr from vegetable samples by vortex-assisted ionic liquid-based dispersive liquid–liquid microextraction prior to atomic absorption spectrometric determination. *Food Chemistry*, *245*, 586 – 594.

Barceló, J., & Poschenrieder, C. (2002). Fast root growth responses, root exudates, andinternal detoxification as clues to the mechanisms of aluminium toxicity andresistance: a review. Environmental and Experimental Botany, 48, 75–92.

Baylor, N. W., Egan, W., & Richman, P. (2002). Aluminium salts in vaccines – U.S. perspective. *Vaccine*, *20*, 18 – 23.

Berke, H. (2014). 'Counting ions' in Alfred Werner's coordination chemistry using electrical conductivity measurements. *Educación Química*, *25* (E1), 267 – 275.

Chaiyo, S., Mehmeti, E., Zagar, K., Siangproh, W., Chailapakul, O., & Kalcher, K. (2016). Electrochemical sensors for the simultaneous determination of zinc, cadmium and lead using a Na^+ion/ionic liquid/graphene composite modified screen-printed carbon electrode. *Analytica Chimica Acta*, *918*, 26 – 34.

Diao, Q., Ma, P., Lv, L., Li, T., Sun, Y., Wang, X., & Song, D. (2016). A water-soluble and reversible fluorescent probe for $Al^{3+}$and F^- in living cells. *Sensors and Actuators B*, *229*, 138 – 144.

Dravecz, G., Bencs, L., Beke, D., & Gali, A. (2016). Determination of silicon and aluminium in silicon carbide nanocrystals by high-resolution continuum source graphite furnace atomic absorption spectrometry. *Talanta*, *147*, 271 – 275.

Ensafi, A. A., Amini, M., & Rezaei, B. (2013). Detection of DNA damage induced by chromium/glutathione/H2O2 system at MWCNTs–poly (diallyldimethylammonium chloride) modified pencil graphite electrode using methylene blue as an electroactive probe. *Sensors and Actuators B: Chemical*, *177*, 862 – 870.

Elečková, L., Alexovič, M., Kuchár, J., Balogh, I. S., & Andruch, V. (2015). Visual detection and sequential injection determination of aluminium using a cinnamoyl derivative. *Talanta*, *133*, 27 – 33.

Ferancová, A., Hattuniemi, M. K., Sesay, A. M., Räty, J. P., & Virtanen, V . T. (2016). Rapid and direct electrochemical determination of Ni(II) in industrial discharge water. *Journal of Hazardous Materials*, *306*, 50 – 57.

Fu, Y., Jiang, X. J., Zhu, Y. Y., Zhou, B. J., Zang, S. Q., Tang, M. S., … Mak, T. C. W. (2014). A new fluorescent probe for Al^{3+} based on rhodamine 6G and its application to bioimaging. *Dalton Transactions*, *43*, 12624 – 12632.

Gilbert, R., Siddiquee, S., Tamrin, M. L., Saallah, S., Yusuf, N. H. M., & Amin, Z. (2018). Electrochemical methods for detection of zinc ion in drinking water. *International Journal of Pharma and Bio Science*, *9*, 268 – 276.

Gilbert, R., Siddiquee, S., Saallah, S., & Tamrin, M. L. (2019). Optimisation of parameters for detection of manganese ion using electrochemical method. *IOP Conference Series: Materials Science and Engineering*, *606*, 012009. DOI: 10.1088/1757-899X/606/1/012009

Gholivand, M. B., Akbari, A., Faizi, M., & Jafari, F. (2017). Introduction of a simple sensing device for monitoring of hydrogen peroxide based on ZnFe2O4 nanoparticles/chitosan modified gold electrode. *Journal of Electroanalytical Chemistry*, *796*, 17 – 23.

Gumpu, M. B., Veerapandian, M., Krishnan, U. M., & Rayappan, J. B. B. (2017). Simultaneous electrochemical detection of Cd (II), Pb (II), As (III) and Hg (II) ions using ruthenium (II)-textured graphene oxide nanocomposite. *Talanta*, *162*, 574 – 582.

Honeychurch, K. C., Rymansaib, Z., & Iravani, P. (2018). Anodic stripping voltammetry determination of zinc at a 3-D printed carbon nanofiber-graphite-polystyrene electrode using a carbon pseudo-reference electrode. *Sensors and Actuators B: Chemical*, *267*, 476 – 482.

Khanhuathon, Y., Siriangkhawut, W., Chantiratikul, P., & Grudpan, K. (2015). Spectrophotometric method for determination of aluminium content in water and beverage samples employing flow-batch sequential injection system. *Journal of Food Composition and Analysis*, *41*, 45 – 53.

Kim, H. S., Angupillai, S., & Son, Y. A. (2016). A dual chemosensor for both $Cu^{2+}$and Al^{3+}: A potential $Cu^{2+}$and Al^{3+}switched YES logic function with an INHIBIT logic gate and a novel solid sensor for detection and extraction of Al^{3+}ions from aqueous solution. *Sensors and Actuators B*, *222*, 447 – 458.

Lima, L. C., Papai, R., & Gaubeur, I. (2018). Butan-1-ol as an extractant solvent in dispersive liquid-liquid microextraction in the spectrophotometric determination of aluminium. *Journal of Trace Elements in Medicine and Biology*, *50*, 175 – 181.

Ma, Y. H., Yuan, R., Chai, Y. Q., & Liu, X. L. (2010). A new aluminium(III)-selective potentiometric sensor based on N,N'-propanediamide bis(2-salicylideneimine) as a neutral carrier. *Materials Science and Engineering C*, *30*, 209 – 213.

Manjumeena, R., Duraibabu, D., Rajamuthuramalingam, T., Venkatesan, R., & Kalaichelvan, P. T. (2015). Highly responsive glutathione functionalized green AuNP probe for precise colorimetric detection of Cd^{2+} contamination in the environment. *Royal Society of Chemistry Advances*, *5*, 69124 – 69133.

Mergu, N., Singh, A. K., & Gupta, V. K. (2015). Highly sensitive and selective colorimetric and off–on fluorescent reversible chemosensors for Al^{3+} based on the rhodamine fluorophore. *Sensors*, *15*, 9097 – 9111.

Engineering Service Division, Ministry of Health, Malaysia. (2016). *Drinking water quality standard*. Retrieved from https://environment.com.my/wp-content/uploads/2016/05/Drinking-Water-MOH.pdf.

Mohseni, H. K., Matysiak, W., Chettle, D. R., Byun, S. H., Priest, N., Atanackovic, J., & Prestwich, W. V. (2016). Optimization of data analysis for the in vivo neutron activation analysis of aluminium in bone. *Applied Radiation and Isotopes*, *116*, 34 – 40.

Peng, D., Hui, B., Kang, M., Wang, M., He, L., Zhang, Z., & Fang, S. (2016). Electrochemical sensors based on gold nanoparticles modified with rhodamine B hydrazide to sensitively detect Cu (II). *Applied Surface Science*, *390*, 422 – 429.

Ramezani, S., Jahani, R., Mashhadizadeh, M. H., Shahbazi, S. & Jalilian, S. (2018). A novel ionic liquid/polyoxomolybdate based sensor for ultra-high sensitive monitoring of Al(III): Optimization by Taguchi statistical design. *Journal of Electroanalytical Chemistry*, *814*, 7 – 19.

Rana, S., Mittal, S. K., Singh, N., Singh, J., & Banks, C. E. (2017). Schiff base modified screen printed electrode for selective determination of aluminium(III) at trace level. *Sensors and Actuators B: Chemical*, *239*, 17 – 27.

Rastogi, L., Dash, K., & Ballal, A. (2017). Selective colorimetric/visual detection of Al^{3+}in ground water using ascorbic acid capped gold nanoparticles. *Sensors and Actuators B*, *248*, 124 – 132.

Sarkar, D., Ghosh, P., Gharami, S., Mondal, T. K., & Murmu, N. (2017). A novel coumarin based molecular switch for the sequential detection of $Al^{3+}$and F^{-}: Application in lung cancer live cell imaging and construction of logic gate. *Sensors and Actuators B: Chemical*, *242*, 338 – 346.

Skalny, A. V., Kaminskaya, G. A., Krekesheva, T. I., Abikenova, S. K., Skalnaya, M. G., Bykov, A. T., & Tinkov, A. A. (2018). Assessment of hair metal levels in aluminium plant workers using scalp hair ICP-DRC-MS analysis. *Journal of Trace Elements in Medicine and Biology*, *50*, 658 – 663.

Siddiquee, S., Yusof, N. A., Salleh, A. B., Tan, S. G., & Bakar, F. A. (2010). Electrochemical DNA biosensor for the detection of Trichoderma harzianum based on a gold electrode modified with a composite membrane made from an ionic liquid ZnO nanoparticles and chitosan, and by using acridine orange as a redox indicator. *Microchimica Acta*, *172*, 357 – 363.

Silva, E. D. N. D., Heerdt, G., Cidade, M., Pereira, C. D., Morgon, N. H., & Cadore, S. (2015). Use of in vitro digestion method and theoretical calculations to evaluate the bioaccessibility of Al, Cd, Fe and Zn in lettuce and cole by inductively coupled plasma mass spectrometry. *Microchemical Journal*, *119*, 152 – 158.

Soni, M. G., White, S. M., Flamm, W. G., & Burdock, G. A. (2001). Safety evaluation of dietary aluminium. *Regulatory Toxicology and Pharmacology*, *33*, 66 – 79.

Suherman, A. L., Tanner, E. E. L., Kuss, S., Sokolov, S. V., Holter, J., Young, N. P., & Compton, R. G. (2018). Voltammetric determination of aluminium(III) at tannic acid capped-gold nanoparticle modified electrodes. *Sensors and Actuators B*, *265*, 682 – 690.

Tarley, C. R., Basaglia, A. M., Segatelli, M. G., Prete, M. C., Suquila, F. A. C., & Oliveira, L. L. G. (2017). Preparation and application of nanocomposite based on imprinted poly(methacrylic acid)-PAN/MWCNT as a new electrochemical selective sensing platform of Pb^{2+} in water samples. *Journal of Electroanalytical Chemistry*, *801*, 114 – 121.

Trachioti, M. G., Hrbac, J., & Prodromidis, M. I. (2018). Determination of Cd and Zn with "green" screen-printed electrodes modified with instantly prepared sparked tin nanoparticles. *Sensors and Actuators B: Chemical*, *260*, 1076 – 1083.

Tripathi, R. M., Gupta, R. K., Singh, P., Bhadwal, A. S., Shrivastav, A., Kumar, N., & Shrivastav, B. R. (2014). Ultra-sensitive detection of mercury(II) ions in water sample using gold nanoparticles synthesized by Trichoderma harzianum and their mechanistic approach. *Sensors and Actuators B: Chemical*, *204*, 637 – 646.

Wang, J. (2001). *Analytical electrochemistry* (2nd ed.). New York: Wiley-VCN.

Wang, C. X., Wu, B., Zhou, W., Wang, Q., Yu, H., Deng, K., Li, J. M., Zhuo, R. X., & Huang, S. W. (2018). Turn-on fluorescent probe-encapsulated micelle as colloidally stable nanochemosensor for highly selective detection of Al^{3+} in aqueous solution and living cell imaging. *Sensors & Actuators: B. Chemical*, *271*, 225 – 238.

Wen, S. H., Wang, Y., Yuan, Y. H., Liang, R. P., & Qui, J. D. (2018). Electrochemical sensor for arsenite detection using graphene oxide assisted generation of Prussian blue nanoparticles as enhanced signal label. *Analytica Chimica Acta*, *1002*, 82 – 89.

World Health Organization. (1998). Guidelines for drinking water quality (Second edition, Volume 2, p. 3). Retrieved from https://www.who.int/water_sanitation_health/dwq/2edaddvol2a.pdf.

Wu, W., Jia, M., Zhang, Z., Chen, X., Zhang, Q., Zhang, W., … Chen, L. (2019). Sensitive, selective and simultaneous electrochemical detection of multiple heavy metals in environment and food using a low cost Fe3O4 nanoparticles/fluorinated multi-walled carbon nanotubes sensor. *Ecotoxicology and Environmental Safety*, *175*, 243 – 250.

Xuan, X., & Park, J. Y. (2018). A miniaturized and flexible cadmium and lead ion detection sensor based on micro-patterned reduced graphene oxide/carbon nanotube/bismuth composite electrodes. *Sensors and Actuators B*, *255*, 1220 – 1227.

Yang, Y., Kang, M., Fang, S., Wang, M., He, L., Zhao, J., … Zhang, Z. (2015). Electrochemical biosensor based on three-dimensional reducedgraphene oxide and polyaniline nanocomposite for selective detection of mercury ions. *Sensors and Actuators B*, *214*, 63 – 69.

Zioła-Frankowska, A., Kuta, J., & Frankowski, M. (2015). Application of a new HPLC-ICP-MS method for simultaneous determination of Al^{3+} and aluminium fluoride complexes. *Heliyon*, e00035. DOI: http://dx.doi.org/10.1016/j.heliyon.2015.e00035

Borneo International Journal of Biotechnology (BIJB)
Vol. 1 (December 2020), 125 – 143

e-ISSN 2716-697X

REASSESSMENT OF THE CATALYTIC ACTIVITY AND SUBSTRATE SPECIFICITY OF FKBP35 FROM *Plasmodium knowlesi* USING PROTEASE-FREE ASSAY

Cahyo Budiman[1*], Carlmond Goh Kah Wun[1], Lee Ping Chin[2], Rafida Razali[1], Thean Chor Leow[3]

[1]Biotechnology Research Institute, Universiti Malaysia Sabah, Kota Kinabalu Sabah, Malaysia
[2]Faculty of Science and Natural Resources, Universiti Malaysia Sabah, Kota Kinabalu Sabah, Malaysia
[3]Enzyme and Microbial Technology Research Center, Department of Cell and Molecular Biology, Faculty of Biotechnology and Biomolecular Sciences, Universiti Putra Malaysia, Serdang, Selangor, Malaysia
*Corresponding author's email: cahyo@ums.edu.my
Received date: 1 September 2020 | Accepted date: 21 September 2020

ABSTRACT

FK506-binding protein35 of *Plasmodium knowlesi (*Pk-FKBP35) is a member of peptidyl prolyl *cis-trans* isomerase (PPIase) and is considered as a promising avenue of antimalarial drug target development. This protein is organized into the N-terminal domain responsible for PPIase catalytic activity followed and the tetratricopeptide repeat domain for its dimerization. The protease-coupling and protease-free assays are known to be the common methods for investigating the catalytic properties of PPIase. Earlier, the protease-coupling assay was used to confirm the catalytic activity of Pk-FKBP35 in accelerating *cis-trans* isomerization of the peptide substrate. This report is aimed to re-assess the catalytic and substrate specificity of Pk-FKBP35 using an alternative method of a protease-free assay. The result indicated that while Pk-FKBP35 theoretically contained many possible cleavage sites of chymotrypsin, experimentally, the catalytic domain was relatively stable from chymotrypsin. Furthermore, under protease-free assay, Pk-FKBP35 also demonstrated remarkable PPIase catalytic activity with k_{cat}/K_M of $4.5 \pm 0.13 \times 10^5$ M^{-1} s^{-1}, while the k_{cat}/K_M of active site mutant of D55A is $0.81 \pm 0.05 \times 10^5$ M^{-1} s^{-1}. These values were considered comparable to k_{cat}/K_M obtained from the protease-coupling assay. Interestingly, the substrate specificities

of Pk-FKBP35 obtained from both methods are also similar, with the preference of Pk-FKBP35 towards Xaa at P1 position was Leu>Phe>Lys>Trp>Val>Ile>His>Asp>Ala>Gln>Glu. Altogether, we proposed that protease-free and protease-coupling assays are reliable for Pk-FKBP35.

Keywords: malaria, *Plasmodium knowlesi*, Peptidyl prolyl *cis-trans* isomerases, FKBP

INTRODUCTION

Plasmodium knowlesi is known as the fifth species of *Plasmodium*, causing malaria in humans through a long tail macaque (Singh et al., 2004; Sing & Daneshvar, 2013). Statistically, Malaysia is considered the epicentre of *Plasmodium knowlesi* malaria, which accounts for 90% of human malaria cases. A recent report showed that more than 7,000 of *P. knowlesi* infection cases were reported in Malaysia, 86.8% of which were detected in Malaysian Borneo (Divis et al., 2020). In Sabah, *P. knowlesi* infection cases were scattered all regions of Sabah, including Tawau, interior division, West Coast division, Sandakan division, and also Kudat division (Lau, Joveen-Neoh, & Chong, 2011; Goh et al., 2013; William et al., 2014). Rajharam et al. (2019) also reported 6 malaria deaths in Sabah during 2015 – 2017, all were from *P. knowlesi*. Altogether, this demonstrates that *P. knowlesi* remains a severe issue in Sabah and urges more collective attempts to fight it.

The genome sequence of *P. knowlesi* harbours a single gene encoding a 35 kDa FK506-binding protein (Pk-FKBP35), a member of peptidyl prolyl *cis-trans* isomerase (PPIase) family proteins. PPIase is a group of enzymes capable of catalysing slow isomerization of a *cis*-proline bond which is known to be a rate-limiting step of protein folding. It is therefore predicted that this protein plays a vital role in the cellular function of *P. knowlesi* due to its involvement in protein folding machinery of the parasite. Hariskishore et al. (2014) proposed that *Plasmodium* FKBP35 is indeed a viable target for the development of novel antimalarial drugs. Accordingly, comprehensive structure and functional studies, as well as attempts to find inhibitors targeting this protein were widely reported (Yoon et al., 2006; Hariskishore et al., 2014; Goh et al., 2018). This protein is a dimeric protein in solution with the size of about 78 kDa and structurally organized into two functional domains of the N-terminal FK506-binding domain (FKBD) and tetratricopeptide repeat (TPR) domain.

The study on the kinetics of a reaction catalysed by the enzyme targeted by the drug is an important avenue for further drug development. Accordingly, extensive studies were reported on the catalytic properties of *Plasmodium* FKBP35, with the aim is to understand the mechanism behind the catalysis as a platform for the discovery

of drug-able spots for inhibiting the catalysis. Two approaches were reported to determine the catalytic activity of PPIase family members: protease-coupling and protease-free assays. In the protease-coupling assay, chymotrypsin was used as the protease and synthetic prolyl bond containing tetrapeptide conjugated with fluorophore moiety assay relies on the released of *p*-nitroaniline from the substrate due to cleavage by chymotrypsin when the proline residue in the substrate assumes the *trans* conformation. The cleavage has not occurred when the prolyl bond is in the *cis* conformation. Accordingly, the increase in isomerization is implicit in the increased *p*-nitroaniline release rate because catalysis of isomerization produces *trans* substrate with increased frequency. While this method is widely used in the measurement of catalytic activity of PPIase, a major drawback of this method is the possibility of PPIase degradation by chymotrypsin used in the assay.

On the other hand, an alternative method of uncoupled PPIase assay was proposed by Janowski, Wöllner, Schutkowski, and Fischer (1997), which omitted the use of any protease and relied on *cis* prolyl bond changes conformers upon a solvent jumping event. The solvent jumping is based on the ability of lithium chloride (LiCl) in anhydrous tetrahydrofuran (THF) or trifluoroethanol (TFE) to shift the equilibrium between *cis* and *trans* of Xaa-Pro peptide bonds in favour of the *cis* conformer. Under a normal solvent, the *cis* prolyl bond population is about only 10 – 20% at the equilibrium state. This population is extremely increased when the solvent changed to LiCl in TFE or THF to 80 – 90% (Kofron et al., 1992). The absence of protease in the uncoupling method also provides an opportunity to have more reliable kinetic parameters of the isomerization and substrate specificity. In the protease-coupling assay, the kinetic parameters and substrate specificity of PPIase might be intersected by the protease due to the possibility of the protease in binding and degrade the substrate during the isomerization. While the limitation of the protease-free assay lies in the high noise of the spectroscopic signal between *cis* and *trans* isomers, this method is recommended for the multidomain PPIase and sensitive towards chymotrypsin.

Earlier, catalytic properties of Pk-FKBP35 were studied using a protease-coupling method, which indicated that FKBD acted as the catalytic domain for this protein, and TPR has no role in the catalytic activity (Goh et al., 2018). Therefore, it is interesting if the catalytic activity of Pk-FKBP35 under protease-coupling assay reflects its real activity without the interference of chymotrypsin. Accordingly, in this report, the sensitivity of Pk-FKBP35 towards chymotrypsin protease was confirmed. Re-assessment of the catalytic activity and substrate specificity of Pk-FKBP35 using the protease-free assay was then discussed and compared to those obtained using the protease-coupling assay.

MATERIALS AND METHODS

Protein Preparation

All proteins were prepared in a His-tagged form. The expression constructs of pET29-Pk-FKBP35 was used to overproduce full-length Pk-FKBP35. Meanwhile, the constructs of pET29-D55A were used to overproduce active site mutants of D55A, where a single amino acid of Asp55 was replaced by Ala. All constructs were obtained as previously reported (Goh et al., 2018) and transformed into *Escherichia coli* BL21(DE3) for overproduction purposes.

Overproduction and Purification

Overproduction and purification of the proteins were carried out as described previously (Goh et al., 2018). Expression and purity of Pk-FKBP35 and D55A were checked by SDS-PAGE using 15% polyacrylamide gel stained under Coomassie Brilliant Blue R250 (Laemmli, 1970). The UV absorption at 280 nm was used to measure the protein concentration with the extinction coefficient at 280 nm of a 0.1% (1 mg mL^{-1}) is 0.73 for Pk-FKBP35 and D55A which was calculated based on Goodwin and Morton (1946).

Stability of Pk-FKBP35 against Chymotrypsin

***In silico* prediction.** The amino acid sequence of Pk-FKBP35 was firstly retrieved from PlasmoDB.org (accession code: PK-NH_1467100). The sequence was then subjected to PeptideCutter (https://web.expasy.org/peptide_cutter/). Chymotrypsin-low specificity (C-terminal to [FYWML], not before P) and chymotrypsin-high specificity (C-terminal to [FYW], not before P) were selected as the proteases to digest. The display of cleavage sites was set as the default.

Limited proteolysis assay. Pk-FKBP35 was prepared in 35 mM HEPES buffer pH 7.8 at a final concentration of 0.5 mg mL^{-1}. This solution was then incubated at 25°C for 3 min. The chymotrypsin was then added into the solution at the final concentration of 15 µM. The mixture was then incubated at 10, 20 and 30 min at 25°C. The reaction was stopped by the addition of 0.5 mM phenylmethylsulfonyl fluoride (PMSF). The proteins were then visualized and analyzed by using 15% SDS-PAGE (Laemmli, 1970) using a 15% polyacrylamide gel, followed by staining with Coomassie Brilliant Blue. The concentrations of Pk-FKBP35 and chymotrypsin were higher than the assay conditions for the visibility of the proteins in SDS-PAGE.

The N terminal amino acid sequencing. The gel obtained from limited protease assay as obtained above was transferred electrophoretically to polyvinylidenedifluoride (PVDF) membrane followed by staining and destaining using 0.5% Coomassie blue R-250 and 50% methanol, respectively. The membrane was then dried at 37°C and the bands of interest were excised gently and placed individually in sterilized 1.5 mL Eppendorf tube, treated with 100 µl anhydrous trifluoroacetic acid (TFA) and incubated for 1 h at 40°C followed by evaporation. The PVDF membrane carrying the bands of interest were then further treated with 100 µl of 0.6 N HCl at 25°C for 12 h. The sequencing of N-terminal amino acids was carried out using Edman degradation with a Procise 491 protein sequencer (Applied Biosystems).

PPIase Catalytic Activity

The PPIase catalytic activity was determined by protease-free assay at 25°C according to previous reports (Janowski et al., 1997; Budiman, Tadokoro, Angkawidjaja, Koga, & Kanaya, 2012). Briefly, the enzyme was incubated in 2 mL of 35 mM HEPES buffer (pH 7.8) for 3 min prior to the addition of the substrate. The peptide substrate suc-ALPF-pNA (Wako Pure Chemical Industries, Osaka, Japan) was dissolved in anhydrous TFE containing 0.5 mM LiCl. The reaction was initiated by the addition of 0.25 µM suc-ALPF-pNA (final concentration). The isomerization of the Leu-Pro bond from *cis* to *trans* conformation catalysed by PPIase was measured by monitoring the change in the absorption at 330 nm using a Hitachi U-2010 UV/VIS spectrophotometer (Hitachi High-Technologies, Tokyo, Japan). The catalytic efficiency (k_{cat}/K_M) was calculated from the relationship $k_{cat}/K_M = (kp - kn)/E$, where E represents the concentration of the enzyme, and kp and kn represent the first-order rate constants for the release of *p*-nitroaniline from the substrate in the presence and absence of the enzyme, respectively (Harrison & Stein, 1990).

Substrate Specificity

Substrate specificity of Pk-FKBP35 was measured under protease-free and protease-coupling assays using N-succinyl-Ala-Xaa-Pro-Phe-p-nitroanilide (Suc-AXaaPF-pNA) (Wako Pure Chemical, Osaka, Japan) as a substrate, in which Xaa stands for a variable aminoacyl residue in the P1 position of various substrates. The condition for protease-free as described above. Meanwhile, the protease-coupling assay was performed according to Goh et al. (2018). The catalytic efficiency (k_{cat}/K_M) obtained from Suc-AFPF-pNA was adjusted to 100% activity according to (Rahfeld et al., 1996; Budiman, Lindang, Cheong, & Rodrigues, 2018).

RESULT AND DISCUSSION

Stability of Pk-FKBP35 towards Chymotrypsin

Figure 1 shows 88 possible cleavage sites of chymotrypsin along the primary structure of Pk-FKBP35 predicted under the PeptideCutter (Gasteiger et al., 2005). This indicated that Pk-FKBP35 is prone to degradation of chymotrypsin as indicated by the presence of cleavage sites of the High- or Low-specificity of chymotrypsin along the sequences of Pk-FKBP35 in Figure 1. It is interesting that the cleavage sites are distributed in the whole region of Pk-FKBP35, extending from the N-terminal catalytic domain and C-terminal TPR domain. Nevertheless, a number of the cleavage sites at the catalytic domain was less than that of the TPR domain. This result implied that the presence of chymotrypsin in the protease-coupling assay would possibly degrade Pk-FKBP35. Nevertheless, the cleavage site predicted by the PeptideCutter is under the assumption that the cleavage sites are in exposed positions. In fact, in the folded state, those cleavage sites are possibly buried inside its three-dimensional structure and inaccessible by a protease to cleave. Parsell and Sauer (1989) demonstrated that the folded structure of protein is an important determinant for their proteolytic susceptibility. Ahmad, Kumar, Ramanand, and Rao (2012) proposed that partially or completely unfolded structures of the proteins are the major proteolytic susceptible conformations. Thomson, Hodgman, Yang, and Doyle (2003) also added that the PeptideCutter only relied on the presence of cleavage sites without taking into account cleavage rates affected by the structure of proteins. This leads to the assumption that the susceptibility of Pk-FKBP35 against chymotrypsin as predicted by the PeptideCutter might not reflect the natural environment where the protein is in a correct and completely folded structure.

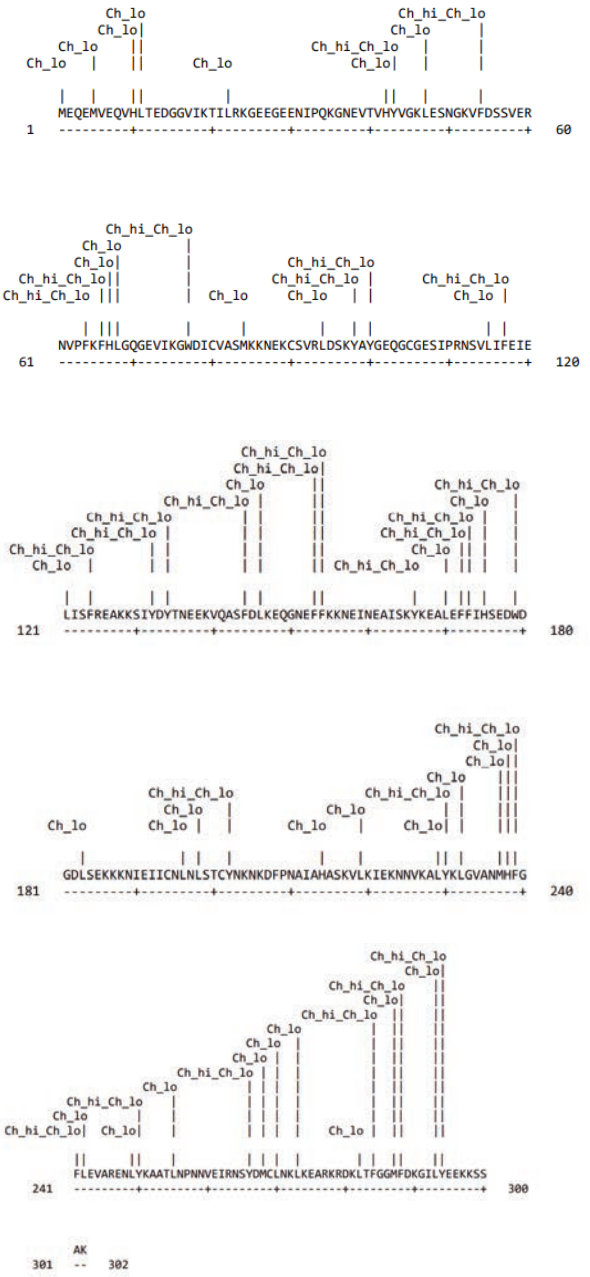

Figure 1 Theoretical cleavage sites of chymotrypsin on the primary sequence of Pk-FKBP35 predicted by the PeptideCutter. This diagram is derived by inputting amino acid sequence of Pk-FKBP35 into ExPASy PeptideCutter. The position of cleavage site is indicated by the dashed line above the sequence. Ch_lo and Ch_li represent the chymotrypsin-low specificity (C-term to [FYWML], not before P) and chymotrypsin-high specificity (C-term to [FYW], not before P), respectively. The numbers at the two ends of the sequence refer to the position of amino acids.

To confirm this, a limited proteolysis assay was conducted experimentally where Pk-FKBP35 was challenged by chymotrypsin at various reaction times. The condition of the proteolysis was adjusted to mimic the protease-coupling assay. Figure 2 shows that Pk-FKBP35 was indeed degraded by chymotrypsin as indicated by the presence of some bands in addition to the bands corresponding to Pk-FKBP35 (38 kDa) and chymotrypsin (25 kDa). Interestingly, degradation of Pk-FKBP35 by chymotrypsin resulted in only two major bands as shown in the Figure 2 as indicated by B and D bands. The apparent sizes of B and C bands were about 26 and 16 kDa, respectively, which are comparable to the sizes of TPR and catalytic domains of Pk-FKBP35, respectively. The N-terminal amino acid sequencing on D band was found to be MGS_H_H, which corresponded to the His-tag tail located at N-terminal of the catalytic domain (Table 1). Meanwhile, the N-terminal sequencing of band B produced two sequences of TNEE_V or EAK_SI (Table 1) corresponding to the residues located at the linker between the catalytic and TPR domain. This confirmed that B and D bands were indeed TPR and catalytic domains of Pk-FKBP35, respectively, which were separated upon degradation by chymotrypsin. This might also suggest that the major cleavage sites of chymotrypsin are located at the linker between these two domains. Earlier, the linker of the catalytic and TPR domains of Pk-FKBP35 structurally is a flexible loop with high solvent accessibility. A fragment between Ser113 and Gln120 of the linker was found to have the highest flexibility and therefore predicted to be susceptible against protease (Silvester, Lindang, Chin, Ying, & Budiman, 2017). Similarly, a multidomain FKBP22, which consisted of N-chaperone and C-catalytic domains, were also cleaved by chymotrypsin at the domain linkers (Budiman et al., 2012). The apparent stability of the functional domains of Pk-FKBP35 toward chymotrypsin was predicted due to the structures of the domains to bury the cleavage sites. This confirms that its folded form, the chymotrypsin cleavage sites on Pk-FKBP35 are much less than that of predicted by the PeptideCutter.

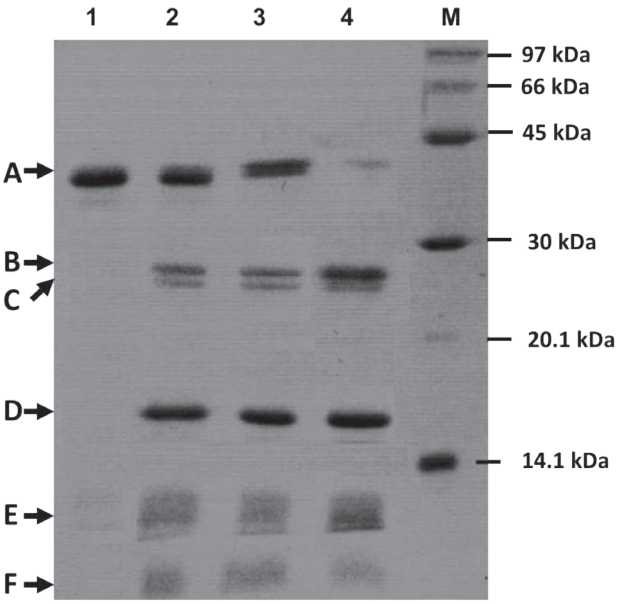

Figure 2 SDS-PAGE pattern of Pk-FKBP35 digestion by chymotrypsin. Lane 1 represented Pk-FKBP35 without chymotrypsin. Lanes 2, 3 and 4 represented Pk-FKBP35 in the presence of chymotrypsin after the incubation for 10, 20 and 30 min at 25°C, respectively. Lane M represented low molecular protein markers (GE Healthcare, Upsalla, Sweden). The protein bands corresponding to Pk-FKBP35 and chymotrypsin are indicated by A and C arrows, respectively. Meanwhile, B, D, E and F arrows indicated the digestion products.

Table 1 The N-terminal sequences of the protein bands from limited proteolysis

Band	Sequence
A	MGSS_HH
B	TNEE_V
	EAK_SI
D	MGS_H_H
E	Unable to be sequenced
F	Unable to be sequenced

"_" indicated the residue is unable to read due to low signal.

Interestingly, the band corresponding to the catalytic domain (D band) was relatively stable up to 30 min reaction time. Meanwhile, the band's thickness corresponds to the TPR domain was shown to decrease during the proteolytic time. These indicated that the catalytic domain was relatively much more stable than the TPR domain. The decrease in the band of the TPR domain indicated that this protein was further digested by chymotrypsin. To note, some minor fragments were also observed in Figure 2 (labelled by E and F arrows) which indicated that the chymotrypsin also able to cleave some fragments of Pk-FKBP35 apart from the linker. Nevertheless, these fragments are considered minor degradation products and might be resulted from the degradation of the surface region of this protein. Altogether, the digestion of Pk-FKBP35 by chymotrypsin occurred primarily at the domain linker producing free forms of the catalytic and TPR domains. The chymotrypsin further digested the TPR domain producing smaller fragments (E and F bands). Further digestion might also occurred in the catalytic domain, yet, at a much lower rate than the TPR domain. Structurally, the catalytic domain folded into a more globular structure, while the TPR domain folded into a more elongated structure (Silvester et al., 2017; Alag et al., 2009), which made this domain is theoretically more prone to proteolytic degradation. Unfortunately, the N-terminal sequencings on E and F bands were unsuccessful (Table 1)**,** which might be due to various fragments accumulated in these bands.

To note, despite this protein is degradable by chymotrypsin, remarkable catalysis of slow *cis* prolyl bond isomerization by Pk-FKBP35 was observed (Goh et al., 2018). This indicated that the cleavage of Pk-FKBP35 by chymotrypsin was not in the region responsible for catalysis. The domain linker of Pk-FKBP35 was indeed found not to play any role in catalysis (Silvester et al., 2017). Similarly, the TPR domain, which was apparently sensitive toward chymotrypsin, was not involved in the catalytic activity of Pk-FKBP35. Besides, the isolated catalytic domain (without TPR domain) remains exhibit comparable catalytic activity to its full-length (Goh et al., 2018).

Catalytic Activity

Figure 3 shows that the time course of reversible prolyl isomerization of Suc-Ala-Phe-Ala-pNA upon the solvent jumping in the presence of 30 nM of Pk-FKBP35 or D55A active site mutant, was found to be considerably different to the spontaneous isomerization reaction. While the isomerization time courses as shown in Figure 3 were found to have scattered light noise appearance, the courses were well first-order fitted with R^2 more than 95% for both reactions. The first-order reaction rate (k) of the cis-trans isomerization in the absence of Pk-FKBP35 was calculated to be $4.0 \pm 0.81 \times 10^{-3}$ s^{-1}, which is comparable to the previous report on the isomerization rate constant in the absence of PPIase (Janowski et al., 1997; Schiene-Fischer, Habazetti, Tradler, &

Fischer, 2002; Fanghanel & Fischer, 2004; Kofron et al., 1992). Interestingly, Goh et al. (2018) found that under protease-coupling assay, the *k* value of the isomerization in the absence of Pk-FKBP35 was in the range 3.70 – 4.52 × 10^{-3} s^{-1}, which is close enough to the *k*-value obtained in this study. This suggested that the presence of chymotrypsin has no serious effect on the isomerization rate of the substrate.

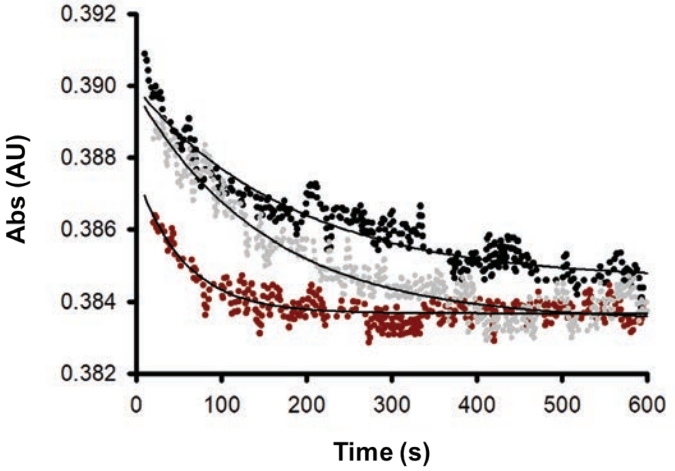

Figure 3 Progress curves of the prolyl cis-trans isomerization of Suc-AlaPhe-Pro-Phe-4-nitroanilide after jumping from the peptide stock solution in TFE/LiCl into the final buffer solution in the absence (black circle) or in the presence of Pk-FKBP35 (red circle) or D55A mutant (grey circle). The solid black line represents the fitting curve of a first order-rate reaction for each curve.

Further, Figure 4 indicated that the *k* value of the isomerization rate in the presence of Pk-FKBP35 was found to be concentration-dependent, which follows the general trend of PPIase catalytic activity (Fanghanel & Fischer, 2004; Schiene-Fischer et al., 2002). Earlier, Goh et al. (2018) also found that the PPIase activity of Pk-FKBP35 measured under protease-coupling assay was a concentration-dependent. The calculated k_{cat}/K_M from this was found to be 4.5 $\pm$ 0.13 × 10^5 M^{-1} s^{-1}, which is remarkable enough to demonstrate the ability of this protein to catalyse the slow cis-trans isomerization. Nevertheless, Goh et al. (2018) reported that k_{cat}/K_M of Pk-FKBP35 under protease-coupling assay was found to be slightly higher (5.0 $\pm$ 0.18 × 10^5 M^{-1} s^{-1}). This might be due to differences in the structural freedom of the catalytic domain of Pk-FKBP35 in the absence or in the presence of chymotrypsin. In the protease-coupling assay, chymotrypsin likely digested the linker of catalytic and TPR domain yielding a free catalytic domain in the assay cocktail. In the absence of chymotrypsin, the catalytic domain remains in its intact form with the TPR domain in a dimeric form. Structurally, the catalytic domain is more restricted due to the dimerization of this protein

as previously reported (Goh et al., 2018). The free forms of the catalytic domain of Pk-FKBP35 are predicted to have more flexibility to bind to more substrate which consequently exhibiting higher catalytic activity than in the dimeric form. Similarly, Budiman et al. (2009) experimentally confirmed that the monomeric catalytic domain of FKBP was found to be more active than its dimeric form due to the less structural constraints to bind to the substrate.

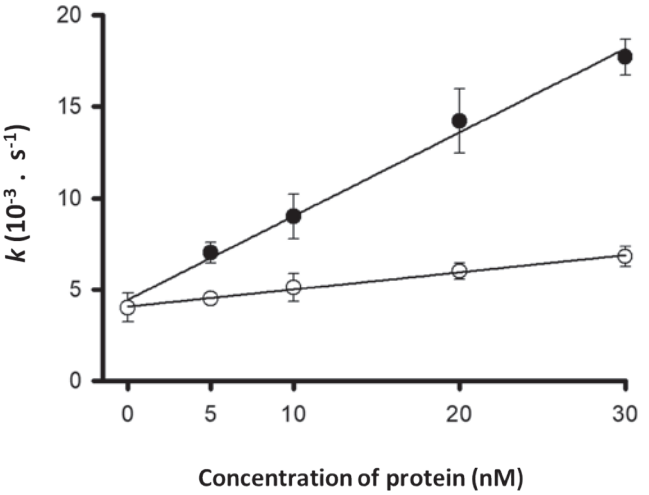

Figure 4 The first-order reaction rates (*k*) of the prolyl cis-trans isomerization in the presence of a various concentrations of Pk-FKBP35 (black circle) and D55A mutant (white circle)

To note, the k_{cat}/K_M values for Pk-FKBP35 obtained from protease-free and protease-coupling assays were different by less than 10%. This magnitude is considered minor for enzymatic activity (Bisswanger, 2014), and therefore we considered that the catalytic activity of Pk-FKBP35 measured using both assays was comparable. Further, the k_{cat}/K_M of D55A mutant under the protease-free assay was calculated to be 0.81 $\pm$ 0.05 $\times$ 10^5 M^{-1} s^{-1}. This value is considerably comparable to the previous report by Goh et al. (2018) showing that the D55A mutant of Pk-FKBP35 exhibited k_{cat}/K_M of 1.01 $\pm$ 0.14 $\times$ 10^5 M^{-1} s^{-1} under a protease-coupling method. Low activity of D55A mutant was previously proposed due to the possible role of this residue to reduce a resonance effect of the peptide bond through the formation of a hydrogen bond to the peptide bond nitrogen (Goh et al., 2018). Fanghanel and Fisher (2004) proposed earlier that disrupting the resonance of a peptide bond is an essential step in the acceleration of the isomerization of the bond. The resonance structure caused the bond is structurally rigid and has restricted rotation.

As the k_{cat}/K_M values of Pk-FKBP35 and D55A mutant measured under protease-free and protease-coupling assays were comparable, we, therefore, assumed that that protease-coupling assay is considered to be reliable for measuring the catalytic activity of Pk-FKBP35. In fact, as Figure 2 obviously showed catalytic domain of Pk-FKBP35 is relatively stable against chymotrypsin which leads to an assumption that the essential region for catalytic activity was not interfered by chymotrypsin. In addition, the stability of both domains might also due to the low concentration of chymotrypsin used in the protease-coupling assay was relatively low. Noteworthy, the protease-free assay was found to have less signal-to-noise ratio as indicated in Figure 3. Janowski et al. (1997) and Kofron et al. (1992) indicated that the high spectroscopic noise is due to small differences in spectroscopic absorbance between *trans* and *cis* prolyl bond isomers. In combination with the apparent stability of the catalytic domain of Pk-FKBP35 against chymotrypsin and the spectroscopic noise, we are in the opinion that the protease-coupling assay is acceptable and preferable for assessment of catalytic Pk-FKBP35. Fanghanel and Fischer (2004) also indicated that the protease-coupling assay is experimentally proven and scientifically acceptable for many types of PPIase. The protease-free assay is, nevertheless, recommended for PPIase members having low stability against chymotrypsin. In addition, to address the noise observed in UV-vis spectroscopy, NMR spectroscopy is more preferable for assessing the direct isomerization rate of the prolyl bond under protease-free assay.

Substrate Specificity

A tetrapeptide substrate containing different amino acid preceding proline residue (Suc-Ala-Xaa-Pro-Pro-pNA) was used to determine the substrate specificity of Pk-FKBP22. Figure 5 indicated the position of the Xaa residue which refers to the P1 position in the nomenclature according to the Schechter and Berger nomenclature (Berger & Schechter, 1970). Based on the nomenclature, the residues involved in the catalytic activity of Pk-FKBP35 (active site residues) were assumed to form a contiguous pocket termed subsite. Each subsite (S2, S1, S1′ and S2′) represents a single active site residue of Pk-FKBP35 that binds to corresponding residues of the peptide substrate (P2, P1, P1′ and P2′). The bond to be isomerized (prolyl-bond) is located between P1 – P1′ sites of the substrate. Figure 5 showed the subsites S2, S1, S1′ and S2′ would interact to P2, P1, P1′ and P2′, respectively. Any changes on the P2, P1, P1′ and P2′ sequence might affect the interaction with the subsites. In this study, eleven (11) variants of the tetrapeptide substrates, with different chemical properties and bulkiness, were used by replacing Xaa to Leu/Phe/Trp/Ala/Gln/Val/Ile/His/Asp/Lys/Glu. Schiene, Reimer, Schutkowski, and Fischer (1998) reported that the residue prior to the proline was found to be critical for spontaneous bond rotation due to its role in formation of the non-covalent enzyme/substrate complex.

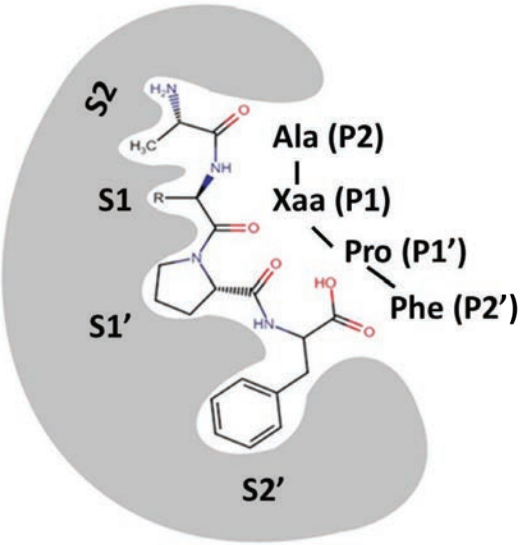

Figure 5 Schematic and nomenclature for binding of the peptide substrate to Pk-FKBP35 according to the Schechter and Berger nomenclature for binding of a peptide substrate to a peptidase. Pk-FKBP35 is represented by the shaded area. R is the side chain of Xaa amino acid. P2, P1, P1′ and P2′ are the amino acid residues of the substrate. S2, S1, S1′ and S2′ are the corresponding subsites on Pk-FKBP35. The figure is not drawn to scale.

Figure 6 shows that the overall preference of Pk-FKBP35 to Xaa is more to the hydrophobic residues. The highest catalytic efficiency (k_{cat}/K_M) was observed for Leu at Xaa position. Meanwhile, no activity was detected when Glu was at Xaa site. In overall, the preference of Pk-FKBP35 towards Xaa at P1 position followed the following order: Leu>Phe>Lys>Trp>Val>Ile>His>Asp>Ala>Gln>Glu. This suggested that Pk-FKBP35 behaves similarly as other FKBP family proteins in which hydrophobic residues as a residue preceding the proline (Fanghanel & Fischer, 2004; Rahfeld et al., 1996; Budiman et al., 2018). Interestingly, while Ile and Val are considerably more hydrophobic than Leu, Phe and Trp, based on their hydropathy index (Kyte & Doolittle, 1983), the activity against Ile or Val was much lower than that of Leu or Phe or Trp. This might be due to the stereochemical properties of Val or Ile side chains which are not appropriate for S1 site. The side chain of Ile is believed to be too bulky to fit the S1 site, while Val's side chain is too short and branched thus unable to interact to the S1 site properly. A similar explanation also applied for Ala, where its single methyl side chain is not sufficient to interact property to the S1 site. Besides, study on human FKBP12 by Schiene et al. (1998) indicated that the methyl group of Ala's side chain was at opposite orientation of the S1 site. Interestingly, while Lys is considered as a hydrophilic residue, the activity against this residue was higher than some hydrophobic residues (Trp, Val, Ile). It is believed that this due to the hydrophobicity of the carbon atom (Cα – Cε) of this residue that fit well the S1 site as also supported by Fanghanel & Fischer (2004).

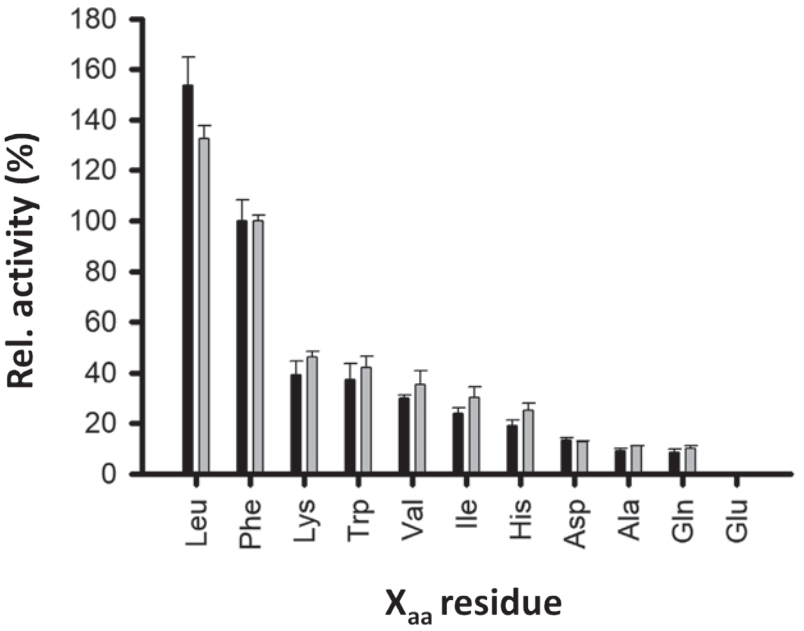

Figure 6 Substrate specificity of Pk-FKBP35 as measured under protease-free (black bars) and protease-coupling (grey bars) assays. The PPIase activity towards Phe as the Xaa residue in the substrate was adjusted to 100% activity.

To note, the catalytic domain of Pk-FKBP35 displays high similarity to the other FKBPs members (Goh et al., 2018) assuming that the proteins share the substrate binding and catalytic mechanisms. Nevertheless, the uniqueness of Pk-FKBP35 lies in the loop corresponding to the loop 80's of human FKBP12, whereby some residues of the FKBP35's loop were found to be different from that of human FKBP12. Nevertheless, the low conservation on the loop apparently has no serious effect on the substrate specificity as human FKBP12 was also reported to prefer bulky hydrophobic residues at Xaa position (Ikura & Ito, 2007). Meanwhile, the preferences of cyclophilin and parvulin toward the Xaa position were reported to be different. Cyclophilin has wide specificity at Xaa position (Rahfeld et al., 1994), while Parvulin having a unique specificity for a phosphorylated Ser or Thr preceding the Pro (Fanghanel & Fischer, 2004; Rahfeld et al., 1994). The discrepancy in the specificity among PPIase member is believed due to structural differences in substrate binding pocket that affect the fitting of each substrate (Fanghanel & Fischer, 2004).

Interestingly, when the protease-coupling assay was used to measure the substrate specificity, the preferences of the Xaa residues were also similar to that of the protease-free assay. This indicated that the presence of chymotrypsin in the assay has no serious effect on the substrate fitting into the catalytic activity. This supports our assumption earlier that the catalytic domain was relatively resistant towards chymotrypsin under

assay condition. Noteworthy, the catalytic domain of Pk-FKBP35 is assumed to be in free monomeric form due to the digestion of the domain linker. Meanwhile, the catalytic domain is in an intact dimeric form when the chymotrypsin is an absence in the assay. This suggested that the substrate specificity of this protein is independent from its dimerization. However, as the catalytic efficiency of Pk-FKBP35 deducted from the protease-coupling assay was slightly higher than that of from the protease-free assay, this also suggests that there is no structural relationship between catalytic efficiency and substrate specificity. Catalytic efficiency might be more related to the flexibility of overall the catalytic domain, located at the tip of the dimeric structure of Pk-FKBP35, in capturing the substrate. Structural dimerization might affect the binding constant (k_{on} or k_{off}) to the catalytic domain. Specificity was then speculated to be more related to the local structural configuration at the active site. Similar evidence was also reported for the dimeric form of FKBP22 from *Shewanella* sp. SIB1 (Budiman et al., 2009; Budiman et al., 2018). Inoue et al. (2019) and Parker, Corey, Stansfeld, and Newstead (2019) also implied that structural basis regulating the substrate specificity heavily relied on the local configuration of the substrate-binding cavity.

CONCLUSION

The current study confirmed the structural sensitivity of Pk-FKBP22 towards chymotrypsin, particularly the linker connecting catalytic and dimerization domains of this protein. Nevertheless, the disruption of the linker by chymotrypsin showed no apparent effect on its catalytic properties. This is based on the results that the catalytic activity of Pk-FKBP35 assessed using protease-coupling and protease-free assays were comparable. In addition, the substrate specificity of Pk-FKBP35 towards Xaa residues at the P1 position measured using protease-coupling and protease-free assays also revealed the same substrate pattern, whereby the hydrophobic bulky residues are preferable at Xaa site. This confirmed that both protease-coupling and protease-free assays are reliable enough to assess the catalytic properties of Pk-FKBP35. Nevertheless, due to the high spectrophotometric noise issue under protease-free assay, the protease-coupling is believed to be practically more preferable for the assay.

ACKNOWLEDGEMENTS

This project is supported by the Skim Penyelidikan Berimpak, Universiti Malaysia Sabah (SPB0003-2020) and the International Collaborative Grant of Protein Research Institute, Osaka University, Japan 2019 (TLA1902). The authors would like to thank Dr Takashi Kodama for his technical support.

REFERENCES

Ahmad, S., Kumar, V., Ramanand, B., & Rao, N. M. (2011). Probing protein stability and proteolytic resistance by loop scanning: A comprehensive mutational analysis. *Protein Science*, *21*, 433 – 446. DOI: 10.1002/pro.2029

Alag, R., Bharatham, N., Dong, A., Hills, T., Harikishore, A., Widjaja, A.A, … Yoon, H. S, (2009). Crystallographic structure of the tetratricopeptide repeat domain of Plasmodium falciparum FKBP35 and its molecular interaction with Hsp90 C-terminal pentapeptide. *Protein Science: a Publication of the Protein Society*, *18* (10), 2115 – 2124. DOI: 10.1002/pro.226.

Berger, A., & Schechter, I. (1970). Mapping the active site of papain with the aid of peptide substrates and inhibitors. *Philosophical transactions of the Royal Society of London. Series B, Biological Sciences*, *257* (813), 249 – 264. DOI: 10.1098/rstb.1970.0024

Bisswanger, H. (2014). Enzyme assays. *Perspectives in Science*, *1*, 41 – 55. DOI: http://dx.doi.org/10.1016/j.pisc.2014.02.005

Budiman, C., Bando, K., Angkawidjaja, C., Koga, Y., Takano, K., & Kanaya, S. (2009). Engineering of monomeric FK506-binding protein 22 with peptidyl prolyl cis-trans isomerase. *FEBS Journal*, *276* (15), 4091 – 4101. DOI: https://doi.org/10.1111/j.1742-4658.2009.07116.x

Budiman, C., Lindang, H. U., Cheong, B. E., & Rodrigues, K. F. (2018). Inhibition and substrate specificity properties of FKBP22 from a psychrotrophic bacterium, *Shewanella* sp. SIB1. *Protein Journal*, *37* (3), 270 – 279. DOI: https://doi.org/10.1007/s10930-018-9772-z

Budiman, C., Tadokoro, T., Angkawidjaja, C., Koga, Y., & Kanaya, S. (2012). Role of polar and nonpolar residues at the active site for PPIase activity of FKBP22 from *Shewanella* sp. SIB1. *FEBS Journal*, *279* (6), 976 – 986. DOI: 10.1111/j.1742-4658.2012.08483.x

Divis, P. C., Hu, T. H., Kadir, K. A., Mohammad, D., Hii, K.C., Daneshvar, C., … Singh, B. (2020). Efficient surveillance of *Plasmodium knowlesi* genetic subpopulations, Malaysian Borneo, 2000–2018. *Emerging Infectious Diseases*, *26* (7), 1392 – 1398. DOI: https://dx.doi.org/10.3201/eid2607.190924

Fanghanel, J., & Fischer, G. (2004). Insight into catalytic mechanism of peptidyl prolyl cis/trans isomerase. *Frontiers Bioscience*, *9*, 3453 – 3478. DOI: 10.2741/1494.

Gasteiger, E., Hoogland, C., Gattiker, A., Duvaud, S., Wilkins, M.R., Appel, R. D., & Bairoch, A. (2005). Protein identification and analysis tools on the ExPASy server. In J. M. Walker (Ed.), *The proteomics protocols handbook* (pp. 571 – 607). Totowa, New Jersey: Humana Press.

Goh, C. K. W., Silvester, J., Wan Mahadi, W. N. S., Lee, P. C., Lau, T. Y., Thean, C. L., … Budiman, C. (2018). Expression and characterization of functional domains of FK506-binding protein 35 from *Plasmodium knowlesi*. *Protein Engineering, Design and Selection*, *31* (12), 489 – 498. DOI: 10.1093/protein/gzz008

Goh, X. T., Lim, Y. A., Vythilingam, I., Chew, C. H., Lee, P. C., Tan, T. C., ... Chua, K. H. (2013). Increased detection of *Plasmodium knowlesi* in Sandakan division, Sabah as revealed by PlasmoNex™. *Malaria Journal*, *12*, 264. DOI: https://doi.org/10.1186/1475-2875-12-264

Goodwin, T. W., & Morton, R. A. (1946) The spectrophotometric determination of tyrosine and tryptophan in proteins. *Biochemical Journal*, *40* (5 – 6), 628 – 632. DOI: 10.1042/bj0400628

Harikishore, A., Niang, M., Rajan, S., Preiser, P. R., & Yoon, H. S. (2013). Small molecule Plasmodium FKBP35 inhibitor as a potential antimalaria agent. *Scientific Reports*, *3*, 2501. DOI: https://doi.org/10.1038/srep02501

Ikura, T., & Ito, N. (2007). Requirements for peptidyl-prolyl isomerization activity: a comprehensive mutational analysis of the substrate-binding cavity of FK506-binding protein 12. *Protein Science*, *16* (12), 2618 – 2625. DOI: 10.1110/ps.073203707

Inoue, Y., Ogawa, Y., Kinoshita, M., Terahara, N., Shimada, M., Kodera, N., … Minamino, T. (2019). Structural insights into the substrate specificity switch mechanism of the type III protein export apparatus. *Structure*, *27* (6), 965 – 976. DOI: 10.1016/j.str.2019.03.017

Janowski, B., Wöllner, S., Schutkowski, M., & Fischer, G. (1997). A protease-free assay for peptidyl prolyl cis/trans isomerases using standard peptide substrates. *Analytical Biochememistry*, *252* (2), 299 – 307. DOI: 10.1006/abio.1997.2330

Kyte, J., & Doolittle, R. F. (1983). A simple method for displaying the hydropathic character of a protein. *Journal of Molecular Biology*, *157* (1), 105 – 132.

Laemmli, U. K. (1970). Cleavage of structural proteins during the assembly of the head of bacteriophage. *Nature*, *227*, 680 – 685.

Lau, T. Y., Joveen-Neoh, W. F., & Chong, K. L. (2011). High Incidence of *Plasmodium knowlesi* Infection in the Interior Division of Sabah, Malaysian Borneo. *International Journal of Bioscience, Biochemistry and Bioinformatics*, *1* (2), 163 – 167. DOI: 10.7763/IJBBB.2011.V1.30

Kofron, J. L., Kuzmic, P., Kishore, V., Gemmecker, G., Fesik, S. W., & Rich, D. H. (1992). Lithium chloride perturbation of cis-trans peptide bond equilibria: effect on conformational equilibria in cyclosporin A and on time-dependent inhibition of cyclophilin. *Journal of the American Chemical Society*, *114* (7), 2670 – 2675. DOI: https://doi.org/10.1021/ja00033a047

Parker, J. L., Corey, R. A., Stansfeld, P. J., & Newstead, S. (2019). Structural basis for substrate specificity and regulation of nucleotide sugar transporters in the lipid bilayer. *Nature Communications*, *10*, 4657. DOI: https://doi.org/10.1038/s41467-019-12673-w

Parsell, D. A., & Sauer, R. T. (1989). The structural stability of a protein is an important determinant of its proteolytic susceptibility in *Escherichia coli*. *The Journal of Biological Chemistry*, *264* (13), 7590 – 7595.

Rahfeld, J. U., Rucknagel, K. P., Schelbert, B., Ludwig, B., Hacker, J., Mann, K., & Fischer, G. (1994). Confirmation of the existence of a third family among peptidyl-prolyl *cis/trans* isomerases. Amino acid sequence and recombinant production of parvulin. *FEBS Letters*, *352* (2), 180 – 184. DOI: https://doi.org/10.1016/0014-5793(94)00932-5

Rahfeld, J. U., Rucknagel, K. P., Stoller, G., Horne, S. M., Schierhorn, A., Young, K. D., & Fischer, G. (1996). Isolation and amino acid sequence of a new 22-kDa FKBP-like peptidyl-prolyl cis/trans-isomerase of *Escherichia coli* similarity to Mip-like proteins of pathogenic bacteria. *The Journal of Biological Chemistry*, *271* (36), 22130 – 22138.

Rajharam, G. S., Cooper, D. J., William, T., Grigg, M. J., Anstey, N. M., & Barber, B. E. (2019). Deaths from *Plasmodium knowlesi* Malaria: Case series and systematic review. *Clinical Infectious Diseases*, *69* (10), 1703 – 1711. DOI: 10.1093/cid/ciz011

Schiene, C., Reimer, U., Schutkowski, M., & Fischer, G. (1998). Mapping the stereospecificity of peptidyl prolyl cis/trans isomerases. *FEBS Letter*, *432* (3), 202 – 206. DOI: 10.1016/s0014-5793(98)00871-0

Schiene-fischer, C., Habazetti, J., Tradler, T., & Fischer, G. (2002). Evaluation of similarities in the *cis/trans* isomerase function of trigger factor and DnaK. *Biological Chemistry*, *383*, 1865 – 1873. DOI: 10.1515/BC.2002.210

Silvester, J., Lindang, H. U., Chin, L. P., Ying, L. T., & Budiman, C. (2017). Structure and molecular dynamic regulation of FKBP35 from *Plasmodium knowlesi* by structural homology modeling and electron microscopy. *Journal of Biological Sciences*, *17* (8), 369 – 380. DOI: 10.3923/jbs.2017.369.380

Singh, B., & Daneshvar, C. (2013). Human infections and detection of *Plasmodium knowlesi*. *Clinical Microbiology Reviews*, *26* (2), 165 – 184. DOI: 10.1128/CMR.00079-12

Singh, B., Sung, L. K., Matusop, A., Radhakrishnan, A., Shamsul, S. S. G., Cox-Singh, J., ... Conway, D. J. (2004). A large focus of naturally acquired *Plasmodium knowlesi* infections in human beings. *Lancet*, *363* (9414), 1017 – 1024. DOI: 10.1016/S0140-6736(04)15836-4

Thomson, R., Hodgman, T. C., Yang, Z. R., & Doyle, A. K. (2003). Characterizing proteolytic cleavage site activity using bio-basis function neural networks. *Bioinformatics*, *19* (14), 1741 – 1747. DOI: 10.1093/bioinformatics/btg237

William, T., Jelip, J., Menon, J., Anderios, F., Mohammad, R., Mohammad, T. A. A., ... Barber, B. E. (2014). Changing epidemiology of malaria in Sabah, Malaysia: increasing incidence of *Plasmodium knowlesi*. *Malaria Journal*, *13* (1), 390. DOI: https://doi.org/10.1186/1475-2875-13-390

Yoon, H. R., Kang, C. B., Chia, J., Tang, K., & Yoon, H. S. (2006). Expression, purification, and molecular characterization of *Plasmodium falciparum* FK506-binding protein 35 (PfFKBP35). *Protein Expression and Purification*, *53* (1), 179 – 185. DOI: https://doi.org/10.1016/j.pep.2006.12.019